The Influence of Dopamine Signaling on the Central Circadian Clock: Implications for Jet lag and Obesity

Ryan Michael Grippo

Basking Ridge, NJ

B.S., Pennsylvania State University, 2012

A dissertation presented to the Graduate Faculty of the University of Virginia in Candidacy for the Degree of Doctor of Philosophy

Department of Biology

University of Virginia

August, 2019

Committee Members
Ali Güler
Ignacio Provencio
Michael Menaker
Michael Scott
Karsten Siller

Abstract

Circadian rhythms, or biological oscillations of approximately twenty-four hours, impact almost all aspects of our lives by regulating the sleep-wake cycle, hormone release, body temperature fluctuation, and timing of food consumption. Circadian entrainment, or temporal synchrony with one's environment, is essential for survival. In mammals, the central circadian pacemaker resides within the suprachiasmatic nucleus (SCN) and mediates an organism's entrainment to environmental conditions. While the light-dark cycle is the primary environmental cue, arousal-inducing, non-photic signals such as food consumption, exercise, and social interaction are also potent synchronizers. Many of these stimuli enhance dopaminergic signaling suggesting that a cohesive circadian physiology depends on the relationship between circadian clocks and the dopamine (DA) neuromodulatory circuits that govern motivational behaviors. Here, we identify a direct connection between DA producing neurons of the ventral tegmental area (VTA) and D1 dopamine receptor (Drd1) expressing SCN neurons that mediates resynchronization of activity rhythms to phase-shifted light:dark cycles. Additionally, we discovered that Drd1 null mice are resistant to diet-induced obesity, while rescue of Drd1 expression specifically within the SCN is sufficient to restore obesity, metabolic disease, and circadian disruption associated with an energy-dense diet. From these studies, it is evident that the SCN-Drd1 signaling is essential for adjusting to changes in environmental conditions as experienced during jet lag, shiftwork, and consumption of palatable foods.

Dedication

This work is dedicated to everyone who has made it possible for me to find success in graduate school. There are too many to list, but know that I remember you all, and your contributions will not be forgotten. Primarily I must acknowledge my advisor Ali Güler, who pushed me to breach my self-limitations, and selflessly mentored me for years with my best interests always in mind. I also thank Aundrea Rainwater for teaching me organization, mouse colony maintenance, and the importance of diligence, dedication, and determination. Aarti Purohit, the last of the original three members of the Güler team, inspired me on a daily basis to never give up and keep pressing forward. She made science fun. Her curiosity, tenacity, and dedication to the lab was instrumental to my success.

Additionally, I am eternally grateful for family support over the years: Vicki Coffin, Jack Coffin, Gerrie Coffin, Carol Caring, Eva Grippo, Frank Grippo, Joseph Grippo, Bonnie Brennan, Bill Brennan, James Grippo, Katie Grippo, and Jessie Grippo. I further dedicate the completion of this work to my partner in life and love Xin Yuan, who has helped me to become a greater scientist and person than I ever imagined possible. Her intelligence, generosity, and willingness to sacrifice provided me with the endless encouragement and support I needed. I am forever grateful for her presence in my life and the impact she has made on my career as well. Finally, I would like to thank the mice themselves. Their sacrifice often goes unnoticed, but they are the life source of our discoveries. Throughout this document, names in bold are used to indicate significant contributions from specific co-authors and collaborators who made this research possible.

Table of contents

Abstract 2

Dedication 3

Table of contents 4

List of abbreviations 5

Chapter I: Dopamine Signaling in Circadian Photoentrainment: Consequences of Desynchrony 7

The Suprachiasmatic Nucleus (SCN) and Circadian Photoentrainment 9

Evaluating Endogenous Circadian Rhythms 10

Peptides and Neurotransmitters of Photic and Non-Photic Entrainment 14

Consequences of Aberrant Entrainment Conditions 15

Dopamine Signaling and Circadian Rhythms 18

Circadian Disruption in Addiction, Mood Disorders and Parkinson's Disease 22

Dopamine signaling in the SCN 25

Chapter II: Direct Midbrain Dopamine Input to the Suprachiasmatic Nucleus Accelerates Circadian Entrainment 28

Chapter III: Weight Gain Associated with Hedonic Feeding Requires Dopamine Signaling in the Suprachiasmatic Nucleus 69

Chapter IV: Conclusions and Future Directions 134

References 140

List of abbreviations

AAV	Adeno associated virus
AgRP	Agouti related peptide
ARC	Arcuate nucleus
BAT	Brown adipose tissue
ChR2	Channelrhodopsin
CLOCK	Circadian locomotor output cycles kaput
CNO	Clozaine-N-Oxide
CNS	Central nervous system
Cre	Cre recombinase
CT	Circadian time
DA	Dopamine
DAPI	4',6-diamidino-2-phenylindole
DAT	Dopamine re-uptake transporter
DIO	Diet induced obesity
DIO	Double inverted open reading frame
Drd1	D1 dopamine receptor
Drd2	D2 dopamine receptor
DS	Donkey serum
FEO	Food entrainable oscillator
GABA	Gamma-Aminobutyric acid
GTT	Glucose tolerance test
GWAT	Gonadal white adipose tissue
H & E	Hemotoxilyn and Eosin
HA-	Human influenza hemagglutinin
HFD	High-fat diet
HPLC	High pressure liquid chromatography
hSyn	Human synapsin
IHC	Immunohistochemistry
IPN	Interpeduncular nucleus
ITT	Insulin tolerance test
KO	Knockout
LD	Light:dark cycle
MASCO	Methamphetamine sensitive oscillator
NAc	Nucleus accumbens
OB	Olfactory bulb
ORO	Oil Red O
PBS	Phosphate buffered saline
PBST	Phosphate buffered saline Triton X
Per2	Period 2
PVN	Paraventricular nucleus
RB	Retrobeads
RER	Respiratory exchange ratio

RRF	Retrorubral field
SCAT	Subcutaneous white adipose tissue
SCN	Suprachiasmatic nucleus
SCD	Standard chow diet
SNc	Substantia Nigra pars compacta
TH	Tyrosine hydroxylase
VIP	Vasoactive intestinal peptide
VTA	Ventral tegmental area
WAT	White adipose tissue
WT	Wild-type
YFP	Yellow fluorescent protein
ZI	Zona incerta
ZT	*Zeitgeber* time

Chapter I: Dopamine Signaling in Circadian Photoentrainment: Consequences of Desynchrony

Published as a review article in *Yale Journal of Biology and Medicine*, 06/27/19

Accessible at PMID: 31249488

Abstract

Circadian rhythms impact almost all aspects of our lives by regulating the sleep-wake cycle, hormone release, body temperature fluctuation, and timing of food consumption. The molecular machinery governing these rhythms is similar across organisms ranging from unicellular fungi to insects, rodents, and humans. Circadian entrainment, or temporal synchrony with one's environment, is essential for survival. In mammals, the central circadian pacemaker is located in the suprachiasmatic nucleus (SCN) of the hypothalamus and mediates entrainment to environmental conditions. While the light:dark cycle is the primary environmental cue, arousal-inducing, non-photic signals such as food consumption, exercise, and social interaction are also potent synchronizers. Many of these stimuli enhance dopaminergic signaling suggesting that a cohesive circadian physiology depends on the relationship between circadian clocks and the neuronal circuits responsible for detecting salient events. Here, we review the inner workings of mammalian circadian entrainment, and describe the health consequences of circadian rhythm disruptions with an emphasis on dopamine signaling.

Introduction

Circadian rhythms regulate biological processes ranging from gene expression to behavior. The period, amplitude, phase, and waveform of these oscillations are governed by an internal clock that has evolved in a variety of organisms to anticipate events such as sunrise and sunset (Aschoff, 1960; Panda et al., 2002). Proper phase alignment of the circadian pacemaker to environmental timing cues is critical for an organism's well-being and survival. Darwinian pressures have changed for humans as many of the emergent stressors of modern society burden our ancient circadian physiology. Varying environmental conditions experienced during shift work or transmeridian travel create desynchrony between the time of day and the internal clocks (Zee and Goldstein, 2010). When prolonged, such misalignments result in higher incidences of mood disorders, obesity, cardiovascular disease, and cancer (West and Bechtold, 2015). As such, pathologies associated with circadian dysfunction are increasing at an alarming rate, creating the pressing need to better understand the basis of circadian physiology in order to advance the practice of psychiatry, nutrition, and medicine (Smolensky et al., 2016; Stevens et al., 2007).

The synchronization of an organism's internal cycles to an external rhythm, termed entrainment, requires the molecular clock machinery, that drives endogenous rhythms, to align with the exogenous daily cycles (Golombek and Rosenstein, 2010). During photoentrainment (entrainment by light), ambient light information is detected by retinal photoreceptors and conveyed to the central circadian clock located in the suprachiasmatic nucleus (SCN) of the hypothalamus

(Berson et al., 2002; Guler et al., 2008; Hattar et al., 2002). This brain region has been studied extensively in the last few decades, revealing a nucleus of vast importance.

The Suprachiasmatic Nucleus (SCN) and Circadian Photoentrainment

For proper adaptation to a dynamic world, a circadian timing system needs to anticipate salient events such as food and mate availability. In mammals, the SCN, or master circadian clock, is situated in the basal hypothalamus dorsal to the optic chiasm and orchestrates rhythms throughout the rest of the brain and body (Albrecht, 2012; Mohawk et al., 2012). The diverse cellular components of SCN are both necessary and sufficient for circadian rhythm maintenance as surgical ablation of this nucleus produces behavioral arrhythmia, while grafts of neonatal SCN into a SCN-ablated host restores rest-activity rhythms (Moore and Eichler, 1972; Ralph et al., 1990; Stephan and Zucker, 1972). Molecular circadian oscillations are generated by a core set of clock genes that form a transcriptional-translational feedback loop to temporally coordinate gene expression and drive behavioral output. For a detailed description of the molecular components of the circadian pacemaker, refer to the following reviews (Asher and Sassone-Corsi, 2015; Takahashi, 2017).

In the absence of external time cues, such as during constant darkness (DD), SCN neurons continue firing rhythmically and driving overt behavioral activity with a period of approximately twenty-four hours (Herzog et al., 1998; Welsh et al., 1995; Welsh et al., 2010). For instance, in DD, mice exhibit a free running period

that is slightly less than twenty-four hours, initiating their activity earlier with each new cycle. While the endogenous circadian clock remains functional in constant conditions (Herzog et al., 1998; Welsh et al., 1995; Welsh et al., 2010), it relies on environmental signals (*Zeitgebers)* to synchronize the organism's physiology to daily external rhythms, such as the earth's 24-hour light-dark (LD) cycle. The synchronization of an organism's internal rhythms to an external cycle, termed entrainment, requires the molecular clock machinery to align endogenous rhythms with the exogenous daily cycles (Golombek and Rosenstein, 2010). In mammals, entrainment by light, termed photoentrainment, is mediated by the light-activated neural circuits originating in the retina that project to the SCN through the retino-hypothalamic tract (Berson et al., 2002; Moga and Moore, 1997; Morin et al., 2003). Non-image-forming, irradiance information is primarily transmitted to the SCN by the melanopsin-expressing intrinsically photosensitive retinal ganglion cells (ipRGCs) (Gooley et al., 2001; Guler et al., 2008; Provencio et al., 2002; Rollag et al., 2003).

Evaluating Endogenous Circadian Rhythms

In humans, the circadian system remains entrainable even in visually blind patients, given that the ipRGCs survive (Czeisler and Brown, 1999; Czeisler and Gooley, 2007; Zaidi et al., 2007). However, complete loss of retinal function results in significant impairments of circadian entrainment (Nakagawa et al., 1992; Sack et al., 1992). While humans (diurnal) and rodents (nocturnal) are active in opposite phases of the day, the anatomical and physiological components of their circadian

system are conserved. As such, hamsters, rats, and mice have been indispensable models in elucidating the molecular mechanisms driving circadian rhythms and entrainment. Analysis of wheel running activity is the gold-standard technique for evaluating the behavioral output of circadian rhythms in rodents (Jud et al., 2005). Mice are particularly useful for mechanistic understanding of circadian behaviors as they voluntarily use running wheels, are easily entrained to a 12 hour light: 12 hour dark cycle, and enable use of a readily available transgenic toolkit (Bucan and Abel, 2002; Meijer and Robbers, 2014; Song and Palmiter, 2018; van der Weyden et al., 2011).

An entrainable circadian pacemaker requires phase-dependent resetting by which the intensity, duration, and phase of the applied stimulus determines the extent and direction of the phase change in behavioral response (Czeisler and Gooley, 2007; Takahashi et al., 1984). The phase sensitivity of resetting is best summarized by a phase-response curve (PRC), which plots the amplitude of phase change against the circadian phase at which the phase shifting stimulus was provided. For instance, the photic PRC is achieved by administering light pulses to free running animals at distinct time points across the circadian day (Figure 1A). The circadian day is defined as one activity-rest cycle, and by convention, the onset of activity is denoted as circadian time 12 (CT 12). Animals exposed to a light pulse during the subjective day, known as the dead zone, experience no physiological change within the SCN or in wheel running activity in the subsequent days (Figure 1B). However, a light pulse in the early subjective night (CT 14) produces a phase delay in the initiation of locomotor activity (Figure 1C), while a

pulse at CT 18 results in a phase advance (Figure 1D). Interestingly, animals exposed to non-photic cues such as restricted availability of food and behavioral arousal, exhibit a similar but antiphasic PRC, with large phase advances occurring during the subjective day (Challet et al., 2003; Hastings and Maywood, 2000; Rosenwasser and Dwyer, 2001). Both photic and non-photic entrainment cues influence the period and phase of the SCN to properly align rest/activity cycles.

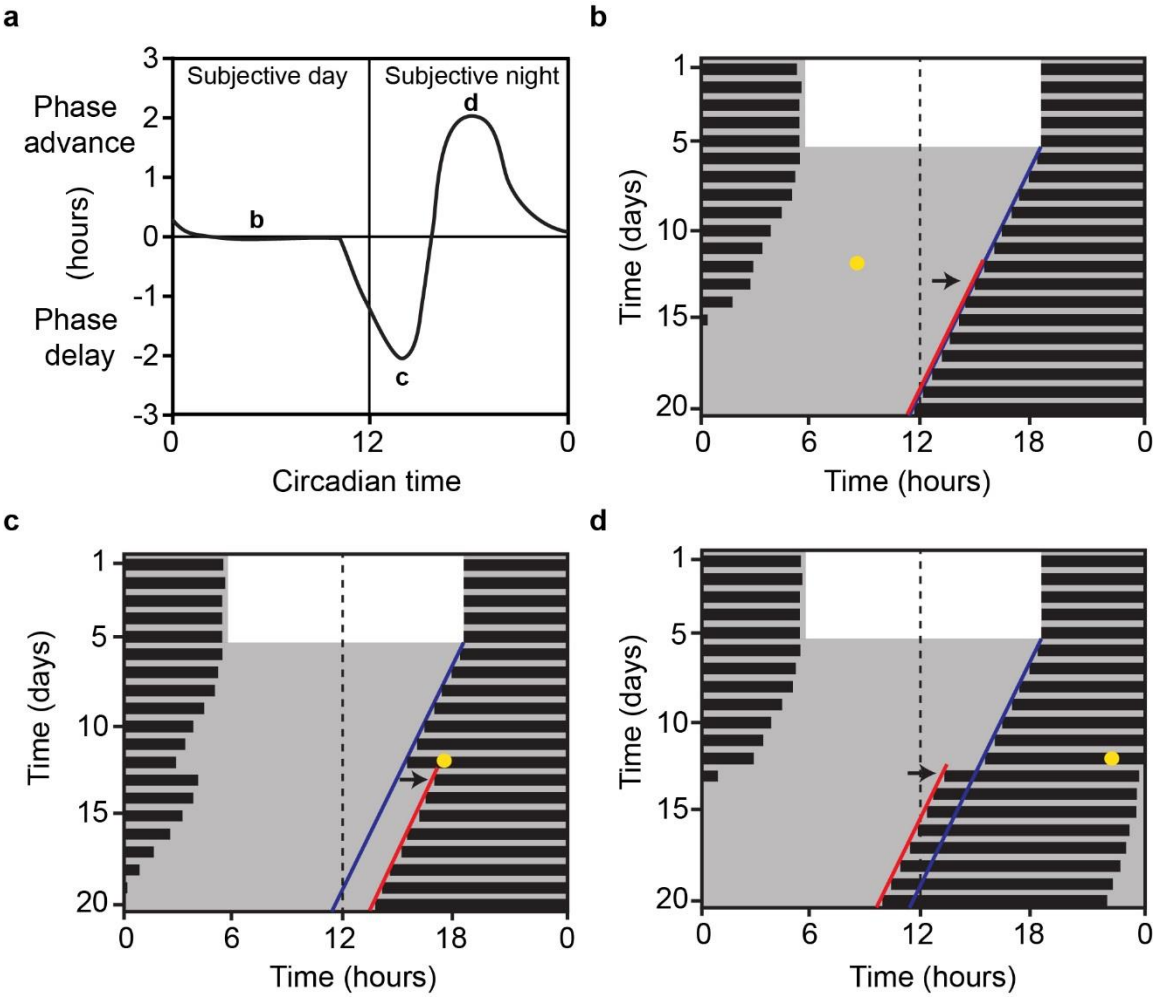

Figure 1. Phase response curve of circadian rhythms to light. A. Illustration of the photic PRC in mice. By convention, phase advances are recorded as positive values and phase delays as negative. Plot of wheel running actograms representing the locomotor response of to a brief light pulse during the B,

subjective day, C, early subjective night (inducing a phase delay), and D, late subjective night (inducing a phase advance). Black bars represent wheel running activity; yellow dots indicate time of light pulses in DD; dark blue lines represent an extended regression line derived by activity onsets prior to the light pulse; red lines follow actual onset of activity after the light pulse. The duration of phase shift is quantified as Delta t between the two regression lines on the day after the light pulse marked by the black arrows.

For adaptation to a dynamic world, this circadian timing system also requires the ability to anticipate salient events such as food or mate availability. While light is the primary entraining agent, arousal-inducing non-photic cues such as palatable foods, social interaction, and physical exercise also influence the phase of the SCN molecular clock (Hastings et al., 1997; Mrosovsky et al., 1989). Dopamine (DA), a neurotransmitter mostly known for its role in reward processing and motivation, is a significant modulator of the aforementioned behaviors that drive non-photic circadian entrainment (Horvitz, 2000; Wise and Rompre, 1989). Additionally, patients suffering psychiatric and neurodegenerative pathologies associated with DA signaling dysregulation such as depression, bipolar disorder, schizophrenia, drug addiction, and Parkinson's disease are known to have perturbations of circadian rhythms (Maywood et al., 2006; Van Veen et al., 2010; Wilson and Argyropoulos, 2012; Wulff et al., 2010; Zanini et al., 2015). As such, DA is emerging as an important regulator of central and peripheral circadian rhythms (Korshunov et al., 2017; Mendoza and Challet, 2014).

Peptides and Neurotransmitters of Photic and Non-Photic Entrainment

The regulation of circadian entrainment is accomplished through various neuropeptides and neurotransmitters such as; vasoactive intestinal peptide (VIP), arginine vasopressin (AVP), neuromedin S (NMS), glutamate, gamma aminobutyric acid (GABA), serotonin, NPY and DA (An et al., 2013; Aton et al., 2005; Grippo et al., 2017; Ingram et al., 1998; Lee et al., 2015). In particular, light-mediated entrainment of the SCN is modulated by the neuropeptide pituitary adenylate cyclase-activating polypeptide (PACAP) and the excitatory neurotransmitter glutamate (Hannibal, 2002). Direct applications of glutamate receptor agonists to the SCN induce similar behavioral phase shifts as those observed in response to light, while glutamate antagonist treatments block light-induced phase shifts (Franken et al., 1999; Meijer et al., 1988).

In addition to retinal-dependent photoentrainment, light-independent neural circuits likewise directly influence SCN neurons to regulate circadian phase. The most prominent non-photic entrainment cue in mammals is behavioral activation or arousal induced by sleep deprivation, animal handling, or introduction of a novel running wheel (Hastings et al., 1998; Mistlberger and Antle, 2011). While the mechanism of phase-resetting by behavioral arousal remains unknown and understudied, both serotonin and NPY directly change SCN molecular rhythms and induce phase shifts of circadian activity during the subjective day, when the SCN is least sensitive to light and most sensitive to non-photic entrainment cues (Glass et al., 2000; Harrington and Rusak, 1989; Johnson et al., 1988; Mrosovsky, 1995). As presented here, resetting the circadian clock through photic or non-

photic cues is accomplished by neurotransmission to induce slight corrections to the phase of the SCN, to maintain a stable relationship with the solar day. However, larger phase shifts in environmental cycles, as experienced in rotational shift work, exert profound challenges to the circadian system.

Consequences of Aberrant Entrainment Conditions

For humans, the advent of electricity and artificial lights has disrupted the sun's role in entraining circadian rhythms, resulting in serious health consequences including a range of metabolic disorders (Arble et al., 2010). Even brief exposure to dim light at night can lead to significant weight gain and metabolic disruption (Fonken et al., 2010). Interestingly, a genetic mutation of the circadian core gene *Clock,* results in elevated DA signaling, dampened feeding rhythms, and metabolic disease in mice, suggesting an important role for circadian rhythms in energy regulation (Turek et al., 2005). Notably, mice given time-restricted access to a high-fat diet (HFD) only at night, gain significantly less weight than mice consuming the same diet *ad libitum* despite isocaloric daily food intake (Hatori and Panda, 2010; Hatori et al., 2012). While still early in their implementation, time-restricted feeding studies in humans show promising results (Gabel et al., 2018; Longo and Panda, 2016). Recently, one study found temporal restriction of meals from 8:00 am to 3:00 pm significantly improved the metabolic profiles of prediabetic men, despite producing no significant changes in body weight (Sutton et al., 2018). Further characterization of time restricted feeding is necessary to evaluate its effectiveness as a weight-loss regimen. Still, these findings emphasize the

importance of aligning daily activities with the astronomical day, and the metabolic consequences of circadian desynchrony created by modern lifestyles.

Along these lines, access to high-fat, palatable foods also alters the timing of food intake and lengthens the period of free-running activity and temperature rhythms in mice (Blancas-Velazquez et al., 2017; Kohsaka et al., 2007). This alteration of circadian timing suggests a connection between energy dense food intake and the circadian pacemaker. Recently, circadian peak of dopaminergic activity in and around the SCN has been found to be a modulator of metabolism in rats (Luo et al., 2018). Consequently, consumption of hypercaloric diets impairs adjustment to photic resetting and reduces light mediated c-fos induction within the SCN (Mendoza et al., 2008). Additionally, regularly timed daily access to a palatable snack (chocolate pellet) entrains behavioral rhythms in constant darkness, reduces light-induced phase shifts, increases DA content in the forebrain and increases c-Fos activity within DA neurons of the midbrain (Mendoza et al., 2010). These important findings uncover an underappreciated relationship between disrupted circadian rhythms and the dysregulation of the DA signaling. Future work must address how aberrant lighting conditions and rewarding foods impact the SCN, the consequence of this interaction, and how to reduce its negative impact.

In addition to hypercaloric food consumption, the circadian system is also challenged by rapid changes in external lighting conditions. Transmeridian travel across several time zones also creates a rapid change in environmental conditions leading to the general malaise and compromised daytime function associated with

jet lag disorder (Zee and Goldstein, 2010). Jet lag primarily is a consequence of imposed internal desynchrony within the SCN resulting from an incongruence between the endogenous circadian pacemaker and the local time. Reducing the duration of this desynchrony is a paramount concern for shift-workers who are constantly exposed to irregular work and sleep schedules, increasing their susceptibility to cardiovascular disease, ulcers, depression, and obesity (James et al., 2017; Zee and Goldstein, 2010). As such, considerable effort has been placed into understanding the mechanism of circadian resynchronization in response to abrupt changes in environmental lighting conditions (Adamovich et al., 2017; Grippo et al., 2017; Nagano et al., 2003; Pilorz et al., 2014).

Jet lag is simulated in the laboratory by advancing the LD cycle (Figure 2a: simulating eastward travel) or delaying it (Figure 2b: simulating westward travel). Resynchronization of wheel running activity to these shifts occurs gradually with incremental phase changes (transients) each day until a stable phase of entrainment has been achieved. Manipulations of LD cycle paired with analysis of activity rhythms have been used to reveal the factors that influence the rate of entrainment. In rodents, introduction of a novel running wheel, exposure to sexually receptive partners or elevated DA tone have all resulted in accelerated circadian photoentrainment, demonstrating that arousal-inducing stimuli influence the rate of circadian resynchrony (Bobrzynska and Mrosovsky, 1998; Grippo et al., 2017; Yamanaka et al., 2008). Further research based on these findings could provide the novel insight needed to develop effective therapeutic strategies to

facilitate entrainment, thereby effectively treating disorders exacerbated by circadian desynchrony to environmental timing cues.

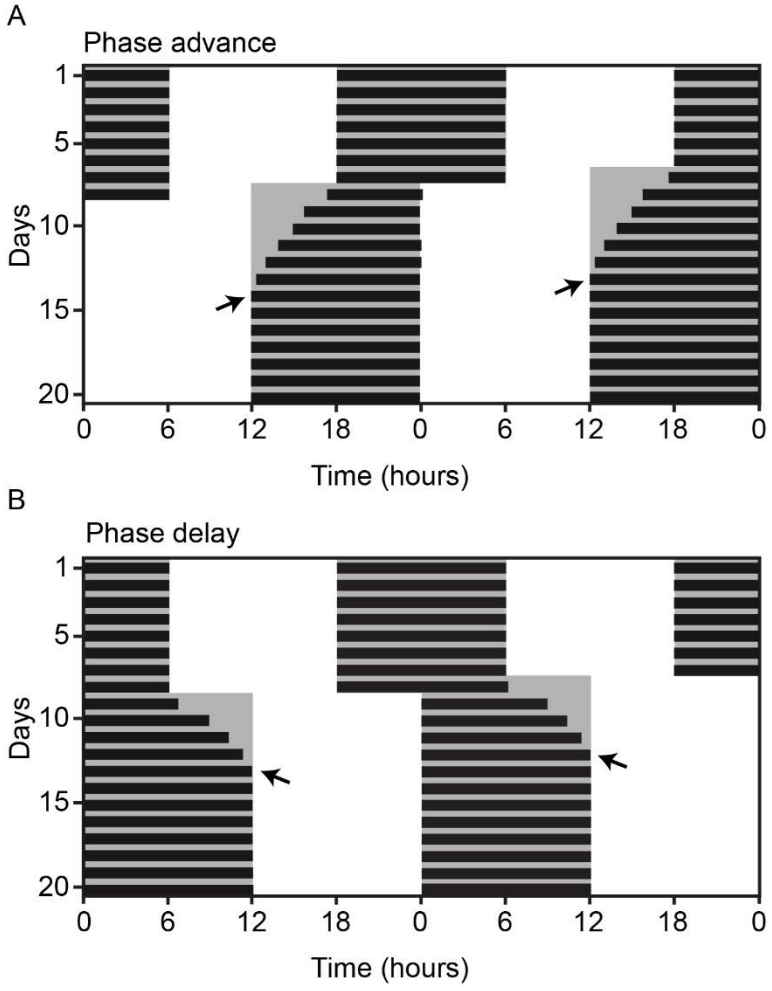

Figure 2. Jet lag paradigms. Representative double-plotted actograms of a light-cycle A. advance and B., delay of the LD phase by six hours. Black arrows indicate the day of entrainment.

Dopamine Signaling and Circadian Rhythms

Dopamine, a monoamine neurotransmitter well known for its role in reward and motivation, is also important for the detection of salient events such as food or mate availability (Horvitz, 2000; Schultz, 1998; Wise, 2004, 2006). To facilitate a

myriad of physiological and behavioral outputs, DA modulates neural activity through a group of G-protein coupled receptors distinguished by their cognate G-proteins—G_s-coupled (D1 and D5), and G_i-coupled receptors (D2, D3, D4)—that are expressed in anatomically distinct regions throughout the brain and body (Beaulieu and Gainetdinov, 2011; Missale et al., 1998; Seeman, 1980). G_s-coupled receptors stimulate cAMP production, while G_i-coupled receptors inhibit both adenylate cyclase activity and cAMP production, promoting different cellular responses following their activation as reviewed in further detail in the following manuscript (Beaulieu and Gainetdinov, 2011). Importantly, DA signaling associated behaviors such as drug self-administration, food reward, and mating all fluctuate in the extent of their expression across the day-night cycle revealing an association with circadian regulation (Abarca et al., 2002; Mendoza and Challet, 2014; Webb et al., 2009). Having a well-coordinated neuronal communication between the dopaminergic and circadian systems is likely necessary for appropriately timed behavioral responses, adaptation to the environment, and survival.

The bi-directional nature of this link has gradually been uncovered in the last few decades. DA synthesis, release and signaling within the retina, olfactory bulb, ventral tegmental area and striatum are all regulated in a circadian manner (Chung et al., 2014; Corthell et al., 2013; Doyle et al., 2002; Ferris et al., 2014). DA has been shown to directly alter clock gene expression in the central circadian pacemaker, and within extra-SCN circadian oscillators (Korshunov et al., 2017; Mendoza and Challet, 2014). Early studies in *Xenopus* revealed an important role

for DA in the entrainment of retinal circadian rhythms whereby *Per2* expression, a core molecular component of the circadian clock, is induced in response to both light and DA (Cahill and Besharse, 1991; Takahashi, 2017; Tosini et al., 2008). Similarly, activation or inhibition of the D1 dopamine receptor (Drd1) in the mammalian retina enhances or attenuates the extent of light induced phase shifts, respectively (Ruan et al., 2008). Additionally, D2 dopamine receptor (Drd2) null mice have significantly diminished suppression of wheel running activity by light (Doi et al., 2006). Taken together these data support that DA signaling outside of the central pacemaker is an important mediator of circadian regulated behaviors.

Midbrain dopaminergic neurons of the ventral tegmental area (VTA) and substantia nigra (SN) are particularly relevant to DA-induced behavioral modification due to their involvement in locomotion, addiction, and reward recognition (Morris et al., 2006; Roeper, 2013; Schultz, 1997). Additionally, the expression of circadian clock genes such as *Per*, *Clock* and *Bmal1* are found within both neuronal populations suggesting a molecular link to circadian regulation (Hampp and Albrecht, 2008; Hampp et al., 2008; McClung et al., 2005; Webb et al., 2009). Selective manipulation of VTA neurons regulates sleep-wake states by promoting salience-induced arousal, enabling the regulation of ethologically relevant behaviors (Eban-Rothschild et al., 2016). Lesioning the VTA of rats with 6-hydroxydopamine treatment has been shown to elongate circadian free-running period, alter the onset of drinking behavior, and decrease wheel running activity rhythms (Isobe and Nishino, 2001). These changes in circadian behavior following alteration of the mesolimbic DA system further highlight the significant interaction

between these two systems. Additionally, the striatum, a midbrain DA-neuron projection site important for learning, reward, and motor control, has been shown to exhibit rhythmic circadian clock gene expression (Balleine et al., 2007; Imbesi et al., 2009). Within this brain region, depletion of DA innervation and pharmacological inhibition of Drd2 signaling disrupts the expression profile of *Per2*, implicating a role for circadian regulators on reward driven processes (Hood et al., 2010; McClung et al., 2005). This is further supported by the evidence that *Per2* mutant mice exhibit heightened sensitivity to cocaine (Abarca et al., 2002). A complete understanding of how DA influences these extra-SCN oscillators will provide important insight into how substance abuse or neurodegenerative disorders that impact the dopaminergic system are able to disrupt circadian rhythms (Fifel and DeBoer, 2014; Logan and McClung, 2018; Videnovic and Golombek, 2013).

When the SCN is compromised, nearly all circadian functions disappear (Stephan and Zucker, 1972). However, non-photic stimuli such as restricted food access or chronic exposure to methamphetamine (MA) can restore rhythmic behavior in SCN lesioned animals. Interestingly, these SCN-independent pacemakers of unknown origin are modulated by the dopaminergic system, which likely mediates additional biological oscillations and their entrainment (Blum et al., 2014; Gallardo et al., 2014; Honma and Honma, 1986; Tataroglu et al., 2006). For instance, scheduled feeding during a restricted portion of the day produces increased locomotion prior to the availability of food, a behavior known as food anticipatory activity (FAA) (Boulos and Terman, 1980; Gallardo et al., 2014;

Mistlberger, 1994). FAA persists even after SCN ablation, suggesting the presence of an independent food entrainable oscillator (FEO) (Krieger et al., 1977; Mistlberger, 2011; Mistlberger and Antle, 2011; Stephan et al., 1979). The dorsal striatum has been implicated as a mediator of FAA, while Drd1 null mice demonstrate reduced FAA implicating DA-Drd1 signaling as a modulator of this important anticipatory behavior of food availability (Gallardo et al., 2014; Liu et al., 2012).

Similar to anticipation of food reward, daily administration of MA, a DA enhancing psychostimulant, increases locomotor activity immediately preceding the time of injection (Mohawk et al., 2013). Strikingly, arrhythmic SCN-lesioned animals regain circadian rhythmicity via a methamphetamine-sensitive circadian oscillator (MASCO) when presented with *ad libitum* access to MA in their drinking water (Honma and Honma, 1986; Tataroglu et al., 2006). Furthermore, a recently described dopaminergic ultradian oscillator (DUO) was found to produce aberrant patterns of arousal when DA tone was elevated through selective activation of the VTA (Blum et al., 2014). Understanding how DA modulates circadian entrainment is an important step in understanding the consequences of aberrant DA signaling on sleep-wake cycles observed in substance abuse and neurodegenerative disease.

Circadian Disruption in Addiction, Mood Disorders and Parkinson's Disease

Based on the recent studies linking DA signaling to the circadian clock, and perturbations of circadian genes with drug addiction, it is critical to evaluate the

connection between circadian rhythm disturbances and the abuse of addictive substances (Logan et al., 2014). DA enhancing drugs such as cocaine or methamphetamine negatively impact circadian entrainment and sleep (Kosobud et al., 2007; McClung, 2007). Cocaine abuse in pregnant females is particularly detrimental to the proper function of the fetal SCN as exposure to cocaine during gestation results in prolonged disruption of photoentrainment after birth (Ferguson et al., 2000). *Clock* mutant mice show overall hyperactivity, exaggerated locomotion in a novel environment, and high levels of sensitization to cocaine after repeated exposures (McClung et al., 2005). These mice also exhibit a greater degree of place preference conditioning with low doses of cocaine, suggesting an elevated reward response to the drug. It is plausible that circadian genes directly regulate dopaminergic circuitry permitting circadian disruptions to alter the true value of a reward and the motivation for addictive substances (Abarca et al., 2002; Logan et al., 2014; McClung et al., 2005; Sleipness et al., 2007a, b).

In addition to drug addiction, several mood disorders and neurodegenerative diseases that involve alterations in DA neurotransmission are accompanied by increased disruptions in circadian rhythms (Hasler et al., 2012; Wulff et al., 2010). Major depressive disorder (MDD) is commonly associated with sleep abnormalities and reduction in the amplitude of daily oscillations of body temperature, cortisol, and melatonin rhythms (Vadnie and McClung, 2017). Bipolar disorder (BD), is characterized by alternating episodes of mania and depression which result in significant sleep and circadian disruptions. Elevated DA contributes to manic episodes in BD and may be a factor in the entrainment disruption.

Circadian disorganization is also observed in Parkinson's disease (PD), a neurodegenerative disorder where loss of nigrostriatal dopaminergic neurons results in tremors, impaired balance, depression, and deterioration of the sleep-wake cycle (Breen et al., 2014; Fifel and DeBoer, 2014; Videnovic and Golombek, 2013). PD patients demonstrate a reduction in nighttime sleep quality, alertness, and cognitive performance which can all be attributed to alterations in circadian entrainment (Videnovic and Golombek, 2013). In a mouse model of PD, in which progressive degeneration of midbrain DA neurons is chemically induced, rest/activity patterns show a gradual decline in amplitude and stability (Fifel and Cooper, 2014). Further evaluation of how neurodegeneration of dopaminergic neurons influence circadian rhythms may provide novel diagnostic tools to detect PD earlier in its progression than currently possible. Additionally, improving the circadian rhythmicity of high-risk patients (ie. through regulation of lighting conditions and feeding times), may help to alleviate negative consequences on the sleep disturbances and inappropriately timed bouts of wakefulness associated with the disease.

In general, circadian disruption is known to occur during the natural aging process. The elderly are susceptible to reduced amplitude in rest-activity cycles, body temperature, hormone levels, SCN firing rate, and they experience fragmented patterns of sleep (Nakamura et al., 2011). Chronobiological treatments in the elderly, using light and physical exercise have shown promising benefits which boost the circadian rhythm amplitude when provided during the correct phase of the circadian cycle (Van Someren et al., 1997). Further elucidation of the

reciprocal relationship between aberrant DA signaling and circadian disruptions may aide in the development of novel chronotherapeutic strategies for psychiatric or some neurodegenerative disorders.

While the extra-SCN oscillators described earlier may account for perturbation of circadian rhythmicity by dopamine, it is also possible that DA signaling directly influences the SCN to relay information about salient events such as food or mate availability. DA signaling within the SCN has been a focus of our work and will be described in detail in the following chapters.

Dopamine Signaling in the SCN

Over twenty years ago, DA signaling within the embryonic SCN was demonstrated to synchronize maternal-fetal circadian rhythms. Administration of dopaminergics to pregnant dams induced *c-fos* expression, a maker for neural activity, within the fetal SCN, while periodic injections of a Drd1 agonist were shown to set the phase of the fetal biological clock (Viswanathan et al., 1994; Weaver et al., 1992). These treatments fail to induce molecular changes within the SCN of the Drd1 null mice, confirming the importance of this G_s-coupled receptor in mediating the effects of DA on the circadian axis (Bender et al., 1997). Despite persistent expression of SCN-Drd1 mRNA in adult rodents, baboons, and humans, administration of Drd1 agonist alone is not sufficient to induce *c-fos* expression within the SCN or behavioral phase shifts of free running animals after postnatal development (Grosse and Davis, 1999; Rivkees and Lachowicz, 1997; Weaver and Reppert, 1995). Based on these findings, it was concluded that sensitivity to DA signaling

within the SCN is transient and is lost after the development of the retinohypothalamic tract, which transmits photic information from the retina to the SCN. However, recent advances in mouse genetics, designer actuators, and viral vector technologies have enabled investigators to challenge this notion and develop a more complete understanding of how Drd1-mediated DA signaling directly modulates the central circadian clock throughout adulthood.

Drd1-expressing neurons represent approximately 60% of the cells within the SCN, including partial overlap with NMS, VIP, and AVP-expressing neurons (Smyllie et al., 2016). Acute treatment of mouse SCN explants with the Drd1 agonist, SKF 38393, lengthens the free running period of circadian molecular rhythms, suggesting that DA signaling remains functional in the adult SCN (Landgraf et al., 2016). Use of advanced genetic tools has recently identified the behavioral phase and period-resetting properties of Drd1-expressing neurons within the SCN (Grippo et al., 2017; Jones et al., 2015; Smyllie et al., 2016). While previous research had concluded a lack of direct communication between DA populations within the brain and the central circadian clock, the question has remained prominent in the literature.

My graduate work was designed to uncover a physiologically relevant link between these two biological systems in the adult mammal that has remained elusive. Answering this question is important because of the significant connections between food and drug addiction, neurodegenerative disease, and mood disorders with disruption of circadian rhythmicity. We sought to answer the following questions: 1) Is there an anatomical connection between DA neurons and

the SCN? 2) Does selective activation of Drd1-SCN neurons modulate free running rhythms? 3) Does elevated DA tone influence circadian photoentrainment? 4) Is DA signaling important for circadian disruption of food intake on highly rewarding, energy dense foods? 5) Lastly, is Drd1 expression selectively within the SCN sufficient to influence circadian entrainment to light and food? In this dissertation, I address these knowledge gaps to reveal a significant role in direct dopamine signaling within the SCN in the modulation of circadian rhythms. Utilizing sophisticated mouse genetic technologies, we were able to precisely target and manipulate Drd1 expressing neurons of the SCN in adult mice to reveal their essential role in circadian entrainment. This work represents the first full characterization of the role of SCN-Drd1 neurons in circadian photoentrainment and diet-induced obesity.

Chapter II: Direct Midbrain Dopamine Input to the Suprachiasmatic Nucleus Accelerates Circadian Entrainment

Published as a research article in *Current Biology* 08/21/2017

Accessible at DOI: https://doi.org/10.1016/j.cub.2017.06.084

Abstract

Dopamine (DA) neurotransmission controls behaviors important for survival including voluntary movement, reward processing, and detection of salient events such as food or mate availability. Dopaminergic tone also influences circadian physiology and behavior. Although the evolutionary significance of this input is appreciated, its precise neurophysiological architecture remains unknown. Here, we identify a connection between the DA-neurons of the ventral tegmental area (VTA) and the central circadian pacemaker located in the suprachiasmatic nucleus (SCN). Furthermore, we demonstrate that activation of SCN-projecting DA-neurons of the VTA accelerates entrainment to phase-shifted light:dark cycles and that D1 dopamine receptor (Drd1) signaling within the SCN is necessary for proper expression of this behavior. Our findings delineate a previously unappreciated role for the direct DA input to the adult mammalian SCN and highlight the importance of an evolutionarily significant relationship between circadian entrainment and the neuromodulatory system that governs motivational behaviors.

Introduction

Circadian rhythms have evolved to synchronize (entrain) physiological processes to predictable environmental events, such as sunrise and sunset. This ensures that coordinated biological responses occur within a temporal niche. In mammals, circadian rhythms are driven by the suprachiasmatic nucleus (SCN), which controls downstream daily oscillatory processes including the sleep-wake cycle, body temperature fluctuation, hormone production, and feeding behavior (Moore and Eichler, 1972; Stephan and Zucker, 1972). The short-term desynchrony between the astronomical day and endogenous circadian rhythms that is experienced by humans during shift work or transmeridian travel (jet lag) leads to general malaise, insomnia, and cognitive deficiencies (Barion and Zee, 2007). When prolonged, such misalignment results in higher incidences of obesity, cardiovascular disease, cancer, and even increased mortality (Arble et al., 2010; Davidson et al., 2006). Light detected by the retina is the main driver synchronizing the phase of endogenous oscillations to external circadian cycles, a process termed photoentrainment (Altimus et al., 2010; Guler et al., 2008; Provencio et al., 2002). In addition, non-photic environmental signals including restricted food access, exercise, and salient cues such as fear-inducing events, also affect circadian entrainment (Hastings et al., 1997). Although the neuronal circuitry governing photoentrainment is well characterized (Golombek and Rosenstein, 2010; Guler et al., 2008), how non-photic information integrates with this system to create a comprehensive circadian response is poorly understood.

Dopamine has been implicated in various behaviors that show periodicity, such as locomotion, reward seeking behavior, and wakefulness (Mendoza and Challet, 2014). Prior to the development of the retinohypothalamic tract, DA is thought to act as a non-photic entrainment cue in the embryonic and early postnatal SCN, synchronizing the circadian rhythm of the mother and her offspring (Viswanathan et al., 1994; Weaver et al., 1992). Since pharmacological stimulation of the DA system in adult rodents and primates fails to elicit behavioral responses or induce c-Fos expression within the SCN, it has been assumed that the SCN loses sensitivity to DA shortly after birth (Bender et al., 1997; Weaver et al., 1992). Nevertheless, dopaminergic agents, such as methamphetamine or cocaine, have been shown to influence entrainment to the light:dark (LD) cycle in adult animals (Mendoza and Challet, 2014). While it remains unclear whether SCN-dependent photoentrainment is directly influenced by the dopaminergic system, DA signaling in the dorsal striatum has been proposed to regulate non-photic entrainment to timed food availability (Gallardo et al., 2014), an SCN-independent behavior (Stephan et al., 1979; Stokkan et al., 2001).

In this study, we challenge the consensus that SCN responsiveness to DA is lost during development and provide evidence that dopaminergic signaling within the SCN continues to influence circadian photoentrainment through adulthood. First, we demonstrate that selective activation of D1 dopamine receptor (Drd1) expressing SCN (Drd1-SCN) neurons shifts the phase of circadian rhythms, mimicking the phase-shifting response to light. Second, we show that *Drd1a*-null (Drd1-KO) mice exhibit a slow rate of photoentrainment in response to a phase

shift in the light cycle, which is rescued by re-expression of Drd1 exclusively within the SCN. Third, we identify a direct neuronal connection from DA-neurons of the ventral tegmental area (VTA) to the central pacemaker, and lastly, we report that specific activation of this midbrain DA-neuron population accelerates entrainment to a light cycle shift. We conclude that Drd1-dependent DA-signaling within the SCN modulates the rate of synchronization of circadian rhythms to changes in the environmental conditions.

Results

Drd1 is Expressed in the SCN Through Adulthood

The presence of dopamine receptor *Drd1a* mRNA is well documented within the SCN of adult rodents, non-human primates, and humans; however, its functional role remains inconclusive (Bender et al., 1997; Rivkees and Lachowicz, 1997; Weaver et al., 1992). In line with reported expression profiles for *Drd1a*, we observed Drd1 immunoreactivity in the SCN of wild-type mice but not in *Drd1a* knockout (Drd1-KO) animals in which both *Drd1a* alleles were replaced by the Cre recombinase open reading frame (Cre; Figure 1A) (Heusner et al., 2008). We confirmed functional Cre expression in the SCN of heterozygous Drd1-Cre mice by crossing them to ROSA26-tdTomato animals (Ai14) that Cre-dependently express tdTomato red fluorescent protein, and we observed signal throughout the SCN (Figures 1B and 1C, Figure S1) (Madisen et al., 2010). As this could be attributable to developmental expression, we validated adulthood *Drd1a* promoter driven Cre expression through bilateral infusion of a Cre-dependent mCherry

reporter adeno associated virus (AAV), AAV-DIO-mCherry, to the SCN of 8 week old rd1-Cre mice and observed mCherry signal within a subset of SCN neurons (Figures 1D and 1E).

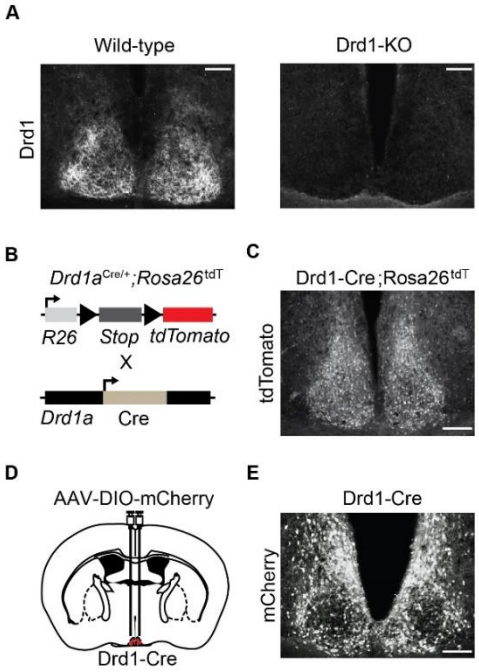

Figure 1. Drd1 is Expressed in the SCN Through Adulthood. (A) Fluorescent IHC with Drd1 antibody labeling in the SCN of wild-type and Drd1-KO mice. Scale bar, 100 µm. (B) Schematic representation of Drd1-neuron specific Cre-mediated recombination in Drd1-Cre mice crossed with *ROSA26-tdTomato* Cre-dependent reporter mice. (C) Presence of tdTomato positive cells within the SCN (central) of *Drd1-Cre;ROSA26^{tdT}* mice. Scale bar, 100 µm. See also Figure S1. (D) Schematic diagram illustrating the site of AAV-DIO-mCherry bilateral injection to the SCN (central) of Drd1-Cre mice. (E) Fluorescent immunohistochemistry of Cre-dependent mCherry expression within the SCN of Drd1-Cre mice. See also Figure S1.

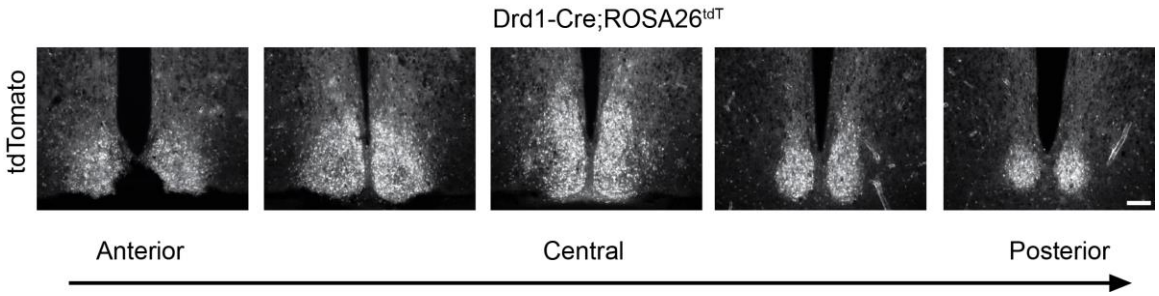

Figure S1. *Drd1a* Driven tdTomato Expression is Present Throughout the SCN. Related to Figure 1. Five representative coronal sections outlining tdTomato red fluorescent protein expression within the SCN. Scale bar, 100 µm.

Activation of Drd1-SCN Neurons Induces Phase Shift of Behavioral Rhythms

The SCN is comprised of a heterogeneous population of cells that differ in their oscillatory activities, neurotransmitters, and responses to light (Antle and Silver, 2005; Cao et al., 2013; Herzog et al., 1998; Welsh et al., 1995). Individual cellular oscillators couple to produce a stable, coherent, rhythmic output; however, not all SCN neurons contribute equally to the production and modulation of circadian rhythms (Welsh et al., 2010). To determine whether Drd1-SCN neurons influence the phase of the endogenous clock, we sought to activate this population using Cre-conditional chemogenetic methods under constant conditions and monitor the effect on wheel running activity rhythms. To this end, we bilaterally delivered a Cre-dependent AAV encoding either hM3Dq-mCherry (hM3Dq), a G_q-coupled designer receptor exclusively activated by a designer drug (DREADD; AAV-DIO-hM3Dq), or mCherry (AAV-DIO-mCherry) as a control, to the SCN of Drd1-Cre mice. After stable entrainment of wheel running activity, we introduced both groups to constant darkness (DD) (Armbruster et al., 2007; Rogan and Roth, 2011). Viral treatment alone had no effect on the phase angle of entrainment during the 12-

hour:12-hour light:dark (LD) cycle or the length of free-running period in DD (Table S1). We then evaluated the behavioral response to selective activation of Drd1-SCN neurons in free running animals at three circadian time points (Figures 2A-2C). Administration of the DREADD-specific agonist, clozapine-N-oxide (CNO; 1 mg/kg, i.p.) six hours prior to activity onset at circadian time (CT) 6 did not produce a significant phase shift in either group (control: -9.00 ± 3.18 minutes; hM3Dq: -14.70 ± 9.71 minutes; $p = 0.633$, Student's two tailed t-test; n = 6-8/group; Figures 2A and 2D). However, CNO administration two hours after activity onset at CT 14 induced a significantly larger phase delay of wheel running activity in hM3Dq mice compared to mCherry controls (control: -7.33 ± 4.54 minutes; hM3Dq: -51.63 ± 28.18 minutes; $p = 0.0009$, Student's two tailed t-test; n = 7-9/group; Figures 2B and 2D). Additionally, CNO administration ten hours after activity onset at CT 22 resulted in a significantly larger phase advance (controls: 0.46 ± 4.08 minutes; hM3Dq: 44.22 ± 8.80 minutes; $p = 0.0007$, Student's two tailed test; n = 8-10/group; Figures 2C and 2D). The responsiveness of hM3Dq-expressing Drd1-SCN neurons to CNO administration was verified by quantification of SCN c-Fos induction two hours after lights-off at *Zeitgeber* time (ZT) 14 (Figure 2E). We observed a robust increase in c-Fos expression within the SCN of hM3Dq mice compared to mCherry controls (control: 32.10 ± 7.00 c-Fos positive cells/mm^2; hM3Dq: 630.30 ± 117.20 c-Fos positive cells/mm^2; $p = 0.0005$, Student's two tailed t-test; n = 7-9/group; 5 SCN sections/mouse). The magnitude of behavioral phase delays at CT 14 correlated positively with the amount of c-Fos induced within the SCN ($R^2 = 0.8844$, $p < 0.0001$; Figure 2F). These findings demonstrate that Drd1-

SCN neuron activation mimics the effects of light pulses during the early and late subjective night, and fails to elicit a response during the mid-subjective day when the circadian clock is sensitive to non-photic entrainment cues (Daan, 1977; Takahashi et al., 1984).

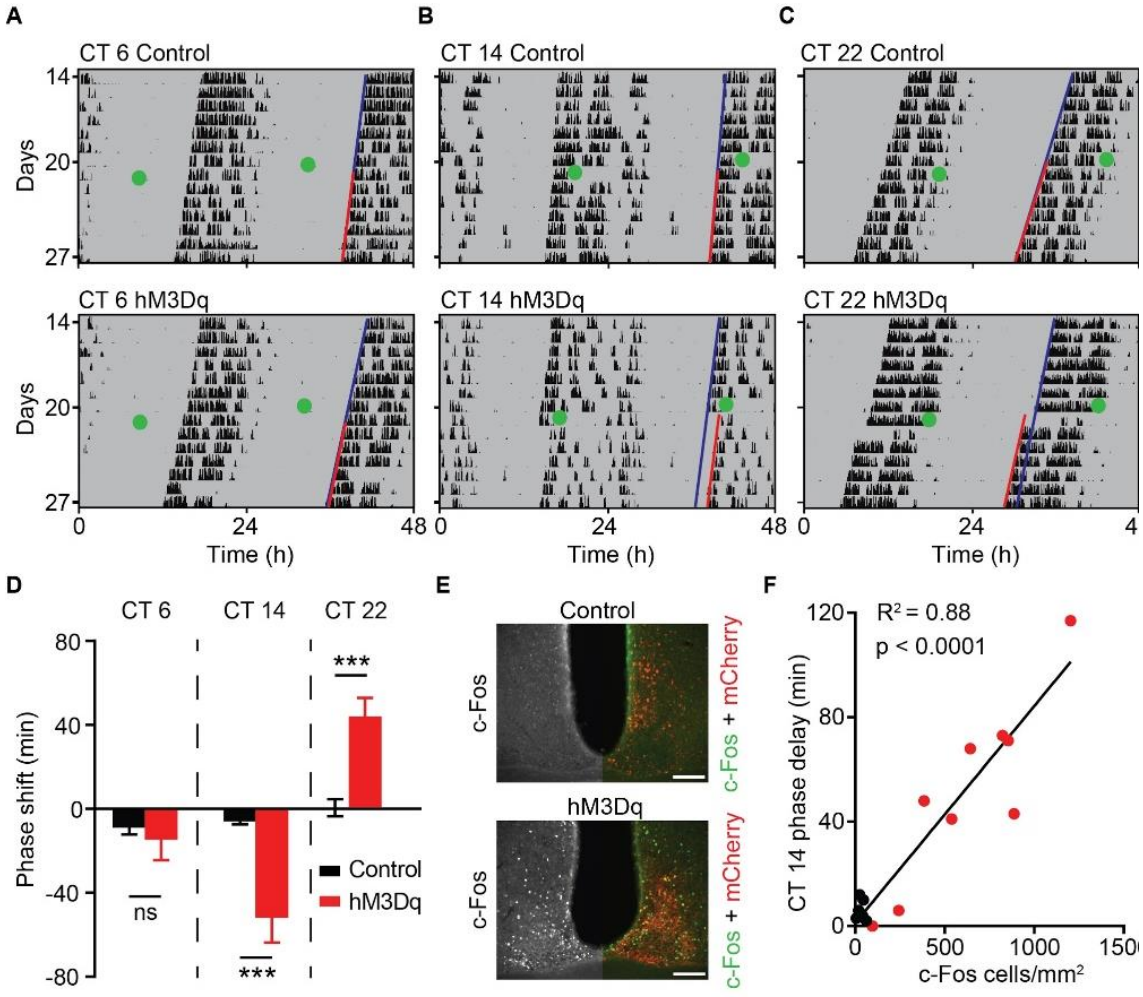

Figure 2. Phase Shift of Behavioral Rhythms by Activation of Drd1-SCN Neurons. (A) Representative double-plotted actograms of circadian time (CT) 6, (B) CT 14 and (C) CT 22 CNO-treated mCherry (control, top) and hM3Dq-mCherry (bottom) mice. Green dot indicates CNO injection (1 mg/kg, i.p.). Grey shading indicates constant darkness; dark blue line represents extended regression line derived by activity onsets prior to CNO; red line follows actual onset of activity after

CNO. (D) Duration of phase shift (minutes) in response to CNO injection (1 mg/kg, i.p.), *** $p < 0.001$. (E) Fluorescent immunohistochemistry of c-Fos within the SCN (anterior) (Left hemisphere: greyscale; right hemisphere: double fluorescent immunohistochemistry of c-Fos (green) and mCherry (red) antibody labelling 120 minutes after CNO. (F) Positive correlation between the duration of phase shift and c-Fos positive cells/mm^2 within the SCN, $R^2 = 0.88$, n = 7-9/group; $p < 0.0001$, linear regression. Scale bars, 100 µm. Data are represented as mean ± SEM. See also Table S1.

Drd1-KO Mice Exhibit a Slow Rate of Photoentrainment

Since Drd1-SCN neuron activation resembles the phase response to photic cues, we sought to determine if Drd1-dependent signaling is an essential component of photoentrainment. Comparison of circadian wheel-running activities between wild-type and Drd1-KO mice revealed no significant differences in several circadian parameters including phase angle of entrainment in a LD cycle or free running period length in DD (Table S1). An acute light pulse (15 minutes, 100 µW/cm^2) presented at CT 14 or CT 22 also produced similar phase delays or advances, respectively (CT 14; wild-type: -114.20 ± 5.09 minutes, Drd1-KO: -126.70± 8.02 minutes; $p = 0.19$, Student's two tailed t-test, n = 6-9/group; CT 22; wild-type: 45.75 ± 3.91 minutes, Drd1-KO: 55.30 ± 5.20 minutes; $p = 0.16$, Student's two tailed t-test; n = 6-8/group, Figures S2A-S2C). Additionally, negative masking behavior in response to a 3-hour light pulse during the active period was normal in Drd1-KO mice, exhibiting significant suppression of wheel running activity that was comparable to wild-type controls (wild-type: 96 ± 2.67%; Drd1-KO: 92 ± 1.60%; $p = 0.28$, Student's two tailed t-test; n = 8/group; Figure S2D and S2E). Despite these

similarities in light-dependent behavioral responses, when challenged by a 6-hour advance in the LD cycle, simulating transmeridian travel, Drd1-KO mice took significantly longer to entrain activity rhythms (wild-type: 6.65 ± 0.28 days; Drd1-KO: 8.58 ± 0.28 days; $p < 0.0001$, Student's two tailed t-test; n = 26/group; Figures 3A-3C). Analysis of daily cumulative phase shifts revealed no differences on day 1 of the LD shift, when the time of 'lights-off' was advanced six hours (Figure 3D). However, on day 2, after the introduction of the new light phase, wild-type animals advanced their activity onset significantly more than Drd1-KO mice (cumulative phase shift on day 2; wild-type: 134.0 ± 19.06 minutes; Drd1-KO: 50.6 ± 7.29 minutes; $p < 0.0001$, repeated-measures two-way ANOVA with Bonferroni *post hoc* comparison; n = 26/group; Figure 3D). As a result, Drd1-KO mice had a marked reduction in the rate of entrainment (minutes/day) during the initial stage of synchronization compared to wild-type controls (days 0-4; wild-type: 70.77 ± 0.09 minutes/day; Drd1-KO: 41.76 ± 3.55 minutes/day; $p < 0.0001$, repeated-measures two-way ANOVA with Bonferroni *post hoc* comparison; n = 26/group; Figure 3E). When the LD cycle was delayed six hours, Drd1-KO mice exhibited similar deficits in photoentrainment duration (wild-type: 5.75 ± 0.25 days; Drd1-KO: 7.67 ± 0.36 days; $p = 0.0002$, Student's two tailed t-test; n = 12/group; Figures S3A and S3B) and rate (days 0-4; wild-type: 87.6 ± 5.99 minutes/day; Drd1-KO: 55.42 ± 3.27 minutes/day; $p < 0.0001$, repeated-measures two-way ANOVA with Bonferroni *post hoc* comparison; n = 12/group; Figure S3C). The delayed rate of resynchronization observed in Drd1-KO mice following advancing or delaying shifts demonstrates that Drd1 signaling is required for efficient re-entrainment.

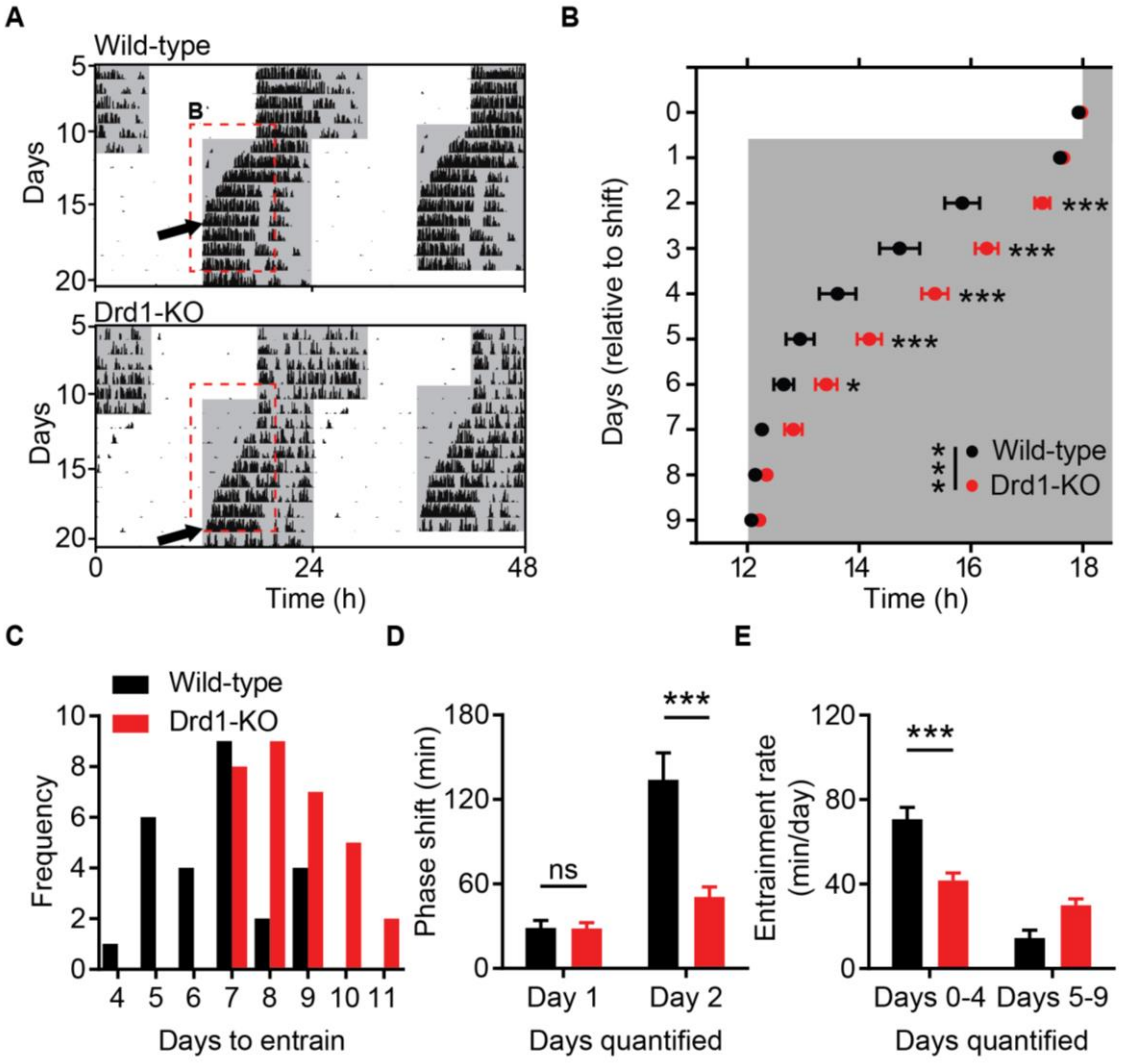

Figure 3. Delayed Entrainment of Behavioral Rhythms in Drd1-KO Mice. (A) Representative double-plotted actograms of light cycle shift comparing wild-type and Drd1-KO mice. White and grey background indicates the; light and dark phase of the LD cycle respectively. Dotted red lines outline onset data represented in b; black arrows indicate the day of entrainment. (B) Group analysis of activity onset; F (1, 50) = 16.55; p = 0.0002, repeated-measures two-way ANOVA with Bonferroni *post hoc* comparison; n = 26/group. * p < 0.05, ** p < 0.01, *** p < 0.001. (C) Frequency of mice per number of days required to entrain wheel running activity to the new light cycle. (D) Group analysis of day 1 and day 2 cumulative phase shift; F (1, 50) = 11.83; p = 0.0012, repeated-measures two-way ANOVA with Bonferroni *post hoc* comparison; n = 26/group. *** p < 0.001. (E) Rate of

entrainment calculated by the slope of activity onsets divided into two segments: days 0-4 and days 5-9 relative to the light cycle shift; repeated-measures two-way ANOVA with Bonferroni *post hoc* comparison, *** $p < 0.001$. Data are represented as mean ± SEM. See also Figures S2, S3 and Table S1.

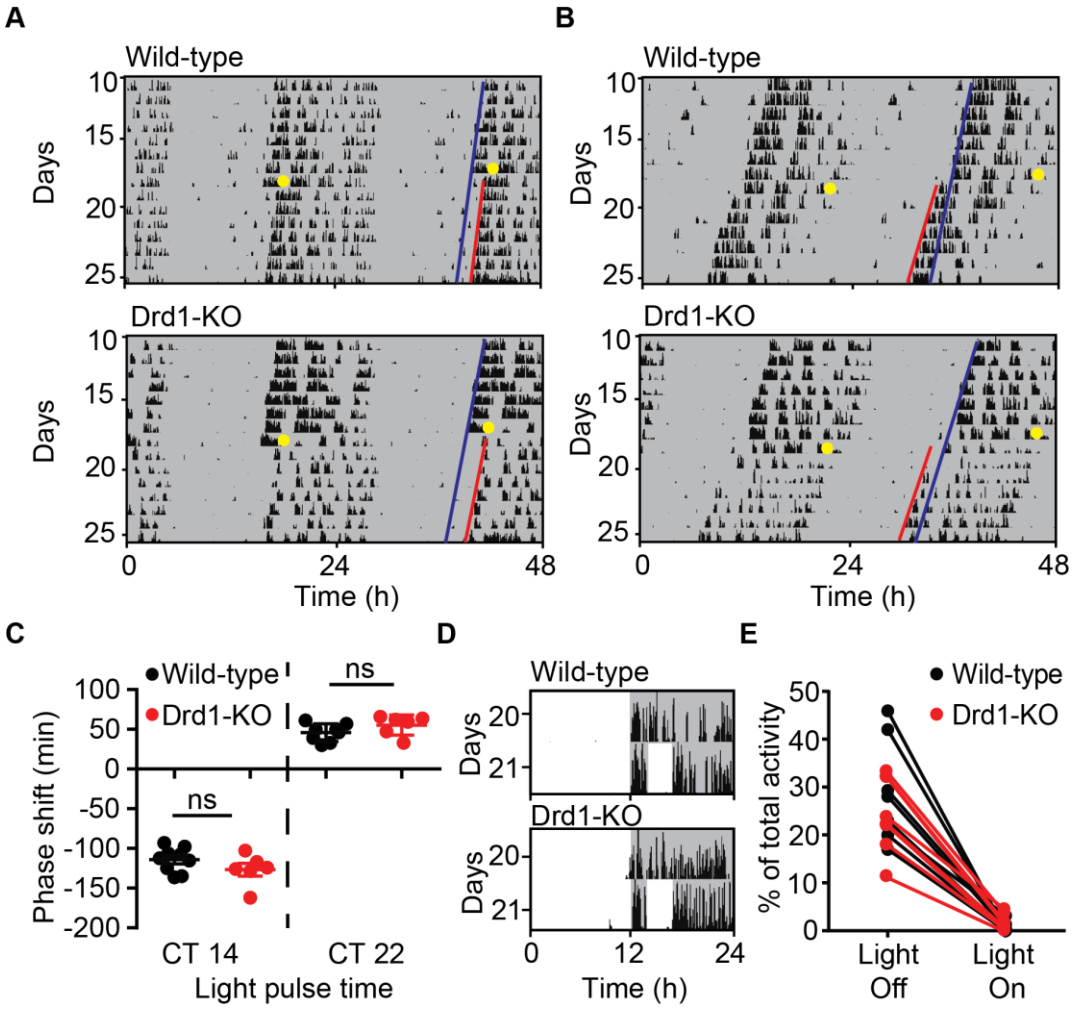

Figure S2. Drd1-KO Mice Have a Normal Response to Light Induced Phase-shifts or Masking. Related to Figure 3. (A) Representative double-plotted actograms of a 15 minute light pulse at CT 14 and (B) CT 22 (yellow dots indicate time of light pulses in DD). The dark blue line represents an extended regression line derived by activity onsets prior to CNO; the red line follows actual onset of activity after CNO. (C) Quantification of phase shift in response to CT 14 and CT 22 light pulses; $p > 0.05$, Student's two-tailed t-test; n = 6-9/group. ns: not

significant. Data reported as mean ± SEM. (D) Representative single-plotted actograms comparing the responses to a 3 hour light pulse from ZT 14 – ZT 17 between wild-type and Drd1-KO mice. White background indicates the time of light exposure. (E) % of total wheel running activity during ZT 14 – ZT 17 on the day prior (light off) and during the 3 hour light exposure (light on).

Drd1 Modulation of Entrainment Rate Requires Light Input

To test whether the influence of Drd1 signaling during circadian re-entrainment requires photic input, we advanced the time of lights-off by six hours and immediately placed wild-type and Drd1-KO mice into constant darkness (Figure 4A). Interestingly, no significant differences in phase shift duration were observed between genotypes on either day 1 or day 2 following the LD cycle shift (cumulative phase shift on day 2; wild-type: 42.53 ± 6.46 minutes; Drd1-KO: 36.38 ± 5.75 minutes; p = 0.9326, repeated-measures two-way ANOVA with Bonferroni *post hoc* comparison; n = 8/group; Figure 4B). However, in line with results observed during the complete 6-hour LD shift (Figures 3B and 3D), wild-type animals exposed to a six hour advance in the dark phase, followed by a 12-hour cycle of light exposure prior to placement into DD (Figure 4C), experienced a robust shift in activity onset on day 2 compared to Drd1-KO mice (cumulative phase shift on day 2; wild-type: 110.80 ± 16.95 minutes; Drd1-KO: 52.18 ± 9.76 minutes; p = 0.0011, repeated-measures two-way ANOVA with Bonferroni *post hoc* comparison; n = 8/group; Figure 4D). Thus, Drd1 signaling may be regulating the photoentrainment rate by modulating the sensitivity of the circadian system to canonical photic inputs.

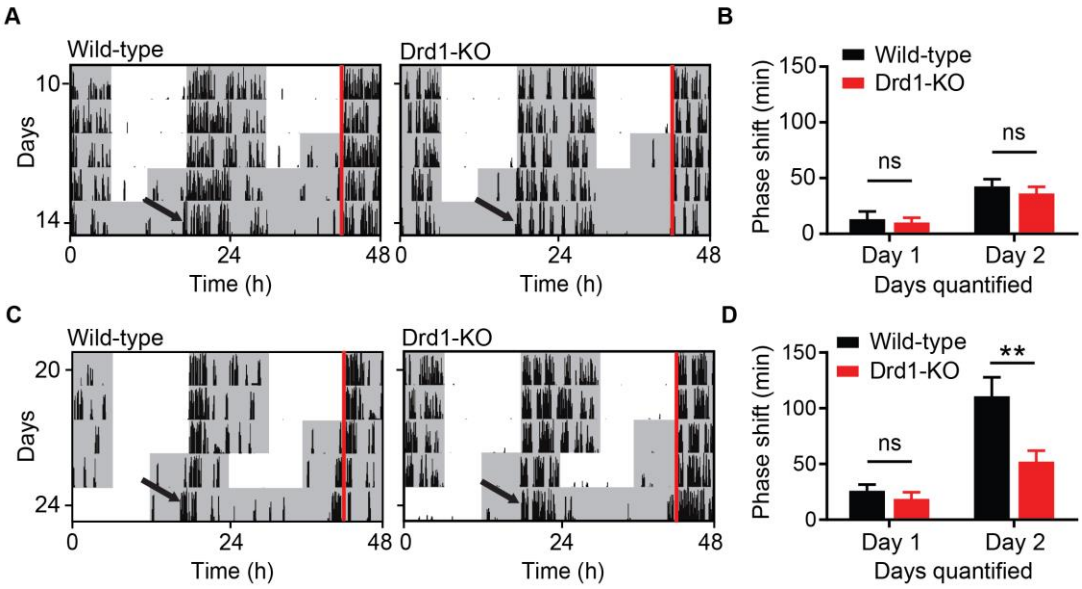

Figure 4. Drd1 Modulation of Entrainment Rate Requires Light Input. (A) Representative double-plotted actograms of wild-type and Drd1-KO mice following a 6-hour advance and immediate release into DD. (B) Group analysis of day 1 and day 2 cumulative phase shift; $F(1, 14) = 0.3684$; $p = 0.5536$, repeated-measures two-way ANOVA; n = 8/group. (C) Representative double-plotted actograms of wild-type and Drd1-KO mice following a 6-hour full LD cycle advance followed by release into DD. Red lines outline ZT 12 prior to LD shift. (D) Group analysis of day 1 and day 2 cumulative phase shift; $F(1, 14) = 7.40$; $p = 0.0166$, repeated-measures two-way ANOVA with Bonferroni *post hoc* comparison; n = 8/group. ** $p < 0.01$. Data are represented as mean ± SEM.

Re-expression of Drd1 within the SCN of Drd1-KO Mice is Sufficient to Rescue Entrainment Rate Deficit

As Drd1 is expressed throughout the brain and peripheral organs (Missale et al., 1998), we sought to determine whether its absence specifically within the central oscillator was responsible for the delayed entrainment rate observed in Drd1-KO mice (Figures 3 and 4). To test the role of SCN-Drd1 signaling during

photoentrainment, we restored Drd1 expression within the SCN of Drd1-KO mice and assessed their ability to entrain to a light cycle shift. We accomplished SCN-specific rescue of Drd1 expression by delivering an AAV containing a Cre-dependent Drd1-HA transgene (AAV-DIO-Drd1-HA) to the SCN of homozygous Drd1-Cre knock-in mice (Drd1-KO-Rescue; Figure 5A) (Gore and Zweifel, 2013). Drd1-KO mice that received AAV-DIO-mCherry or a Cre-dependent AAV encoding the light activated, membrane localized cation channel Channelrhodopsin-2 (AAV-DIO-ChR2-eYFP) were used as controls. Successful introduction of AAV-DIO-Drd1-HA was determined by immunohistochemistry (Figure 5B). In response to a 6-hour advance in the LD cycle, restoration of Drd1 within the SCN completely rescued the rate of circadian photoentrainment in Drd1-KO mice to wild-type levels. No significant differences were observed between mCherry or ChR2 groups, however, both controls took significantly longer to entrain than Drd1-KO-Rescue mice (Drd1-KO-Rescue: 6.31 ± 0.26 days; ChR2: 7.88 ± 0.40 days, $p = 0.0085$; mCherry: 7.92 ± 0.34 days, $p = 0.0023$; one-way ANOVA with Bonferroni *post hoc* analysis; n = 8-13/group; Figures 5C-5E). The most prominent difference once again occurred two days after the shift following the first 'lights-on' segment of the new LD cycle (cumulative phase shift on day 2: Drd1-KO-Rescue: 138.30 ± 31.22 minutes; ChR2: 58.28 ± 11.00 minutes, $p = 0.0117$; mCherry: 70.26 ± 7.82 minutes, $p = 0.0181$; repeated-measures two-way ANOVA with Bonferroni *post hoc* comparison; n = 8-13/group; Figure 5F). Like wild-type mice, only virally restored mice displayed a normal rate of entrainment during the initial phase of the LD shift (days 0-4; Drd1-KO-Rescue: 73.80 ± 6.87 minutes/day; ChR2: 47.9 ± 4.09

minutes/day; p = 0.0024; mCherry: 51.28 ± 3.66 minutes/day, p = 0.0003; repeated-measures two-way ANOVA with Bonferroni *post hoc* comparison; n = 8-13/group; Figure 5G). When the LD cycle was delayed six hours, Drd1-KO-Rescue mice also exhibited a standard duration of photoentrainment (ChR2: 5.17 ± 0.40 days; Drd1-KO: 7.50 ± 0.27 days; p = 0.0003, Student's two tailed t-test; n = 6-8/group; Figures S3D and S3E) and rate (days 0-4; wild-type: 94.45 ± 4.72 minutes/day; Drd1-KO: 59.97 ± 3.32 minutes/day; p < 0.0001, repeated-measures two-way ANOVA with Bonferroni *post hoc* comparison; n = 6-8/group; Figure S3F). These rescue studies demonstrate that delayed photoentrainment in Drd1-KO mice is caused primarily by the absence of Drd1 signaling within the SCN.

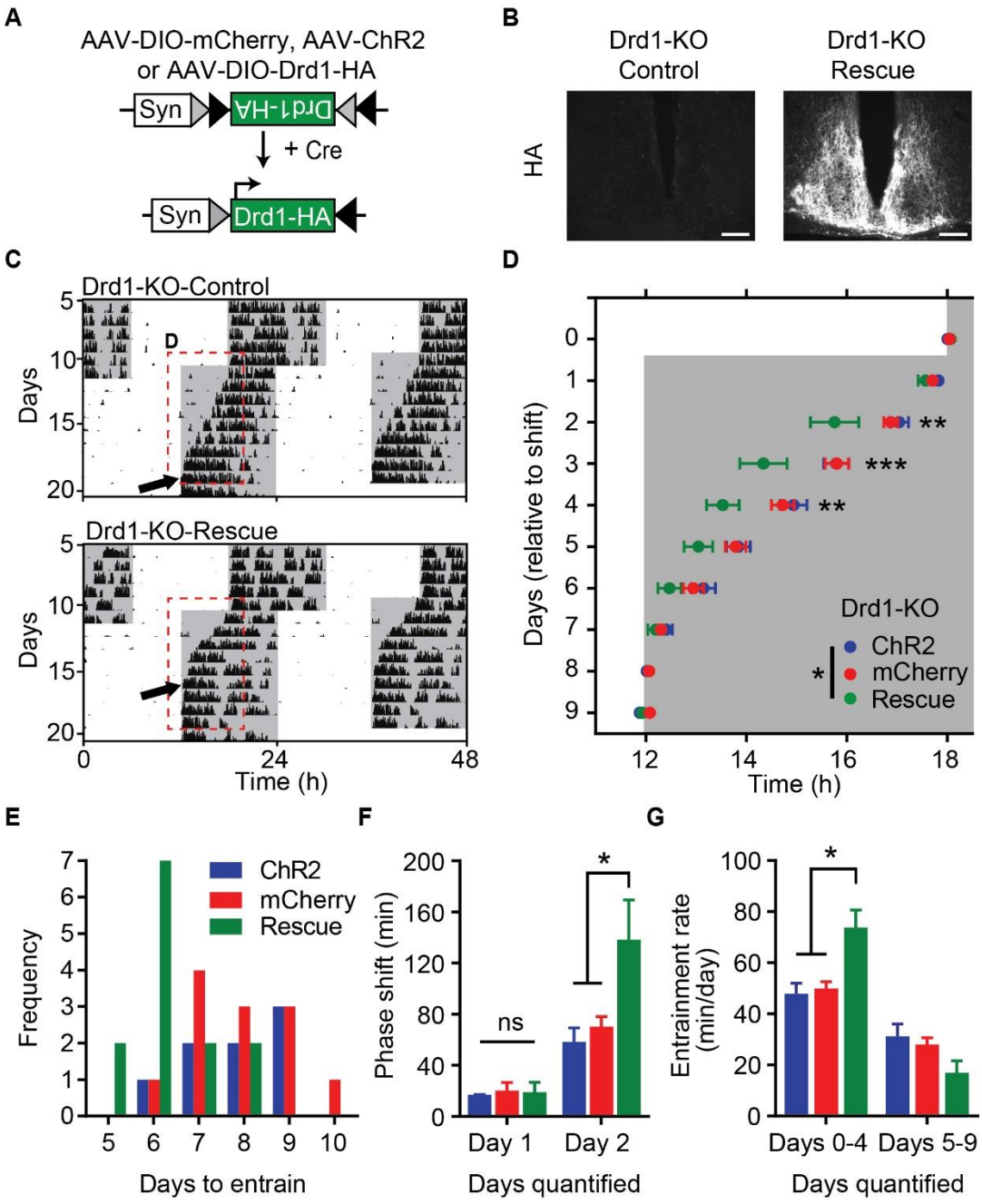

Figure 5. Viral Restoration of Drd1 within the SCN Rescues Entrainment in Drd1-KO Mice. (A) Schematic representation of the Cre-dependent AAV-DIO-Drd1-HA construct. (B) Fluorescent immunohistochemistry of HA antibody labelling within the SCN (central) of mCherry expressing controls (Drd1-KO-Control) and Drd1-HA expressing (Drd1-KO-Rescue) rescue mice. Scale bar, 100 µm. (C) Representative double-plotted actograms of light cycle shift comparing

Drd1-KO-mCherry and Drd1-KO-Rescue mice. (D) Group analysis of activity onset; $F(2, 30) = 5.073$; $p = 0.0127$, repeated-measures two-way ANOVA with Bonferroni *post hoc* comparison; n = 8-13/group; * $p < 0.05$, ** $p < 0.01$, *** $p < 0.001$. (E) Frequency of mice per number of days required to entrain wheel running activity to the new light cycle. (F) Group analysis of day 1 and day 2 cumulative phase shift; $F(2, 30) = 3.319$; $p = 0.0499$, repeated-measures two-way ANOVA with Bonferroni *post hoc* comparison; * $p < 0.05$. (G) Rate of re-entrainment calculated by the slope of activity onsets, repeated-measures two-way ANOVA with Bonferroni *post hoc* comparison, ** $p < 0.01$. Data are represented as mean ± SEM. See also Figure S3 and Table S1.

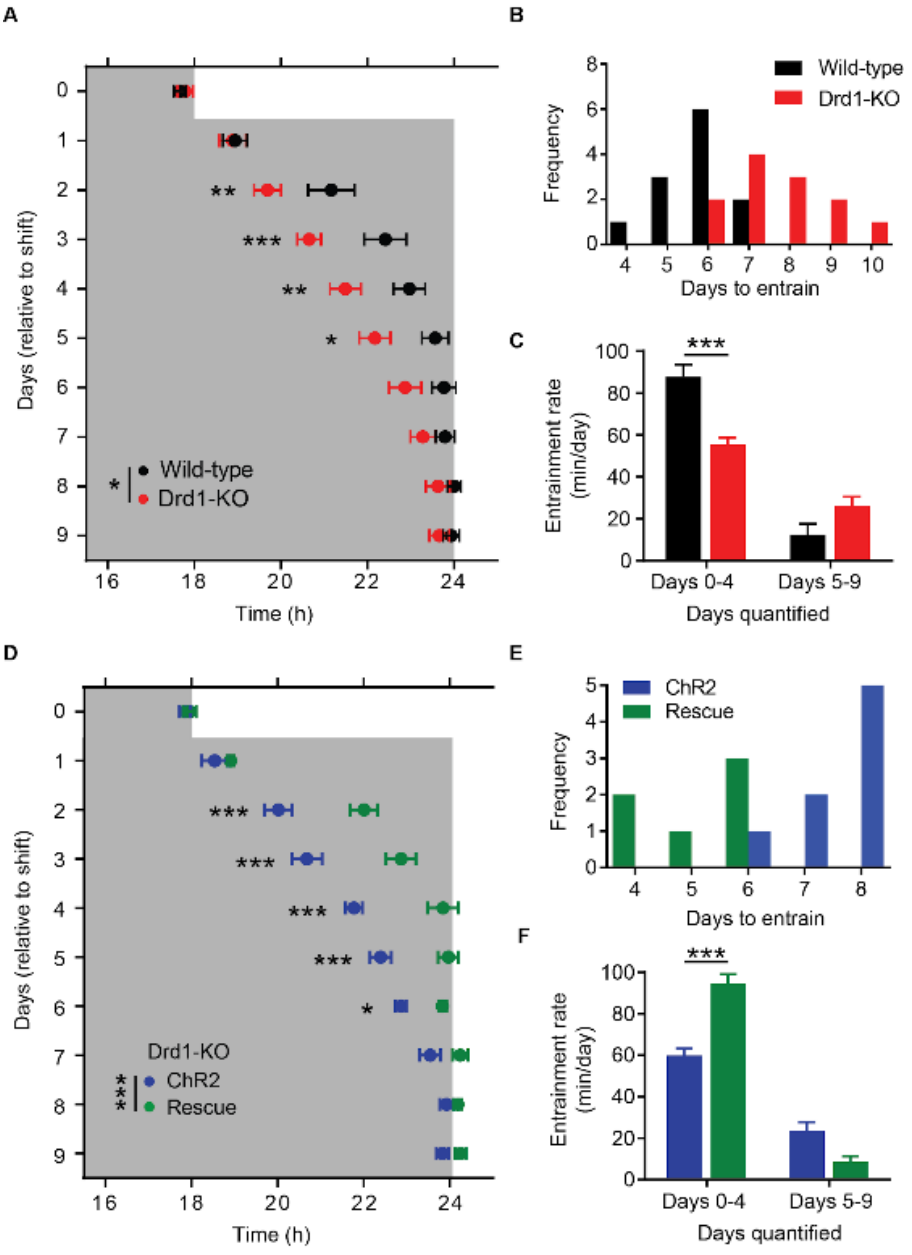

Figure S3. Drd1 Expression Within the SCN Modulates the Rate of Photoentrainment in Response to a 6-hour Delay in the LD Cycle. Related to Figures 3 and 5. (A) Group analysis of activity offsets comparing wild-type and Drd1-KO mice; F (1,20) = 5.20 ; p = 0.0337, repeated-measures two-way ANOVA with Bonferroni *post hoc* comparison; n = 12/group. * p < 0.05, ** p < 0.01, *** p < 0.001. (B) Frequency of mice per number of days required to entrain wheel running activity to the new light cycle. (C) Rate of entrainment calculated by the slope of

activity offsets; repeated-measures two-way ANOVA with Bonferroni *post hoc* comparison, *** $p < 0.001$. (D) Group analysis of activity offsets comparing Drd1-KO-ChR2 and Drd1-KO-Rescue mice; $F(1, 12) = 23.33$; $p = 0.0004$, repeated-measures two-way ANOVA with Bonferroni *post hoc* comparison; n = 8/group. * $p < 0.05$, *** $p < 0.001$. (E) Frequency of mice per number of days required to entrain wheel running activity to the new light cycle. (F) Rate of entrainment calculated by the slope of activity offsets; repeated-measures two-way ANOVA with Bonferroni *post hoc* comparison, *** $p < 0.001$. Data are represented as mean ± SEM.

The SCN Receives VTA DA-neuron Innervation

After establishing a significant role for Drd1 expression in governing the rate of circadian photoentrainment within the adult mammalian SCN, we aimed to determine the potential source of dopaminergic input to the central clock. The existence of dopaminergic axonal fibers within the SCN and peri-SCN previously has been identified in hamsters, rats, and mice (Duffield et al., 1999; Strother et al., 1998; Ugrumov et al., 1989). Consistent with previously published levels in other mammals, we detected 3.79 ± 1.20 pg/mm^3 of DA in the SCN of wild-type mice (n = 5 mice) using high performance liquid chromatography (distinguished from other monoamines and DA metabolites by its specific retention time) (Lin and Pivorun, 1989). To demonstrate the presence of synaptic release machinery in DA-neurons within the SCN, we crossed mice expressing Cre under the control of the DA transporter promoter (DAT-Cre) with ROSA26-Flox-synaptophysin-tdTomato (Ai34D) mice, which facilitated the expression of tdTomato specifically in synaptic terminals of dopaminergic neurons (Figure 6A) (Nirenberg et al., 1996). We observed tdTomato positive structures within the nucleus accumbens (NAc), a

well-known projection site of DA-neuron populations, and the SCN of these mice (Figures 6B and 6C). To screen for potential DA-neuron populations providing this input, we delivered retrogradely transported red fluorescent beads (retrobeads) to the SCN of wild-type mice (Figure 6D and 6E). Three weeks after surgery, we examined the brains of injected mice for retrobeads within the major DA-neuron populations. Colocalization of retrobeads with tyrosine hydroxylase (TH), the rate-limiting enzyme in DA synthesis, was consistently observed within the ventral tegmental area (VTA; Figure 6F). Although we cannot definitively rule out dopaminergic projections from other regions, we did not observe colocalization in the olfactory bulb, zona incerta, substantia nigra, or the retrorubral field (n = 6 mice; Figure S4a). When retrobeads were delivered dorsal to the SCN, no colocalization was observed (n = 12 mice). To determine the efficiency of retrobead uptake by the VTA DA-neurons, we targeted the NAc with retrobeads and observed that a larger portion of DA-neurons project to the NAc relative to the SCN (Figure S4). Next, we sought to confirm direct VTA-DA neuron innervation of the SCN by injecting AAV-DIO-mCherry into the VTA of adult DAT-Cre mice (Figure 6G). We observed dense mCherry positive fiber innervation within the NAc (Figure 6H), and additionally, within and immediately surrounding the SCN (n = 4 mice; two weekspost-injection; Figure 6I). Together, these results demonstrate the existence of a VTA DA-neuron population that directly innervates the SCN.

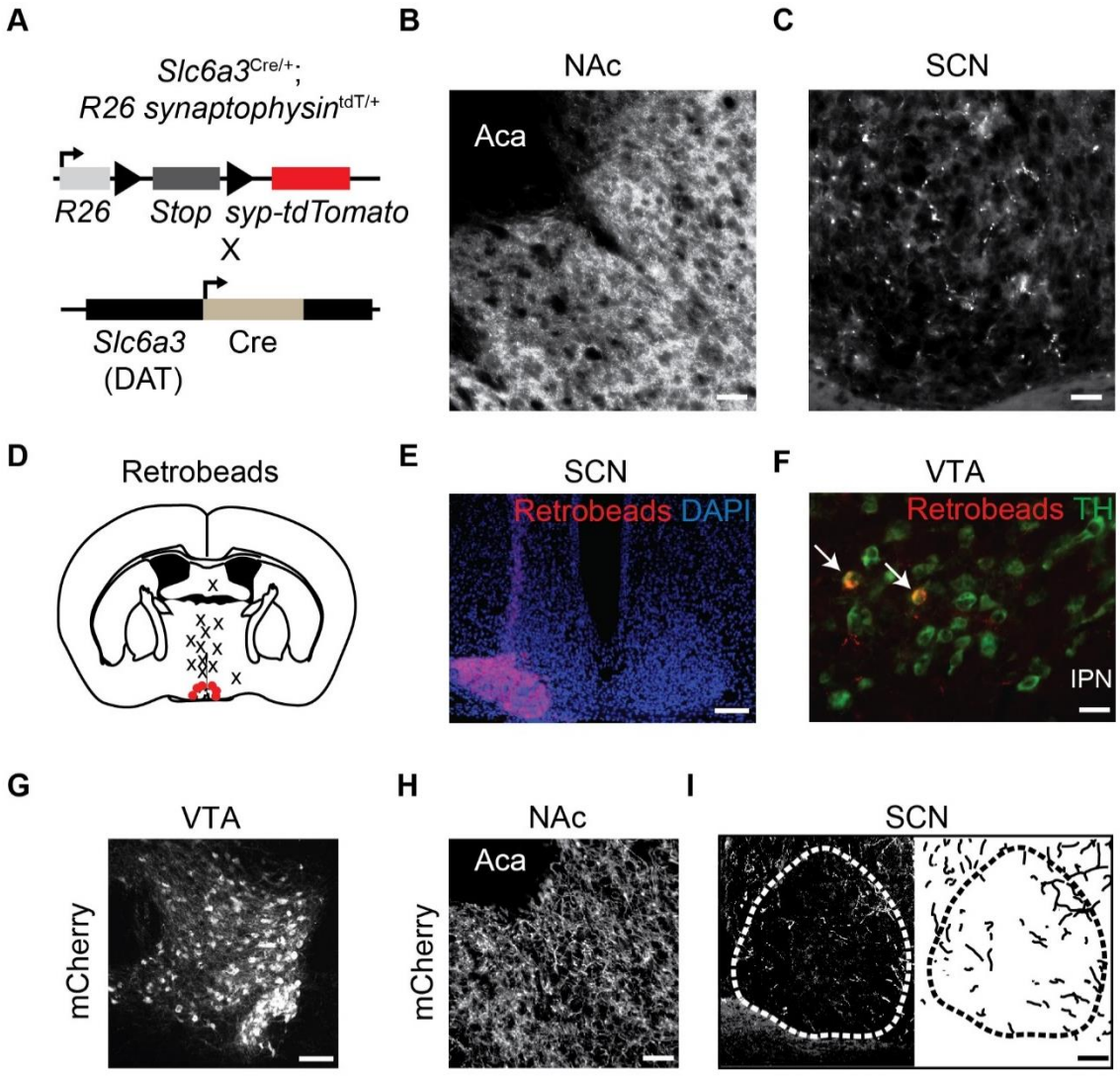

Figure 6. Identification of VTA DA-Neuron Projections and Drd1 Expression within the SCN

(A) Schematic representation of DA-neuron specific expression of synaptophysin-tdTomato in DAT-Cre mice crossed with *ROSA26-synaptophysin-tdTomato* Cre-dependent reporter mice. (B) Dense innervation within the nucleus accumbens and (C) moderate innervation within SCN (central). Scale bar, 50 µm. (D) Coronal diagram indicating retrobead target sites. Red dots specify positive SCN targeting and X's represent dorsal targeted controls. (E) Pseudo-colored images of retrobeads (beads; red) and DAPI (blue) confirming positive targeting of the SCN. Scale bar, 100 µm. (F) Fluorescent immunohistochemistry of retrobeads (red)

colocalized within TH (green) positive neurons in the VTA. Scale bar, 50 µm. (G) Fluorescent immunohistochemistry with mCherry antibody labelling of VTA target site. Scale bar, 100 µm. (H) Immunoreactive mCherry fibers within the nucleus accumbens (NAc). Scale bar, 50 µm. (I) Left: Immunoreactive mCherry fibers within and around the SCN (anterior). Right: trace of innervating mCherry fibers. Scale bar, 50 µm. See also Figure S4.

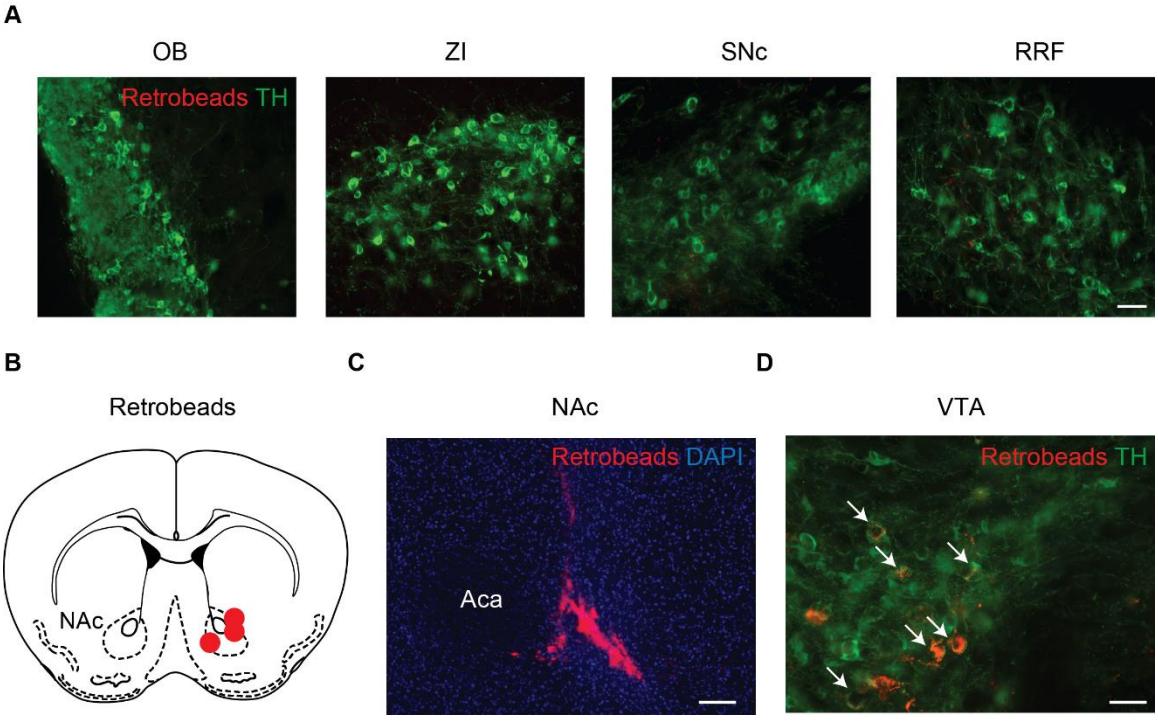

Figure S4. SCN or NAc-targeted Retrograde Tracing. Related to Figure 6. (A) Fluorescent immunohistochemistry with TH (green) and retrobeads (red) in DA neuron populations after retrobead delivery to the SCN. No colocalization was observed in the olfactory bulb (OB), zona incerta (ZI), substantia nigra pars compacta (SNc) or retrorubral field (RRF). Scale bar, 50 µm. (B) Coronal diagram indicating retrobead target sites to the nucleus accumbens (NAc). Red dots specify positive NAc targeting. (C) Pseudo-colored images of retrobeads (beads; red) and DAPI (blue) confirming targeting of the NAc. Scale bar, 100 µm. (D) Fluorescent immunohistochemistry of retrobeads (red) colocalized within TH (green) positive neurons in the VTA. Scale bar, 50 µm.

Activation of VTA DA-neurons Accelerates Rate of Entrainment

DA-neurons of the VTA are regulators of motivational processes and have recently been implicated in ethologically relevant sleep related behaviors (Eban-Rothschild et al., 2016; Roeper, 2013). To examine whether increased activity of VTA DA-neurons influences the rate of circadian photoentrainment, we delivered AAV-DIO-hM3Dq or AAV-DIO-mCherry to the VTA of DAT-Cre mice (Figure 7A) (Blum et al., 2014; Lammel et al., 2015; Zhuang et al., 2005). Immunohistochemical analysis revealed that 93.25 ± 2.65% of mCherry expressing cells co-localized with TH positive neurons in the VTA (Figure 7A, n = 3 mice; 4 VTA sections/mouse). Additionally, administration of CNO at ZT 14 (1 mg/kg; i.p.) resulted in significantly greater c-Fos induction within the VTA of hM3Dq mice compared to mCherry controls (control: 56.53 ± 6.12 c-Fos positive cells/mm^2; hM3Dq: 940.16 ± 74.27 c-Fos positive cells/mm^2; $p = 0.0067$, Student's two tailed t-test; n = 3/group; 4 VTA sections/mouse; Figures 7B and 7C, Figures S5A and S5B). Viral treatment produced no effect on free-running period or the phase angle of entrainment (Table S1). However, following CNO administration immediately prior to a 6-hour advance in the LD cycle, hM3Dq mice entrained significantly faster than mCherry controls (control: 7.50 ± 0.42 days; hM3Dq: 5.78 ± 0.22 days; $p = 0.0020$, Student's two tailed t-test; n = 8-9/group; Figures 7D-7F). Interestingly, in line with the entrainment differences between wild-type and Drd1-KO mice, the most prominent advance occurred on the second day of the LD cycle shift after DA-neuron stimulation (cumulative phase shift duration on day 2; control: 65.40 ± 10.10 minutes; hM3Dq: 158.1 ± 32.14 minutes; $p = 0.0197$, repeated-measures two-way

ANOVA with Bonferroni *post hoc* comparison; n = 8-9/group; Figure 7G). Consequently, hM3Dq mice exhibited an accelerated rate of entrainment within the initial period of the light cycle shift (days 0-4; control: 51.91 ± 5.39 minutes/day; hM3Dq: 72.92 ± 7.07 minutes/day; p = 0.0156, repeated-measures two-way ANOVA with Bonferroni *post hoc* comparison; n = 8-9/group; Figure 7H). To confirm the necessity of photic input following the elevation in the DA tone for this response, we administered CNO or saline to hM3Dq mice prior to a 6-hour advance of the LD cycle and immediately placed them into DD (Figure S5C). No significant difference was observed in the duration of shift between saline or CNO injected hM3Dq mice on either day of analysis (cumulative phase shift duration on day 2; saline: 60.38 ± 8.74 minutes; CNO: 56.32 ± 9.97 minutes; p = 0.9847, repeated-measures two-way ANOVA with Bonferroni *post hoc* comparison; n = 8/group; Figure S5D), demonstrating that elevated DA tone by itself is not sufficient to phase-shift the circadian clock. Rather, these findings demonstrate that the selective activation of VTA DA-neurons increases the responsiveness of the circadian clock to photic inputs, allowing for efficient photoentrainment.

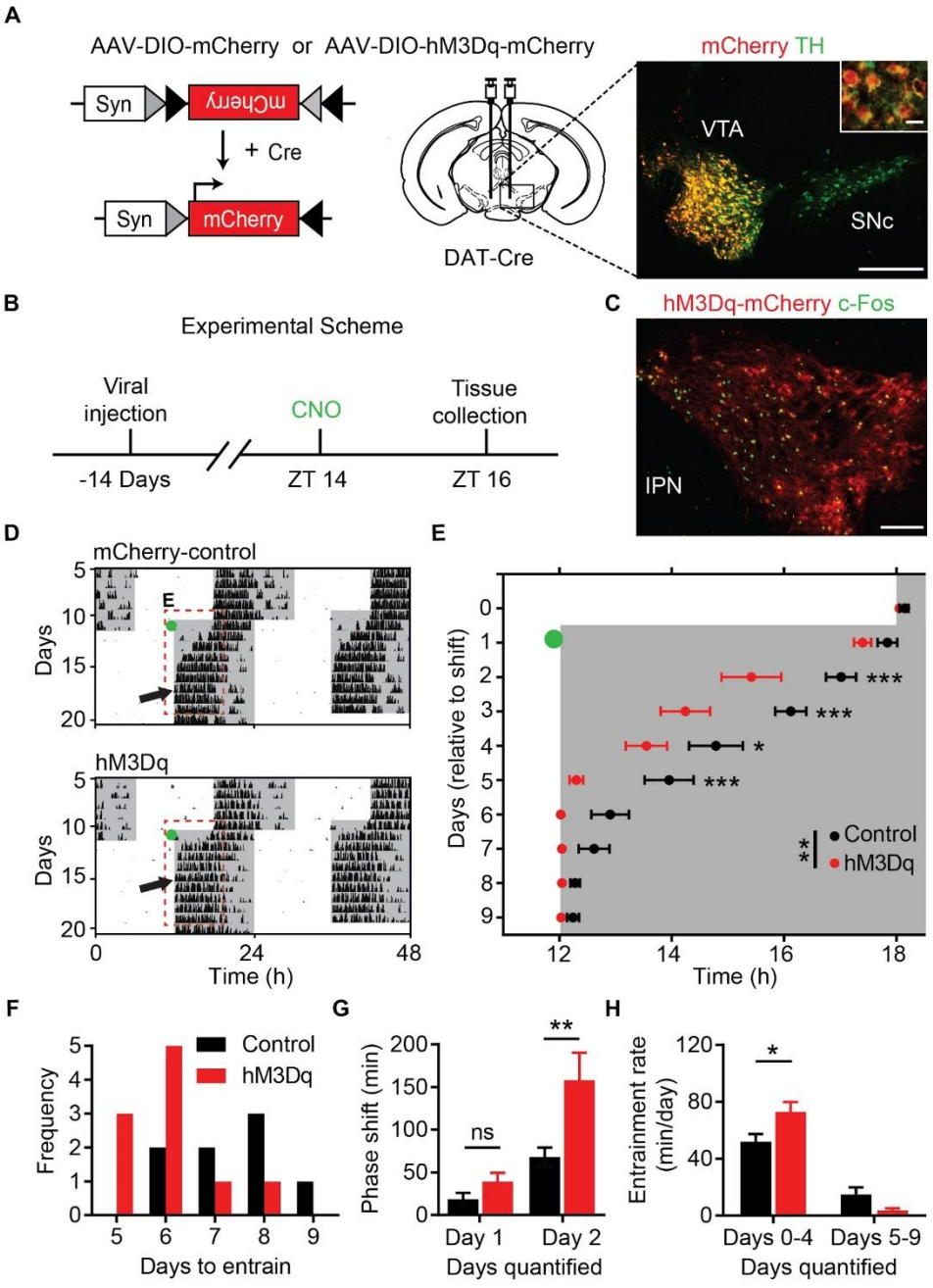

Figure 7. DREADD Activation of VTA Neurons Accelerates Circadian Entrainment. (A) Left: Design of Cre-dependent control virus, AAV-DIO-mCherry, or excitatory G_q-coupled DREADD, AAV-DIO-hM3Dq-mCherry. Syn: human synapsin promotor; Cre: Cre recombinase. Middle: Schematic illustrating injection site to the midbrain of DAT-Cre mice. Right: double fluorescent immunohistochemistry with mCherry (red) and TH (green) antibody labelling

demonstrating selective transgene expression within DA-neurons of the ventral tegmental area. VTA: ventral tegmental area; SNc: Substantia nigra pars compacta. Scale bar, 200 µm; inset scale bar, 20 µm (**Qi Zhang**). (B) Timeline of experiment assessing CNO-induced (1mg/kg, i.p.) c-Fos expression two hours after lights-off; *Zeitgeber* time 14 (ZT 14). (C) Double fluorescent immunohistochemistry with c-Fos (green) and mCherry (red) antibody labelling reveals activation of VTA DA-neurons. Brains were collected for analysis 120 minutes after CNO injection (1 mg/kg, i.p.). IPN: interpeduncular nucleus. Scale bar, 100 µm. See also Figure S1. (**Qi Zhang**) (D) Representative double-plotted actograms of light cycle shift comparing mCherry and hM3Dq-mCherry expressing DAT-Cre mice. Green dots indicate CNO injection (1 mg/kg, i.p); black arrows indicate the day of entrainment. (E) Group analysis of activity onset; $F(1, 14) = 12.74$; $p = 0.0031$, repeated-measures two-way ANOVA with Bonferroni *post hoc* comparison; n = 8-9/group; * $p < 0.05$, ** $p < 0.01$, *** $p < 0.001$. (F) Frequency of mice per number of days required to entrain wheel running activity to the new light cycle. (G) Group analysis of day 1 and day 2 cumulative phase shift; $F(1, 15) = 7.056$; $p = 0.0180$, repeated-measures two-way ANOVA with Bonferroni *post hoc* comparison; n = 8-9/group; ** $p < 0.01$. (H) Rate of entrainment calculated by the slope of activity onsets; repeated-measures two-way ANOVA with Bonferroni *post hoc* comparison; * $p < 0.05$. Data are represented as mean ± SEM. See also Figure S5 and Table S1.

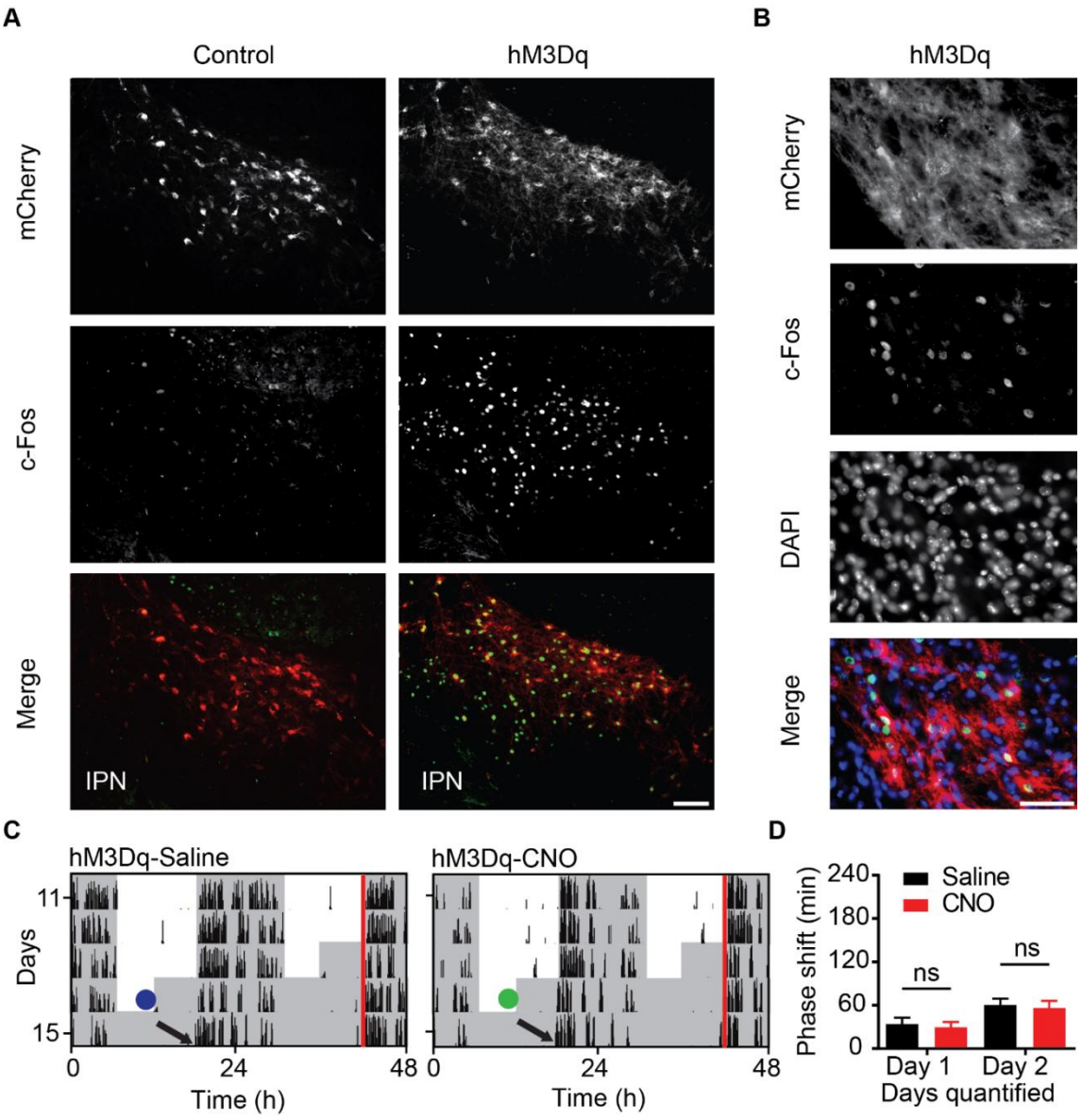

Figure S5. VTA-DA Neuron Activation Mediated c-Fos Expression and Behavioral Responses. **Related to Figure 7.** (A) Double-fluorescent immunohistochemistry with mCherry (top) and c-Fos (middle) antibody labelling within the VTA, 120 minutes after CNO (1 mg/kg) injection to DAT-Cre-mCherry (left) or DAT-Cre-hM3Dq (right) mice . Pseudo-colored images (mCherry: red and c-Fos: green) are merged at the bottom panel. IPN: interpeduncular nucleus. Scale bar, 100 μm. (**Qi Zhang**) (B) High magnification images of fluorescent immunohistochemistry with mCherry, c-Fos, and DAPI labelling within the VTA,

120 minutes after CNO (1 mg/kg) injection to DAT-Cre-hM3Dq mice. Pseudo-colored images (mCherry: red, c-Fos: green, and DAPI: blue) are merged at the bottom panel. Scale bar, 50 μm (**Qi Zhang**). (C). Representative double-plotted actograms of a 6-hour light cycle advance followed by immediate release to DD comparing DAT-Cre-hM3Dq mice treated with an i.p. injection of saline (blue dot) or CNO (green dot; 1mg/kg). Red lines outline ZT 12 prior to LD shift. (D) Group analysis of day 1 and day 2 cumulative phase shift; $F(1, 18) = 0.1291$; $p = 0.7235$, repeated-measures two-way ANOVA; $n = 10$/group. Data are represented as mean ± SEM.

Reference Figure	Genotype	Free-Running Period (h)	Phase Angle of Entrainment (h)	% of Light Activity
Figure 2	Drd1-Cre-mCherry	23.63 ± 0.44	-0.08 ± 0.5	3.72 ± 1.42
	Drd1-Cre-hM3Dq	23.57 ± 0.06	-0.03 ± 0.02	1.96 ± 0.44
Figure 3	Wild-type	23.61 ± 0.04	-0.07 ± 0.02	3.25 ± 0.64
	Drd1-KO	23.57 ± 0.04	-0.08 ± 0.02	3.86 ± 0.57
Figure 5	Drd1-KO-mCherry	23.52 ± 0.12	-0.04 ± 0.02	3.34 ± 0.85
	Drd1-KO-Rescue	23.54 ± 0.06	0.05 ± 0.04	6.94 ± 2.22
	Drd1-KO-ChR2	23.52 ± 0.04	-0.06 ± 0.02	3.60 ± 1.08
Figure 7	DAT-Cre-mCherry	23.56 ± 0.05	-0.05 ± 0.04	6.76 ± 2.22
	DAT-Cre-hM3Dq	23.53 ± 0.04	-0.04 ± 0.04	4.40 ± 1.58

Table S1. Phenotypic Characteristics of Experimental Mice. Related to Figures 2, 3, 5 and 7. Viral treatment had no effect on free running period in constant darkness, the phase angle of entrainment, or % of total wheel running activity during the light period in a LD cycle. Figure 2; Drd1-Cre-mCherry vs Drd1-Cre-hM3Dq: Free-running period: $p = 0.44$, $n = 7$-9/group; Phase angle of entrainment: $p = 0.40$, $n = 7$-9/group; % of light activity: $p = 0.27$, $n = 7$-9/group. Student's two-tailed t-test. Figure 3; Wild-type vs Drd1-KO: Free-running period: p

= 0.46, n = 16/group; Phase angle of entrainment: p = 0.65, n = 24/group; % of light activity: p = 0.22, n = 26/group. Student's two-tailed t-test. Figure 5; Drd1-KO-ChR2 vs Drd1-KO-mCherry vs Drd1-KO-Rescue: Free-running period: F (2, 19) = 0.03667, p = 0.9641, n = 6-8/group; Phase angle of entrainment: F (2, 30) = 0.07922, p = 0.9240, n = 8-13/group; % of light activity: F (2, 27) = 1.976, p = 0.1582, n = 8-12/group; One-way ANOVA. Figure 7; DAT-Cre-mCherry vs DAT-Cre-hM3Dq: Free-running period: p = 0.77, n = 5-7/group. Phase angle of entrainment: p = 0.88, n = 8-9/group. % of light activity: p = 0.40, 8-9/group. Student's two-tailed t-test. Data are represented as mean ± SEM (Quantification was also done by **Aarti Purohit**).

Discussion

The circadian system has evolved to predict and adjust to daily changes in environmental conditions. For humans, the advent of artificial lighting has introduced conditions that exceed the ability of our circadian axis to swiftly synchronize to constantly changing environmental, social, and economic pressures. Here, we show that the SCN receives direct input from VTA DA-neurons (Figure 6) consistent with previous findings demonstrating that electrolytic lesion of midbrain dopaminergic neurons leads to a 40% reduction of DA levels within the SCN (Kizer et al., 1976). Most notably, we demonstrate that stimulation of VTA DA-neurons accelerates entrainment to a shift in the light cycle, especially within the initial first two days of this response (Figure 7). In addition, we observed that the continuation of a shifted LD cycle is necessary for the potentiation of the phase shifts in response to elevated DA tone (Figure S5C and S5D), suggesting that DA signaling enhances photic resetting.

Extensive work has been conducted to discover a variety of DA neurotransmission-associated pacemakers such as the food entrainable oscillator, the dopamine ultradian oscillator, and the methamphetamine-sensitive circadian oscillator (Blum et al., 2014; Boulos and Terman, 1980; Krieger et al., 1977; Mistlberger, 2011; Stephan et al., 1979). Intriguingly, these oscillators have all been found to drive cyclic rhythms in the absence of a functional SCN. However, when the central circadian pacemaker is intact, proper integration with these extra-SCN oscillators is necessary for a comprehensive biological timing process. The persistent expression of Drd1 within the adult SCN suggests the existence of Drd1-dependent dopaminergic modulation of central circadian rhythms. In addition to our findings (Figure 2), two other reports have used Drd1-mediated intersectional genetics to show that, first, altering firing rate in Drd1-SCN neurons entrained behavioral rhythms to the time of optogenetic stimulation (Jones et al., 2015) and second, Drd1-SCN neurons were the rate determining cells within the SCN circuit in a temporally chimeric mouse model (Smyllie et al., 2016). Here, we demonstrate that selective activation of Drd1 neurons within the SCN phase shifts behavioral rhythms when the circadian system is most sensitive to light, thereby proposing a functional role for endogenous Drd1 signaling within the central clock in the modulation of photoentrainment.

Previous studies have shown that DA, Drd1, and Drd2 signaling within the retina and striatum influences circadian clock gene expression, light adapted vision, and circadian wheel-running patterns (Cahill and Besharse, 1991; Doyle et al., 2002; Jackson et al., 2012; Ruan et al., 2008). Our experiments demonstrate

that Drd1 expression within the SCN influences the rate of circadian entrainment to a shifted light cycle. In support of this claim, loss of Drd1 leads to a significantly reduced rate of photoentrainment, which is rescued by re-expression of Drd1 within the SCN (Figures 5 and 6), even though the absence of Drd1 has a moderate increase in locomotor activity (Heusner et al., 2008; Nakamura et al., 2014) and does not affect most circadian parameters (Figure S2 and Table S1). Thus, we reason that Drd1-SCN neurons are responsive to elevated dopaminergic tone in adulthood and account for the accelerated entrainment to a photoperiod shift observed upon specific VTA DA-neuron stimulation (Figure 6). Although increased Drd1 signaling within the developed SCN does not elicit an immediate circadian behavioral effect in constant conditions (Duffield et al., 1998; Weaver et al., 1992), we hypothesize that SCN-Drd1 signaling allows the central oscillator to enter a more “entrainable” state setting the gain on entrainment cues such as light. This is supported by the evidence that: 1. Selective chemogenetic activation of Drd1-SCN neurons mimics phase responses to photic stimuli (Figure 2), 2. Drd1 expression within the SCN is necessary for a normal rate of entrainment in response to LD cycle shifts (Figures 3-5), 3. Acceleration of circadian photoentrainment after elevation of DA tone relies on the introduction of the new light phase (Figure 7). From these results, it is apparent that the incorporation of the Drd1 signaling in the SCN with the photic information is critical for appropriately timed photoentrainment. Determining how DA-dependent arousing or rewarding stimuli primes the central clock to respond more robustly to light input will be important to investigate in subsequent studies.

In summary, Drd1 mediated DA neurotransmission within the SCN is an integral component determining the rate of entrainment following changes in the prevailing light cycle. Intriguingly, arousal inducing stimuli such as introduction of a novel running wheel or exposure to sexually receptive partners, which may result in elevation of DA tone, has been shown to elicit accelerated circadian entrainment (Bobrzynska and Mrosovsky, 1998; Yamanaka et al., 2008). Additionally, pathologies that involve aberrant DA neurotransmission such as Parkinson's disease, depression, attention deficit hyperactivity disorder (ADHD), bipolar disorder, schizophrenia, and drug addiction are associated with abnormal circadian rhythms and sleep patterns (Maywood et al., 2006; Van Veen et al., 2010; Wilson and Argyropoulos, 2012; Wulff et al., 2010; Zanini et al., 2015). Direct midbrain DA-neuron innervation to the central clock demonstrates a promising a link between dopaminergic and circadian pathologies. Delineation of the precise DA-neuronal circuitry governing circadian entrainment provides novel therapeutic targets for enhancing photoentrainment to combat symptoms of jet lag or shiftwork and alleviate the harmful effects of circadian rhythm misalignment.

Materials and Methods

Experimental models and subject details

All animal care experiments were conducted in concordance with University of Virginia Institutional Animal Care and Use Committee (IACUC). Animals were housed in a temperature and humidity-controlled vivarium (22-24°C, ~40% humidity) until experimental use on a 12-hour:12-hour light:dark cycle and were

provided with food and water *ad libitum*. All experiments were conducted in mice that ranged from 2-8 months of age. In addition to wild-type C57BL6/J mice, the following mouse lines were used: *Drd1a*$^{Cre/+}$ (Drd1-Cre) (Heusner et al., 2008), B6.129(Cg)-*Slc6a3*$^{tm1(cre)Xz}$/J (DAT-Cre) (Zhuang et al., 2005), B6.Cg-*Gt(ROSA)26Sor*$^{tmt(CAG-tdTomato)Hze}$/J (Ai14, ROSA26-tdTomato) (Madisen et al., 2010), B6;129S-*Gt(ROSA)*$^{26Sortm34.1(CAG-Syp/tdTomato)Hze}$/J (Ai34D, ROSA26-synaptophysin-tdTomato; The Jackson Laboratory #012570). For circadian behavioral studies, littermate males were exclusively used and were backcrossed to C57BL/6 for at least 10 generations. Drd1-KO*,* Drd1-Cre, and wild-type littermates were raised on a special diet of Teklad 8660 (Envigo, United Kingdom) and Bio-Serv Transgenic Dough Diet (S3472, Flemington, New Jersey) until weaning to promote Drd1-KO survival, then fed with standard Teklad 8664 (Envigo, United Kingdom) on the cage floor as Drd1-KO mice were more likely to consume food when it was readily accessible (Gallardo et al., 2014).

Viral Expression and Stereotaxic Surgery

During surgery, animals were anesthetized with isoflurane (induction 5%, maintenance 2%-2.5%; Isothesia) and placed in a stereotaxic apparatus (Kopf). A heating pad was used for the duration of the surgery to maintain body temperature and ocular lubricant was applied to the eyes to prevent desiccation. A Double-floxed inverted open reading frame (DIO) cassette containing recombinant AAV were used to express specific transgenes in Cre-expressing neurons. AAV was delivered using a 10 µl syringe (Hamilton) and 26-gauge needle (Hamilton) at a

flow rate of 100 nl/min driven by a microsyringe pump controller (World Precision Instruments, model Micro 4). The syringe needle was left in place for 10 minutes and was completely withdrawn 20 min after viral delivery. Following surgery, mice were administered ketoprofen (3 mg/kg) subcutaneously as an analgesic. Animals were tested at least two weeks following virus injection to ensure optimal transgene expression. Reporter expression was evaluated through immunohistochemistry. All surgical procedures were performed in sterile conditions and in accordance with University of Virginia IACUC guidelines.

Viral Constructs

Viruses were obtained from the University of North Carolina Gene Therapy Center (Chapel Hill) and the University of Pennsylvania School of Medicine Penn Vector Core. All viral cargos were cloned into the same parental construct. AAV8-hSyn-DIO-mCherry, AAV8-hSyn-DIO-hM3Dq-mCherry, AAV1-hSyn-ChR2-(H134R)-eYFP, and AAV1-CAG-DIO-Drd1-HA (500 nl; 1.1 x 10^13 viral genomes/ul) were injected into the NAc (ML: + 1.15 mm, AP: + 0.98 mm, DV: - 5.75 mm), SCN (ML: ± 0.28 mm, AP: - 0.30 mm, DV: -5.75 mm) or VTA (ML: ± 0.5 mm, AP: - 3.6 mm, DV: - 4.5 mm) depending on experimental paradigm. All coordinates are relative to bregma (George Paxinos and Keith B. J. Franklin). The original construct for AAV-DIO-Drd1-HA was developed in **Larry Zweifel's** lab (Gore and Zweifel, 2013).

Tracing Studies

For retrograde tracing studies, animals were injected unilaterally with 300 nl of fluorescent retrobeads (Lumafluor) directed towards the NAc or SCN. Brains were processed 3 weeks after retrobead delivery. In anterograde tracing confirmation, AAV8-hSyn-DIO-mCherry (500 nl) was delivered unilaterally into the VTA and the fiber innervation within the SCN was analyzed two weeks after surgery.

Histological Analysis and Imaging

Animals were deeply anesthetized (ketamine:xylazine, 280:80 mg/kg, i.p.) and perfused intracardially with ice cold 0.01 M phosphate buffer solution (PBS) followed by fixative solution (4% paraformaldehyde (PFA) in PBS at a pH of 7.4). After perfusion, brains were dissected and post-fixed overnight at 4°C in PFA. Brains were rinsed in PBS, transferred into 30% sucrose in PBS for 24 hours, and then frozen on dry ice. Coronal sections (30 µm) were cut with a cryostat (Microm HM 505 E). Sections were permeabilized with 0.3% Triton X-100 in PBS (PBS-T) and blocked with 3% normal donkey serum (Jackson ImmunoResearch) in PBS-T (PBS-T DS) for 30 min at room temperature. Sections were then incubated overnight in primary antibodies diluted in PBS-T DS. For visualization, sections were washed with PBS-T and incubated with appropriate secondary antibodies diluted in the blocking solution for 2 hours at room temperature. Sections were washed three times with PBS and mounted using DAPI Fluoromount-G (Southern Biotech). Images were captured on a Zeiss Axioplan 2 Imaging microscope equipped with an AxioCam MRm camera using AxioVision 4.6 software (Zeiss).

The following primary antibodies were used for fluorescent labelling: anti-Drd1 (rat, 1:500, Sigma D2944), anti-TH (chicken, 1:500, Millipore AB9702; rabbit, 1:1000, Millipore AB152), anti-mCherry (rabbit, 1:1000, Abcam ab167453), anti-DsRed (rabbit, 1:1000, Clontech 632496), anti-c-Fos (rabbit, 1:5000, Calbiochem PC38; rabbit, 1:100, Santa Cruz Sc-52), anti-HA (rabbit, 1:500, Cell Signaling Technology C29F41:500). The secondary antibodies (Jackson ImmunoResearch) used were Cy2- or Cy3- conjugated donkey anti-rat IgG (1:250), donkey anti-rabbit (1:250), and goat anti-chicken (1:250).

HPLC

Fresh brains were dissected from adult wild-type male animals and 1 mm coronal slices were collected using a mouse brain matrix (Zivic Instruments). SCN samples were collected with a 1 mm in diameter tissue punch, frozen in liquid nitrogen, and stored at -80°C until further processing. Tissue punches were homogenized by sonication in 50 µl of 0.4 N perchloric acid solution. The homogenate was centrifuged at 15,000*g* for 12 min at 4°C. 25 µl of the resulting supernatant was loaded into an auto-sampler connected to a high-performance liquid chromatography instrument with an electrochemical detector (Decade, Antec Leyden B.V., Zoeterwoude, The Netherlands) to measure the levels of dopamine. Retention time for DA was determined through comparison with DA standards.

Behavioral Analysis

To record the rhythm of locomotor activity, adult male mice were individually housed in activity wheel-equipped cages (Nalgene) in light-tight boxes under a 12-hour:12-hour LD cycle for at least 7 days. Fluorescent lights (100 μW/cm^2) were used for behavioral experiments. Food and water were provided *ad libitum*. Wheel running rhythms were monitored and analyzed with ClockLab collection and analysis system (Actimetrics, Wilmette, IL). The free-running period was calculated according to the onset of activity across seven days in constant darkness. Activity onset was identified through ClockLab software as the first bin above a threshold of 5 counts preceded by at least 6 hours of inactivity and followed by at least 6 hours of activity. Offsets were determined by at least 6 hours of activity and followed by 6 hours of inactivity. When necessary, onset and offset points were edited by eye. Phase angle of entrainment was calculated as the average difference between the time of lights-off and the time of activity onset across three days during LD entrainment. All data was analyzed by a trained scorer blind to genotype or viral treatment (**Ryan Grippo, Aarti Purohit**). In constant darkness, i.p. injections were conducted under infrared light with night vision goggles.

To assess the response to a jet lag light cycle shift, mice were entrained to an LD cycle for at least seven days, then the dark portion of the cycle was abruptly advanced or delayed six hours and locomotor activity was recorded for an additional 15 days. The days required to entrain following the shift in the light cycle was calculated. The duration of re-entrainment was defined as the number of days

required to shift activity onset or offset by 6 ± 0.25 hours followed by two consecutive days of activity onset or offset within this range.

To evaluate the role of photic input during the jet lag light cycle shift, following stable entrainment to the LD cycle for at least seven days, the dark portion of the cycle was abruptly advanced 6 hours and the mice were placed either immediately into constant darkness or after the continuation of one full LD cycle shift (Figure 4). The duration of cumulative phase shift on days 1 and 2 after the LD cycle shift was calculated relative to the onset of activity on the day prior to the shift.

To evaluate the phase responses DREADD activation or light, mice were entrained to the LD cycle for at least seven days then were placed in constant darkness for at least an additional 7 days to establish a free running period. Each animal was administered CNO (1 mg/kg in 0.9% saline) at CT 6, CT 14, or CT 22, or exposed to a 15-minute pulse of white light at either CT 14 or CT 22. Using ClockLab, a regression line was fit through activity onsets for the seven days prior to CNO or light administration and extrapolated for seven days following treatment. The duration of phase shifts was determined by measuring the time difference between the two lines on the day following the treatment.

To examine the acute effects of light on wheel running (masking), a 3-hour light pulse was delivered from ZT 14 to ZT 17. Changes in the number of wheel revolutions during application of light were quantified as percent of baseline activity at the corresponding time on the preceding day for each animal.

c-Fos quantification

Five 30 µm thick sections spanning through the rostro-caudal axis of the SCN and four 30 µm thick sections from the VTA were collected from each brain and labeled for c-Fos. The borders of the SCN were outlined by analysis of DAPI nuclear staining. The region of interest in μm^2 was determined using Axiovision 4.6 software and normalized to counts/mm^2. Quantification was performed by a trained observer blind to treatment (**Ryan Grippo, Qi Zhang**).

Statistical Analysis

Exclusion criteria for behavioral experimental animals were determined by appropriate phase angle of entrainment in LD. Mice that did not entrain to an LD cycle were excluded from analysis (n = 3 D1R-Cre mice after AAV-DIO-hM3Dq to SCN injection, 2 Drd1-Cre mice after AAV-DIO-mCherry to SCN injection, and 12 Drd1-KO mice which were used to troubleshoot the optimal titration of AAV-DIO-Drd1-HA re-expression virus). When comparing two groups of normally distributed data, Student's two tailed t-test was used. To compare the effects of genotype on days to entrain, cumulative phase shift for day 1 or day 2, and the rate of entrainment, two-way repeated-measures ANOVA was used, with *post hoc* Bonferroni's comparisons in the event of significant effects of genotype or time. All n values represent the number of mice used in each experiment.

Chapter III: Weight Gain Associated with Hedonic Feeding Requires Dopamine Signaling in the Suprachiasmatic Nucleus

In review as a research article in *Current Biology* 6/3/2019

Abstract

The increase in global incidence of obesity is paralleled by the widespread availability of energy-dense, rewarding foods. Overeating during mealtimes and unscheduled snacking disrupts timed metabolic processes which further contribute to weight gain. The neuronal mechanism by which the consumption of energy-dense food restructures the timing of feeding is poorly understood. Here, we demonstrate that dopaminergic signaling within the suprachiasmatic nucleus (SCN), the central circadian pacemaker, disrupts feeding schedule resulting in overconsumption of food. D1 dopamine receptor (Drd1) null mice are resistant to obesity, metabolic disease, and circadian disruption associated with energy-dense diets. Conversely, genetic rescue of Drd1 expression within the SCN restores diet-induced overconsumption, weight gain, and obesogenic symptoms. Additionally, access to rewarding food increases SCN dopamine turnover, and elevated Drd1-signaling decreases SCN neuronal activity, which disinhibits downstream orexigenic responses. These findings define a connection between the reward and circadian pathways in the regulation of pathological calorie consumption.

Introduction

Obesity and its comorbid conditions including type 2 diabetes, cardiovascular disease, and metabolic syndrome are pandemics that significantly reduce lifespan (de Mutsert et al., 2014; Eckel et al., 2011; Guh et al., 2009; Hurt et al., 2010). Lifestyle interventions such as decreasing caloric intake and increasing exercise are the primary strategies used to combat obesity, yet they remain ineffective for long-term success (Montesi et al., 2016). Energy-rich, rewarding foods encourage snacking outside of regular mealtimes lowering adherence to dietary interventions, and therefore preventing sustained weight loss (Del Corral et al., 2011; Webb and Wadden, 2017). Determining the neural mechanisms by which palatable foods alter feeding amount and meal-timing is a necessary step toward developing effective therapies against obesity.

Proper maintenance of energy homeostasis requires the synchronization of meals with daily metabolic rhythms (Turek et al., 2005). Surprisingly, even during conditions of isocaloric energy intake, high-fat food consumption out of phase with rhythmic metabolic processes leads to obesity through altered energy utilization and increased energy storage in mice (Arble et al., 2010; Hatori et al., 2012). Consistent with these observations, late-night eaters tend to be refractory to weight-loss therapy (Garaulet et al., 2013), while temporal restriction of meal timing improves the metabolic profiles of pre-diabetic men (Sutton et al., 2018). These findings emphasize the importance of both the amount and timing of calorie intake on metabolic health. While becoming recognized as critically important for well-being, the precise mechanisms by which energy-dense, rewarding foods alter food intake and feeding patterns remain unknown.

Food-seeking is orchestrated by two complementary and interacting neuronal circuits: the homeostatic and hedonic pathways (Liu and Kanoski, 2018; Saper et al., 2002). Homeostatic feeding is driven by depletion of energy stores while hedonic, or reward-based feeding, occurs when highly palatable foods are consumed even during periods of energy surplus. Agouti-related peptide (AgRP)-expressing neurons of the arcuate nucleus are the main orexigenic drivers of homeostatic feeding, while dopaminergic neurons within the ventral tegmental area (VTA) support hedonic feeding (Coccurello and Maccarrone, 2018). Dopaminergic VTA-neurons that project to the nucleus accumbens (NAc) are activated and release dopamine in response to palatable food consumption, sight of food, and stimuli that predict food delivery in both humans and laboratory animals (Berridge and Robinson, 1998; Hernandez and Hoebel, 1988; Kelley and Berridge, 2002; Volkow et al., 2002). In the absence of AgRP-neurons, dopaminergic neuron activation promotes palatable food consumption, emphasizing the cooperative nature of hedonic and homeostatic feeding circuits (Denis et al., 2015).

Dopamine (DA), a neurotransmitter known for its role in reward processing, is required for sustained motivation and execution of goal-directed behaviors (Wise, 2004, 2006). In accordance with these functions, loss of DA signaling leads to hypophagia and eventual death by starvation in mice (Zhou and Palmiter, 1995). Modulation of DA-dependent neural activity and behavior is mediated by a group of G protein-coupled receptors expressed in anatomically distinct regions throughout the central and peripheral nervous systems. Both D1-like (G_s-coupled)

and D2-like (G_i-coupled) receptors have been implicated in non-homeostatic consumption of palatable foods and obesity (Beaulieu and Gainetdinov, 2011; Johnson and Kenny, 2010; Missale et al., 1998). Reduced D2 dopamine receptor (Drd2) expression in the striatum has been linked to obesity in rodents and humans (Volkow et al., 2008; Wang et al., 2001). However, recent evidence suggests that this is not a predictor of weight gain or inactivity, and may be a consequence of obesity rather than a cause (Friend et al., 2017). The D1 dopamine receptor (Drd1) is also involved in the neural circuitry governing feeding. Selective activation of Drd1 expressing neurons in the prefrontal cortex induces food intake (Land et al., 2014), and prolonged access to a high-fat diet alters Drd1 expression within the reward centers of the brain (Alsio et al., 2010; Carlin et al., 2013). Additionally, treatment with a Drd1 antagonist reduces food intake in rodents and causes weight loss in humans (Astrup et al., 2007; Terry and Katz, 1994). Because rewarding foods rich in sugar and fat influences DA signaling (Volkow et al., 2012), we sought to determine the role of this neuromodulatory system in diet-induced obesity.

In this study, we show that Drd1 expression is necessary for overconsumption of a high-fat, high-sugar (HFD) diet. Moreover, Drd1 signaling in response to HFD perturbs circadian feeding and activity rhythms which exacerbate obesity and metabolic disease phenotypes. Unlike wild-type mice, Drd1-knockout mice provided *ad libitum* access to energy-dense, palatable foods are resistant to weight gain and metabolic pathologies associated with diet-induced obesity. Most strikingly, Drd1-knockout mice on a HFD diet maintain robust daily rhythms of food consumption, foraging, and fuel utilization, while wild-type mice demonstrate

altered circadian regulation of metabolism and activity. Selective restoration of Drd1 expression within the nucleus accumbens (NAc), the predominant reward processing center of the brain, fails to rescue the overconsumption of energy-rich food and attendant weight gain observed in wild-type mice. However, Drd1 rescue specifically within the central circadian clock of Drd1-knockout mice completely restores the weight gain and obesogenic phenotype. Surprisingly, while consumption of HFD elevates DA activity in the suprachiasmatic nucleus (SCN), the molecular clockworks of the central circadian pacemaker remain unaltered. However, the overall excitability of the SCN is reduced in response to Drd1 agonist treatment likely due to the increased activity of GABAergic Drd1-expressing-SCN neurons inhibiting local post-synaptic cells. Therefore, we posit that in response to rewarding foods, the increased dopaminergic tone on the circadian pacemaker dampens the SCN neuronal activity, disinhibiting downstream orexigenic targets and thereby promoting out-of-phase foraging.

Results

Drd1-KO Mice are Protected from High-Fat Diet-Induced Obesity

Mice with *ad libitum* access to rewarding, calorically dense food rapidly develop obesity, diabetes, and metabolic disease (Hariri and Thibault, 2010; Winzell and Ahren, 2004). To explore the potential relationship between dopamine D1 receptor (Drd1) signaling and obesity, we monitored response to dietary challenge using *Drd1a*$^{Cre/Cre}$ (KO) mice, in which both *Drd1a* alleles were replaced by Cre recombinase (Cre) (Heusner et al., 2008). First, we compared weekly changes in

body weight between adult wild-type (WT) and KO mice during *ad libitum* access to either a standard chow diet (SCD; 19% fat, 0% sucrose: 3.1 kcal/g) or HFD (45% fat, 17% sucrose:4.73 kcal/g) (Figure 1A). While KO mice raised on SCD are lean throughout development (4-10 weeks old; Figure S1A), their rate of body weight increase is similar to WT and heterozygous (HET) littermates, suggesting that the growth retardation prior to weaning accounts for the majority of their reduced body weight (BW) (Figure S1B (Drago et al., 1994; Xu et al., 1994). At fourteen weeks of age, mice were either maintained on SCD or switched to a HFD to assess their response to calorically dense food consumption (Figure 1A). Percent BW change was indistinguishable between adult WT and KO mice that remained on SCD (WT-SCD: 5.0 ± 2.5% increase; KO-SCD: 5.9 ± 1.1% increase). As expected, WT mice on a HFD (WT-HFD) significantly increased body mass (Figure 1B), however, KO mice fed the same HFD (KO-HFD) were completely resistant to diet-induced weight gain (WT-HFD: 29.5 ± 3.1% increase; KO-HFD: 5.4 ± 1.6% increase) (Figure 1B and 1C). Similar resistance to obesity has been observed in a separate *Drd1a* null (*Drd1*$^{-/-}$) mouse model (Drago et al., 1994), following twelve weeks of access to a palatable, high-fat, low sugar diet (60% fat, 10.7% sucrose; 5.49 kcal/g) (Figure S1E). These data indicate that Drd1 signaling is necessary for weight gain on a variety of calorically dense food sources, and that the effect is not strain dependent.

Diets rich in fats not only increase food consumption, but also alter feeding patterns resulting in food intake that extends into the phase of day when the animal is normally at rest (Arble et al., 2010; Espinosa-Carrasco et al., 2018). This

disruption in feeding rhythms induces weight gain independent of overconsumption, highlighting the importance of maintaining robust feeding rhythms for proper metabolic regulation (Hatori et al., 2012). To evaluate the temporal dynamics of food intake between WT and KO mice, we examined the day:night distribution of consumption on SCD or HFD. During the active (night) phase of the light:dark cycle, intake of either diet was equivalent between the genotypes. However, WT mice exhibited a significant increase in rest (light) phase (day) HFD consumption (Figure 1D). This profound intake increase during the rest phase in WT-HFD mice was nearly absent in KO-HFD mice (WT-SCD: 20.6 ± 0.3%; KO-SCD: 12.9 ± 0.2%; WT-HFD: 40.7 ± 1.8%; KO-HFD: 19.4 ± 1.0%) (Figure 1E). Attenuated daytime consummatory behavior in KO animals was also observed on a highly palatable liquid diet, demonstrating that the observed phenotype is applicable to different hypercaloric food sources (Figure S1F). Consistent with reduced daytime food intake, KO mice exhibited an increased latency to forage and consume a buried pellet of HFD during the day compared to WT controls (ZT 8; WT: 21.9 ± 4.2s; KO: 144.9 ± 68.6s; Student's two tailed t-test, p=0.037). No detectable differences in foraging latency were observed when the test was conducted at night (ZT 15; WT: 52.6 ± 31.0s; KO: 38.4 ± 8.5s; Student's two tailed t-test, p=0.667) demonstrating that Drd1 is required for out-of-phase palatable food-seeking, and the observed daytime reduction of food intake in KO mice is not a generalized impairment in motivation, olfaction, or locomotion (Figure 1F and Video S1 and Video S2; (Riera et al., 2017). Taken together, these data suggest that Drd1-dependent overconsumption of palatable food, predominantly

during the light phase, leads to obesity and metabolic disease. These findings not only reaffirm an essential role of circadian regulation in energy balance (Stenvers et al., 2019), but also implicate a significant role for Drd1-dependent DA-signaling in the neurocircuitry governing rewarding food consumption and alteration of circadian behavioral output.

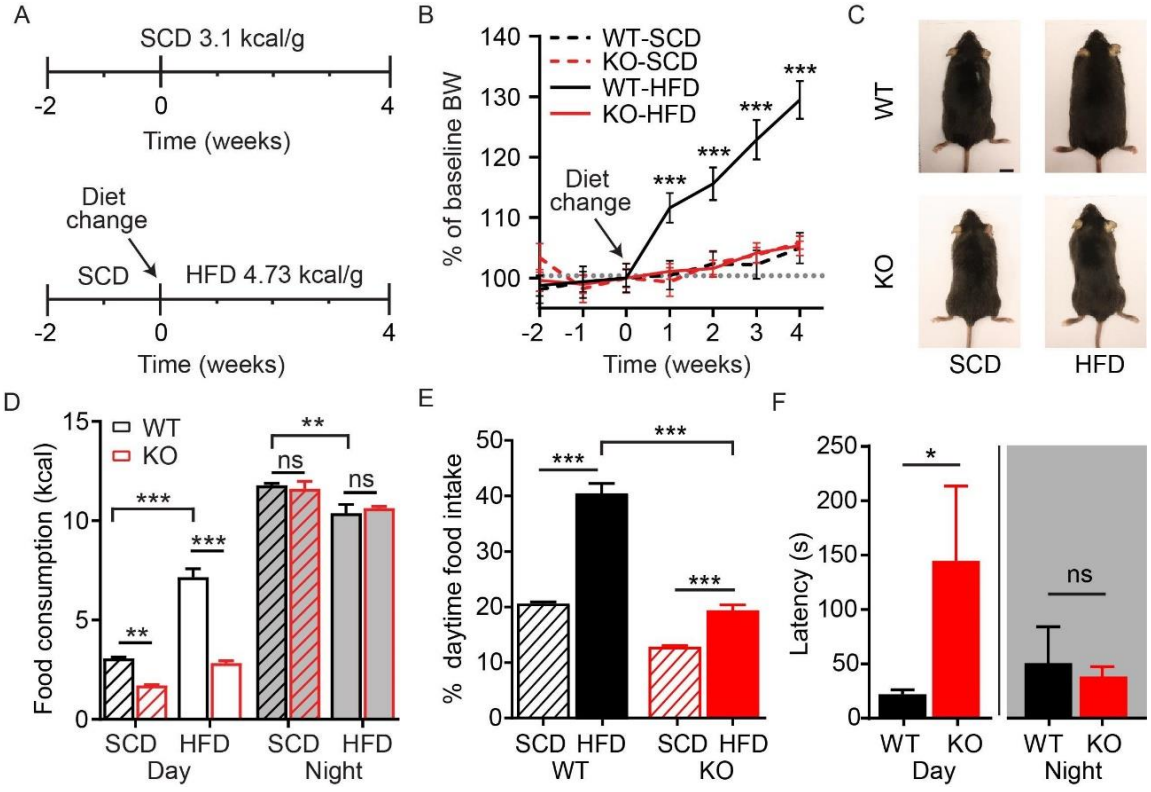

Figure 1. Drd1-KO Mice are Protected from High-Fat Diet-Induced Obesity. (A) Food access paradigm schematic. Diet switch from SCD to HFD is designated as week 0. (B) Percent body weight (BW) change relative to week 0 for WT and KO mice on SCD or HFD. Repeated-measures three-way ANOVA with Bonferroni post hoc comparison, n = 7-13/group; $F_{genotype}(1,37) = 4.825$, $p = 0.034$; $F_{diet}(1,37) = 5.956$, $p = 0.020$. The arrow indicates the time of diet switch from SCD to HFD. Statistical significance between WT-HFD and KO-HFD is depicted in the figure. (C) Representative mouse images of WT or KO mice following the feeding paradigm in figure 1A. Scale bar = 1 cm. (D) Calorie intake during the 12-hour light-

(Day) or dark-phases (Night) for WT and KO mice on SCD or HFD. Repeated-measures three-way ANOVA with Bonferroni post hoc comparison, n = 13/group $F_{time}(1,96) = 1,544$, $p < 0.001$; $F_{genotype}(1,96) = 57.07$, $p < 0.001$; $F_{diet}(1,96) = 12.63$, $p < 0.001$. (E) Percent of total daily food intake consumed during the light-phase for WT and KO mice on SCD or HFD. Two-way ANOVA with Bonferroni post hoc comparison, n = 13/group; $F_{genotype}(1,48) = 203.2$, $p < 0.001$; $F_{diet}(1,48) = 170.2$, $p < 0.001$. (F) Latency to retrieve a buried pellet of HFD during the light- (Day) or dark-phase (Night) for WT and KO mice. Student's two tailed t-test, n = 9-15/group (**Qijun Tang**). Data are represented as mean ± SEM for all panels. *p < 0.05, **p < 0.01, ***p < 0.001, ns = no significance.

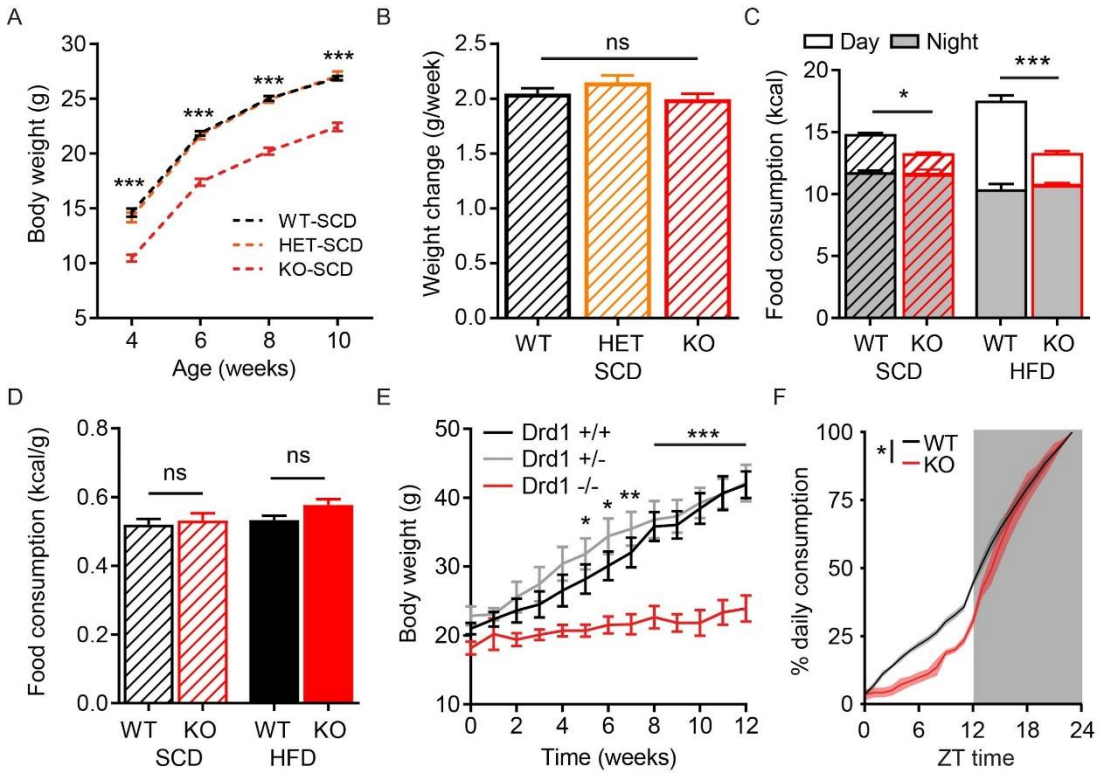

Figure S1. (related to Figure 1) D1 Dopamine Receptor Expression is Required for HFD-induced Obesity. (A) Post-weaning body weight change of $Drd1^{cre/cre}$ (KO), $Drd1^{cre/+}$ (HET) and $Drd1^{+/+}$ (WT) on SCD. Repeated-measures two-way ANOVA with Bonferroni post hoc comparison, n = 23/group; $F_{genotype}(2,66) = 70.06$, $p < 0.001$. Statistical significance between WT and KO is depicted in the figure (**Meghana Sunkara, Aarti Purohit**). (B) Weekly body weight change rate for WT and KO animals from 4 to 10 weeks of age on SCD. One-way ANOVA with Bonferroni post hoc comparison, n = 23/group; $F(2,66) = 2.173$, $p = 0.122$. (C) Daily total calorie consumption of WT and KO mice on SCD or HFD. Light- (white) and dark-phase (grey) consumption are segregated for clarity. Two-way ANOVA with Bonferroni post hoc comparison, n = 13/group; $F_{genotype}(1,48) = 54.49$, $p < 0.001$; $F_{diet}(1,48) = 12.06$, $p = 0.001$. (D) Daily food consumption normalized to body weight. Two-way ANOVA with Bonferroni post hoc comparison, n = 13/group; $F_{genotype}(1,48) = 2.580$, $p = 0.115$. (E) Weekly body weight measurements of Drd1 null (Drd1 -/-), heterozygous (Drd1 +/-) and WT (Drd1 +/+) mice on a high-fat/low-sugar diet. Repeated-measures two-way ANOVA with Bonferroni post hoc

comparison, n = 4-8/group; $F_{genotype}(2,16) = 15.2$, $p < 0.001$. Statistical significance between Drd1 +/+ and Drd1 -/- is depicted in the figure (**Andrew Steele**). (F) Cumulative highly palatable liquid diet consumption represented as percentage of whole-day consumption for KO and WT mice. Zeitgeber time (ZT), where ZT 0 indicates onset of light-phase and ZT 12 indicates onset of dark phase (shaded grey). Repeated-measures two-way ANOVA, n = 4/group; $F_{genotype}(1,6) = 6.499$, $p = 0.044$ (**Ryan Grippo, Meghana Sunkara**). Data in all panels are represented as mean ± SEM. *p < 0.05, **p < 0.01, ***p < 0.001, ns = no significance.

Drd1-KO Mice are Resistant to Dampening of Metabolic Rhythms and Metabolic Disease

One consequence of *ad libitum* calorie-rich food consumption is the adaptation of metabolic processes, which switch from a high amplitude circadian oscillation between carbohydrate utilization (during the active phase) and lipid oxidation (during the rest phase) to a low amplitude oscillation reflective of metabolic shunting towards energy storage (Arble et al., 2009; Kohsaka et al., 2007). To determine whether weight gain resistance in KO mice is accompanied by protection from HFD-induced metabolic disruption, we examined metabolic output of WT and KO mice through indirect calorimetry. WT and KO mice on SCD exhibit robust circadian rhythms of respiratory exchange ratio (RER), which is maintained at a value close to one at night due to elevated carbohydrate utilization following feeding, and reduced to ~0.80 during the day, reflecting increased rest, fasting, and lipid oxidation (Figures 2A-C). In contrast, the circadian amplitude of RER in WT-HFD mice is significantly dampened, as reported previously (Day: 0.871 ± 0.007; Night: 0.873 ± 0.005. Repeated-measures two-way ANOVA, $p>0.999$; Figures 2D and 2E, and Figure S2A) (Hatori et al., 2012). However, KO-HFD mice

sustain high-amplitude RER rhythms favoring increased fat utilization during rest and increased consumption at night (Day: 0.825 ± 0.012; Night: 0.883 ± 0.011. Repeated-measures two-way ANOVA, p=0.001) (Figures 2D and Figure S2A). Elevated daytime (ZT 6) fatty acid oxidation in KO-HFD mice was confirmed by the quantification of the activated form of a lipid hydrolyzing enzyme, phosphorylated hormone sensitive lipase (pHSL) levels (Kraemer and Shen, 2002). We observed an increased pHSL(660)/HSL ratio during the day (ZT 6) in KO-HFD mice indicating increased adipocyte lipolysis compared to WT-HFD animals (WT-HFD: 3.0±0.1; KO-HFD: 4.7±0.5; Student's two tailed t-test, p=0.014) (Figures S2B and Figure S2C) (Akasheh et al., 2013). These data reveal that KO-HFD mice maintain high amplitude metabolic rhythms more similar to the SCD- than HFD-fed animals which support metabolic well-being and protection from weight gain.

While KO-HFD mice exhibit marginal hyperactivity at night, we observed no marked difference in twenty-four hour energy expenditure (EE) or resting metabolic rate (RMR) compared to WT-HFD mice (Figure 2F and Figures S2D and S2E). However, similar to WT-SCD animals, KO-HFD mice maintained lower body temperatures (T_b) during the midday (ZT 6) compared to WT-HFD mice (WT-SCD: 36.5 ± 0.1°C; KO-SCD: 36.4 ± 0.1°C; WT-HFD: 37.2 ± 0.1°C; KO-HFD: 36.5 ± 0.1°C. Two-way ANOVA with Bonferroni post hoc comparison, $p<0.001$). All groups had similar T_b at midnight (ZT 18; WT-SCD: 37.8 ± 0.1°C; KO-SCD: 37.7 ± 0.1°C; WT-HFD: 37.7 ± 0.1°C; KO-HFD: 37.8 ± 0.1°C) resulting in a significant night:day amplitude difference between WT-HFD and KO-HFD mice (Figure S2F). The maintenance of WT-SCD-like T_b in KO-HFD mice suggests that excess energy

is not lost due to increased heat production, and is unlikely to contribute to the defect in weight gain as observed in other obesity resistant models (Mills et al., 2018; Wan et al., 2012). Lastly, we determined whether WT-HFD and KO-HFD groups differ in their ability to absorb calories from food by performing fecal waste calorimetry. No difference in fecal energy density was detected in any group (Figure S2G). In fact, the daily energy assimilation was reduced in KO-HFD mice and hence could not contribute to the reduced body weight in these animals (Figures S2H and Figure 1C).

Obesity from HFD consumption also results in increased adiposity, adipocyte hypertrophy, hepatic steatosis, glucose intolerance and insulin resistance (Hariri and Thibault, 2010; Kopelman, 2000). As expected, excess weight gain in WT-HFD mice was attributed to a significant increase in full body adiposity (Figure 2G). In contrast, KO-HFD animals, while acquiring all their calories from a fat and sucrose enriched diet, maintain similar body fat composition to SCD controls (WT-SCD: 12.5 ± 5.1%; KO-SCD: 10.8 ± 1.5%; WT-HFD: 27.7 ± 6.1%; KO-HFD: 11.4 ± 1.5%; Figure 2G). Adipocyte cell hypertrophy in gonadal white adipose tissue (GWAT) and posterior subcutaneous adipose tissue (SCAT) was also diminished in KO-HFD mice compared to WT-HFD animals (Figures 2H and 2I and Figures S2I-J). Consistent with these observations, KO-HFD hepatic lipid accumulation remained similar to SCD controls and was markedly reduced compared to WT-HFD mice (Figure 2J). Most strikingly, KO-HFD mice were protected from glucose intolerance and insulin resistance, two hallmarks of obesity induced metabolic disease (Figures 1H and Figures S1L and S1M) (Kahn et al.,

2006; Steppan et al., 2001). Despite *ad libitum* consumption of HFD, KO mice maintain high amplitude activity, temperature, and metabolic rhythms, reduced adiposity, and retain robust responsiveness to glucose and insulin fluctuations.

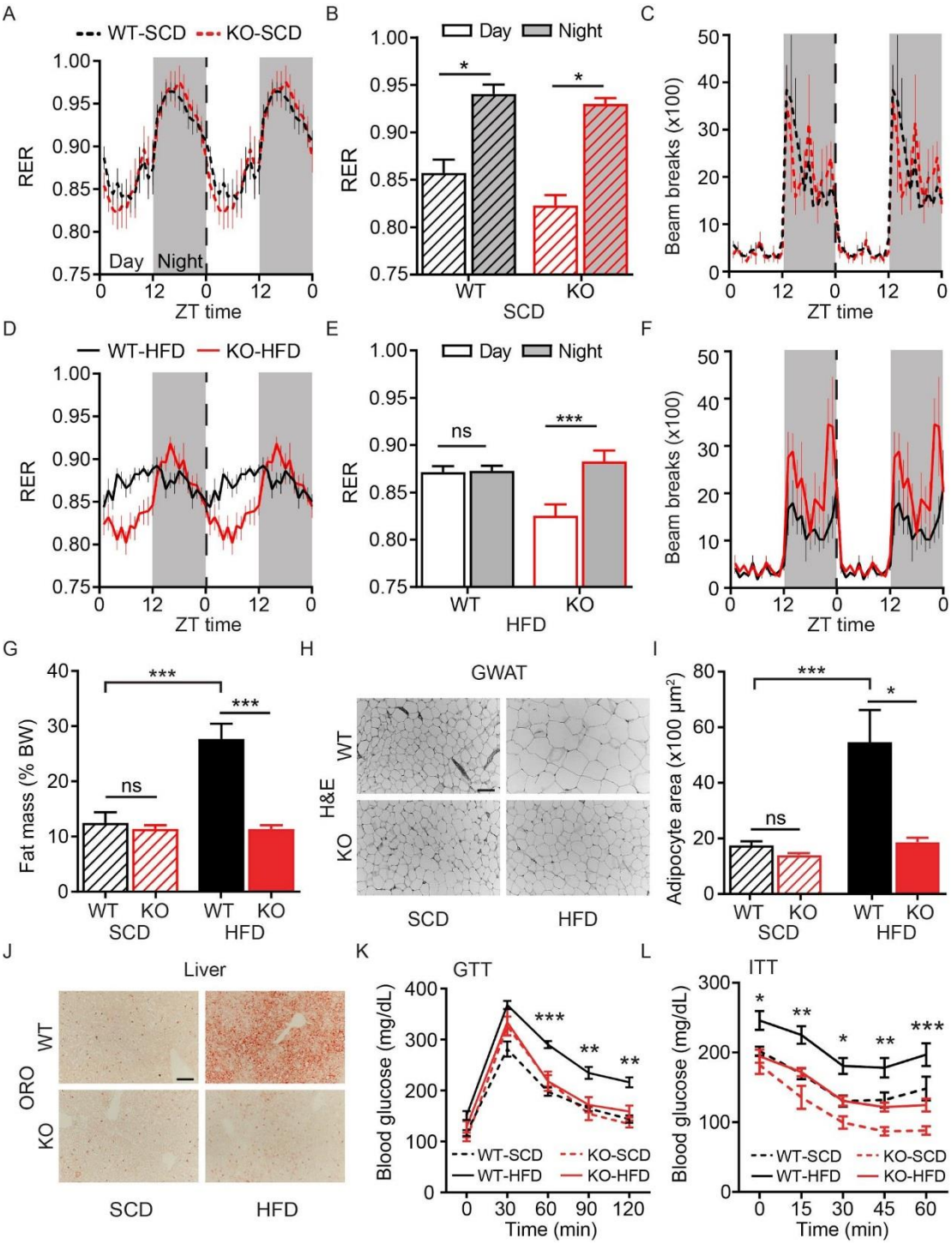

Figure 2. Drd1-KO mice are Resistant to High-Fat Diet-Induced Metabolic Disease. (A) Respiratory exchange ratio (RER) for WT and KO mice on SCD. Repeated-measures two-way ANOVA, n=4-5/group (**Ryan Grippo, Qijun Tang, Michael Scott**). Time is represented as *Zeitgeber* time (ZT), where ZT 0 indicates

onset of light-phase and ZT 12 indicates onset of dark phase (shaded grey). Data are plotted in 1-hour intervals. Vertical dotted line indicates the point at which twenty-four hour data is double-plotted for clarity. Same representation applies to panel (c),(d) and (f). (B) Average RER during the 12-hour light- (Day) or dark-phase (Night) from panel (A). Repeated-measures two-way ANOVA with Bonferroni post hoc comparison, n = 4-5/group; $F_{time}(1,7) = 57.46$, $p < 0.001$. (C) Double-plotted locomotor activity measured by passive infrared beambreaking for WT and KO mice on SCD. Repeated-measures two-way ANOVA with Bonferroni post hoc comparison, n = 4-5/group. (D) Double-plot of RER for mice on HFD for WT and KO mice. Repeated-measures two-way ANOVA with Bonferroni post hoc comparison, n = 5/group. (E) Average RER during the 12-hour light- or dark-phase from panel (D). Repeated-measures two-way ANOVA with Bonferroni post hoc comparison, n = 5/group; $F_{time}(1,8) = 15.83$, $p = 0.004$. (F) Double-plotted locomotor activity measured by passive infrared beambreaking for WT and KO mice on HFD. Repeated-measures two-way ANOVA with Bonferroni post hoc comparison, n = 5/group; $F_{genotype}(1,8) = 5.402$, $p = 0.049$. (G) Fat mass as percent of body weight (BW) for WT and KO mice on SCD or HFD. Two-way ANOVA with Bonferroni post hoc comparison, n = 5-7/group; $F_{diet}(1,19) = 22.33$, $p < 0.001$; $F_{genotype}(1,19) = 26.52$, $p < 0.001$. (H) Representative GWAT histology with Hematoxylin and Eosin (H&E) stain for groups in (G). Scale bar = 100 μm. (I) Quantification of GWAT adipocyte area for groups in (H). Two-way ANOVA with Bonferroni post hoc comparison, n = 3/group; $F_{diet}(1,8) = 13.54$, $p = 0.006$; $F_{genotype}(1,8) = 8.179$, $p = 0.021$. (J) Representative liver histology using Oil-red-O for groups in (G) (**Qijun Tang**), where hepatic lipid content stains as red. Scale bar = 100 μm. (K) Blood glucose levels during glucose tolerance test (GTT) for groups in (G) (**Qi Zhang**). Repeated-measures three-way ANOVA with Bonferroni post hoc comparison, n = 8-12/group; $F_{genotype}(1,35) = 5.49$, $p = 0.034$; $F_{diet}(1,35)=21.92$, $p < 0.001$. Post-hoc statistical significance between WT-HFD and KO-HFD is depicted in the figure. (L) Blood glucose levels during insulin tolerance test (ITT) for groups in (G) (**Qi Zhang**). Repeated-measures three-way ANOVA with Bonferroni post hoc comparison; n = 9-12/group; $F_{genotype}(1,36) = 26.44$, $p < 0.001$;

$F_{diet}(1,36) = 14.83$, $p < 0.001$. Statistical significance between WT-HFD and KO-HFD is depicted in the figure. Data in all panels are represented as mean ± SEM. *p < 0.05, **p < 0.01, ***p < 0.001, ns = no significance.

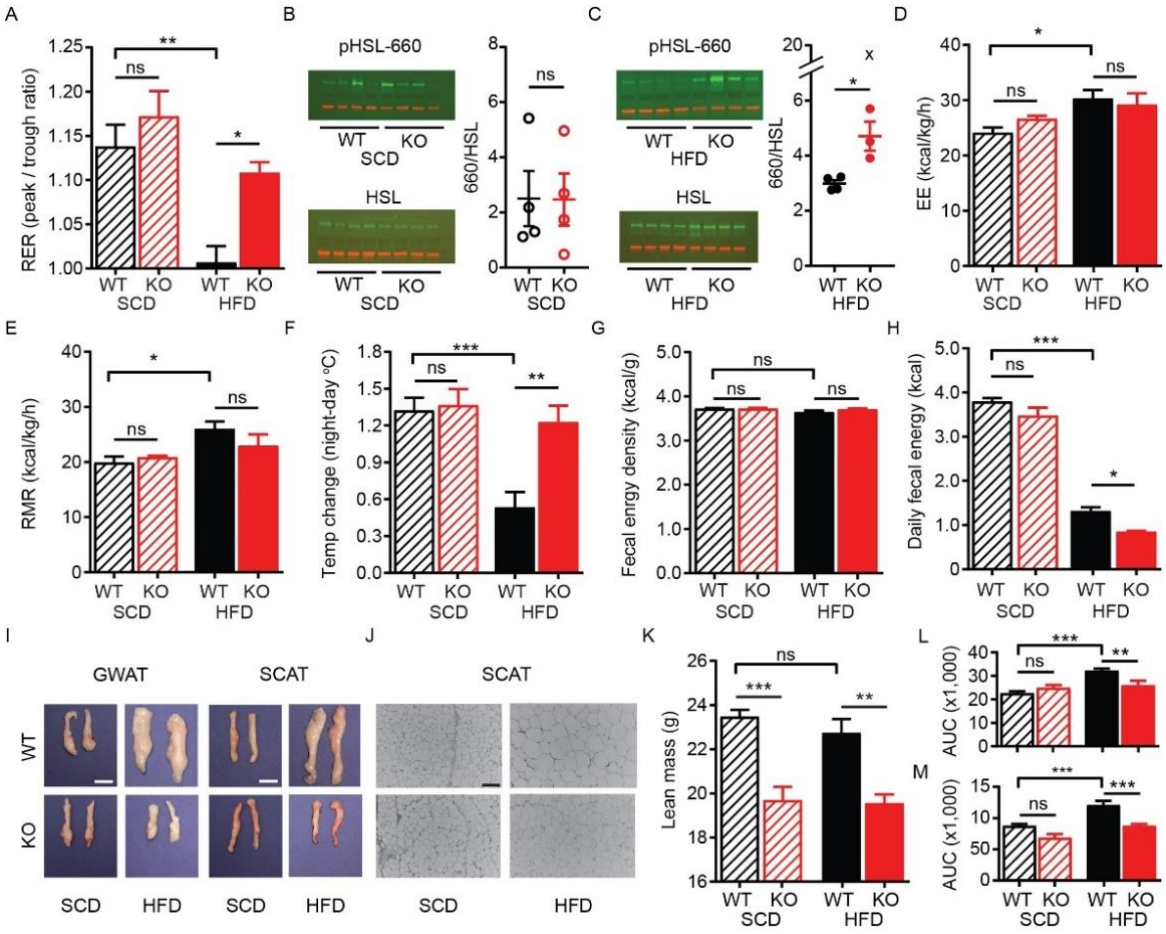

Figure S2. (related to figure 2) Supportive Metabolic Tests Illustrating the Resistance to High-Fat Diet-Induced Metabolic Syndromes of Drd1-KO Mice. (A) Group analysis of night (ZT 14-16)-day (ZT 3-5) RER ratio. Two-way ANOVA with Bonferroni post hoc comparison, n = 4-5/group; $F_{diet}(1,15) = 21.38$, $p < 0.001$; $F_{genotype}(1,15) = 10.36$, $p = 0.006$. (B) Left: Immunoblots visualized in green channel for pHSL 660 (top), and HSL (bottom) collected at ZT 6 from GWAT of WT and KO mice on SCD. Signal is normalized to tubulin levels (red channel). Right: pHSL 660/HSL ratio from left. Student's two tailed t-test, n = 4/group (**Anthony Spano,**

Laura Sipe). (C) Left: Immunoblots visualized in green channel for pHSL 660 (top), and HSL (bottom) collected at ZT 6 from GWAT of WT and KO mice on HFDD. Signal is normalized to tubulin levels (red channel). Student's two tailed t-test, n = 4/group. One outlier in Drd1-KO group was detected by ROUT outlier test (Q = 5 %) and indicated as x (**Anthony Spano**). (D) Energy expenditure (EE; kcal/kg/hour) for WT and KO mice on SCD or HFD. Two-way ANOVA with Bonferroni post hoc comparison, n = 4-5/group (**Qijun Tang**). (E) Resting metabolic rate (RMR; kcal/kg/hour) for groups in (D) (**Qijun Tang**). Two-way ANOVA with Bonferroni post hoc comparison, n = 4-5/group. (F) Change in body temperature between ZT 18 and ZT 6 for groups in (D). Two-way ANOVA with Bonferroni post hoc comparison, n = 9-11/group; $F_{diet}(1,34) = 13.5$, $p < 0.001$; $F_{genotype}(1,34) = 8.539$, $p = 0.006$. (G) Fecal energy density measured by fecal bomb calorimetry for groups in (D). two-way ANOVA with Bonferroni post hoc comparison, n = 3-4/group. (H) Estimated energy lost to fecal waste in twenty-four hours for groups in (D). Two-way ANOVA with Bonferroni post hoc comparison, n = 5/group; $F_{diet}(1,16) = 567.3$, $p < 0.001$; $F_{genotype}(1,16) = 13.37$, $p = 0.002$. (I) Representative dissected GWAT (left) and SCAT (right) images for groups in (D) (**Qijun Tang, Qi Zhang**). Scale bar = 1 cm. (J) Representative SCAT histology with Hematoxylin and Eosin (H&E) stain for groups in (D). Scale bar = 100 um. (K) Lean mass measured by Echo MRI four weeks after SCD or HFD diet in WT and KO mice. Two-way ANOVA with Bonferroni post hoc comparison, n = 5-7/group; $F_{genotype}(1,19) = 49.68$, $p < 0.001$. (L) Area under the curve (AUC) for GTT (from Figure 1H). Two-way ANOVA with Bonferroni post hoc comparison, n = 8-12/group, $F_{diet}(1,35) = 21.14$, $p < 0.001$; $F_{genotype}(1,35) = 3.858$, $p = 0.058$ (**Qi Zhang)**. (M) AUC for ITT (from Figure 1I). Two-way ANOVA with Bonferroni post hoc comparison, n = 9-12/group, $F_{diet}(1,36) = 25.87$, $p < 0.001$; $F_{genotype}(1,36) = 24.02$, $p < 0.001$. Data in all panels are represented as mean ± SEM. *$p < 0.05$, **$p < 0.01$, ***$p < 0.001$, ns = no significance (**Qi Zhang**).

The Effect of HFD on KO Peripheral Circadian Rhythms

Following chronic nutrient overload, the development of diet-induced insulin resistance results at least in part from chronic inflammation in the liver and adipose tissue (Dandona et al., 2004; Xu et al., 2003). These defects associated with obesity and metabolic disease have been linked to the establishment of a dysbiotic gut microbiome (Tilg and Kaser, 2011). To evaluate the effect of diet and feeding pattern changes on the microbiome over a twenty-four hour period, fecal samples were collected every four hours from WT-SCD, WT-HFD, and KO-HFD mice, and their microbiome composition was determined by 16S rRNA profiling. In WT mice, we found that, compared to SCD, HFD significantly reduced the alpha diversity of the fecal microbiome (Mann–Whitney U test, $p < 0.001$), and accounted for over 40% of the variation in microbial composition (PERMANOVA, $R^2 = 0.436$ $p = 0.001$; Figure 3A). While diet had a significant effect on species richness and composition of the microbiome, no substantial genotype differences in alpha diversity (Mann–Whitney U test, p= 0.355; Figure 3B) or microbial composition (PERMANOVA, R^2 0.043; p = 0.173; n = 18/group; Figure 3A) could be detected on a HFD diet. Although circadian cycling of the microbiome has been reported in the caecum (Zarrinpar et al., 2014), we did not observe significant cycling across a twenty-four hour period in the fecal microbiome using JTK analysis (Figure S3A) (Hughes et al., 2010). Because we observed no robust cycling across a twenty-four hour period, we further evaluated whether time of day would influence microbial composition within the same animal. To accomplish this, we collected fecal samples from WT-HFD and KO-HFD mice at both ZT 1 and ZT 13. In this

paradigm, we observed that time of collection had a significant effect on microbial composition (PERMANOVA, $R^2 = 0.147$; $p = 0.001$ n = 8/group), but no substantial differences between genotype could be distinguished (PERMANOVA, $R^2 = 0.036$; $p = 0.055$ n = 8/group; Figure 3C). These data reinforce that the composition of the diet, and not the obese phenotype or timing of food consumption is primarily responsible for our observed differences in the fecal microbiome.

While developing a dysbiotic microbiome, KO-HFD mice remain protected from adipocyte hypertrophy and insulin resistance contrary to the reported associations between gut microbiota and metabolic state (Figures 2 and Figure 3; (Dandona et al., 2004; Xu et al., 2003). However, diet-induced obesity also increases intestinal permeability resulting in enhanced exposure of adipose tissue to proinflammatory bacterial products (Frazier et al., 2011). Since this may cause peripheral inflammation and insulin resistance, we sought to evaluate the effect of diet on intestinal permeability in our animal models (Brun et al., 2007; Caricilli and Saad, 2013). To accomplish this, an oral gavage of fluorescein isothiocyanate labeled dextran (FITC-Dextran) was administered to mice at ZT 6, followed by quantification of fluorescence within the blood plasma (Thevaranjan et al., 2017). As expected, fluorescent signal in the plasma of WT-HFD mice was significantly increased compared to WT-SCD animals. However, KO-HFD mice displayed a reduced fluorescent signal indicative of protection against increased intestinal permeability observed in WT-HFD mice (Figure 3D). While KO-HFD and WT-HFD mice both develop a dysbiotic fecal microbiome, the decreased intestinal permeability may prevent microbial byproduct infiltration resulting in protection

against metabolic consequences of HFD in KO mice (Brun et al., 2007; Chang et al., 2018).

In addition to changes in microbial composition, prolonged access to HFD dampens circadian clock gene rhythms in the peripheral tissues (i.e. WAT and liver) (Kohsaka et al., 2007). Interestingly, the robust cycling of these peripheral circadian oscillators can be restored by time restricted feeding (TRF) of HFD during the active phase (Hatori et al., 2012). Since KO-HFD animals maintain a predominantly nocturnal pattern of feeding and robust metabolic rhythms, we evaluated *Rev-erbα, Per2* and *Bmal1* gene expression in GWAT and liver tissue every four hours throughout the twenty-four hour day. As reported previously, we observed significant dampening in the amplitude of circadian clock genes from GWAT in WT-HFD mice compared to WT-SCD controls (Figure 3E) (Hatori et al., 2012; Kohsaka et al., 2007). However, despite their lean phenotype, the daily oscillation of the clock genes in KO-HFD mice was generally indistinguishable from WT-HFD mice except for *Bmal1* expression at ZT 1 in GWAT, and *Per2* expression at ZT17 in liver (Figure 3F and Table S1). Even with a self-imposed, restricted food consumption pattern in KO animals, the minor differences in peripheral circadian oscillators between WT-HFD and KO-HFD mice are dissimilar to what has been observed in mice on eight hour TRF, which sustain robust peripheral circadian clock rhythmicity compared to their *ad libitum* fed controls (Hatori et al., 2012). Therefore, unlike this TRF model, the protection from metabolic disease in KO-HFD mice cannot be fully explained by a resilient amplitude of clock gene expression in the periphery.

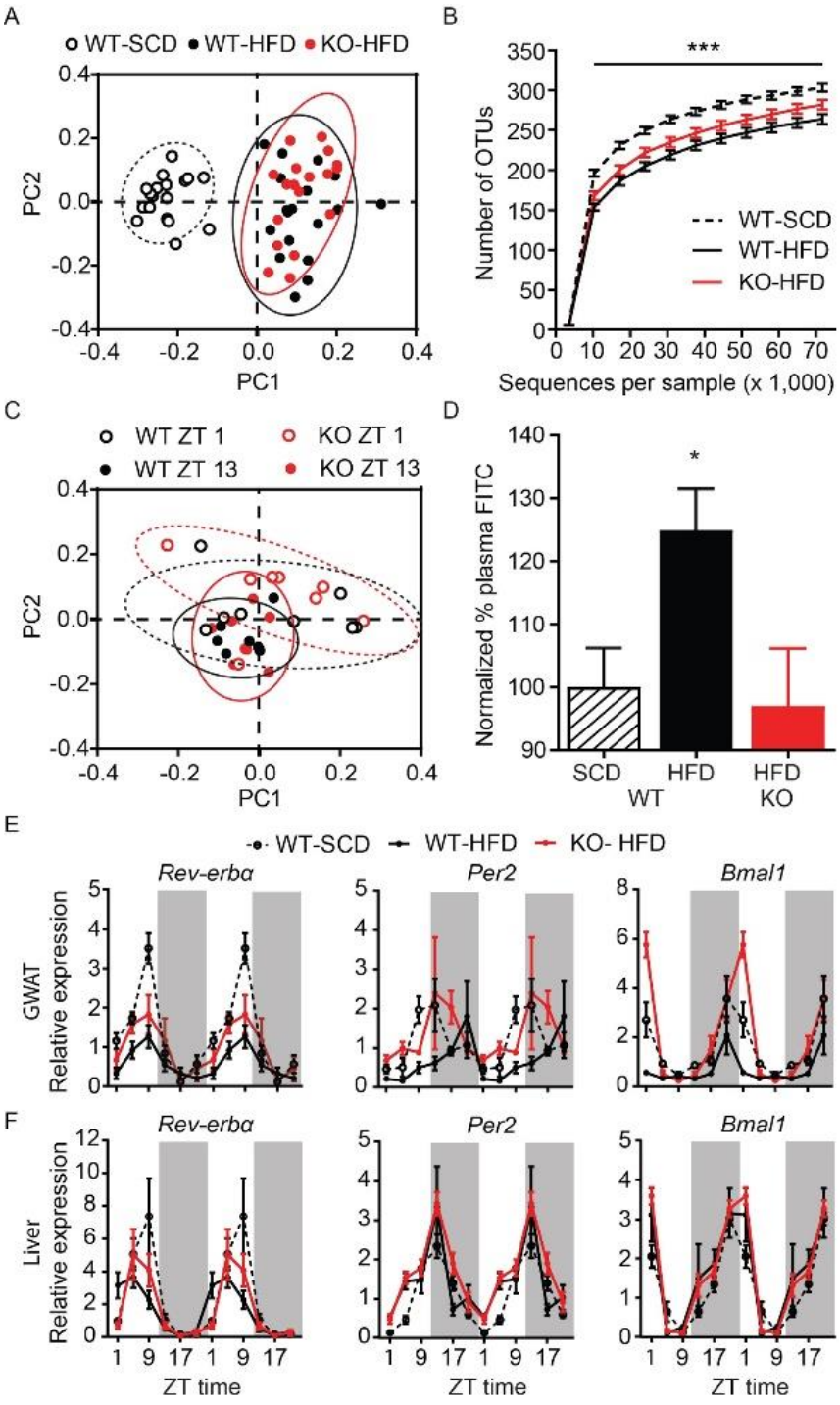

Figure 3 Drd1-KO Mice are Resistant to HFD Induced Peripheral Abnormalities. (A) Weighted UniFrac principal component analysis (PCA) of microbiome composition comparing WT-SCD, WT-HFD, and KO-HFD mice. The 95% normal confidence ellipses are illustrated (**Yingnan Gao, Martin Wu**). (B) Alpha diversity of fecal microbiome operational taxonomic units (OTUs). Repeated

measures two-way ANOVA with Bonferroni post hoc comparison, n = 18/group; $F_{treatment}(2,51) = 15.14$, $p < 0.001$. Statistical significance between WT-SCD and WT-HFD is depicted in the figure (**Yingnan Gao, Martin Wu)**. (C) Weighted UniFrac PCA analysis of fecal samples collected from the same mouse at two different time points (ZT 1 vs ZT 13) for WT-HFD and KO-HFD mice. The 95% normal confidence ellipses are illustrated (**Yingnan Gao, Martin Wu)**.(D) Fluorescent signal in plasma normalized to WT-SCD levels following oral gavage of FITC-Dextran. One-way ANOVA with Bonferroni post hoc comparison, n = 6-10/group; $F(2,21) = 4.943$, $p = 0.017$. (E) Double-plotted RNA expression level of circadian genes *Rev-erbα, Per2* and *Bmal1* in the GWAT every 4 hours throughout the twenty-four hour day. Two-way ANOVA with Bonferroni post hoc comparison, n = 3/time point/group (Table S1). Time is represented in ZT and dark-phase is shaded grey. Same representation applies to panel (F) (**Qi Zhang**). (F) Double-plotted RNA expression level of circadian genes *Rev-erbα, Per2* and *Bmal1* in the liver, every 4 hours throughout the twenty-four hour day. Two-way ANOVA with Bonferroni post hoc comparison, n = 3/time point/group (Table S1). Data in all panels are represented as mean ± SEM. *p < 0.05, **p < 0.01, ***p < 0.001, ns = no significance (**Qi Zhang)**.

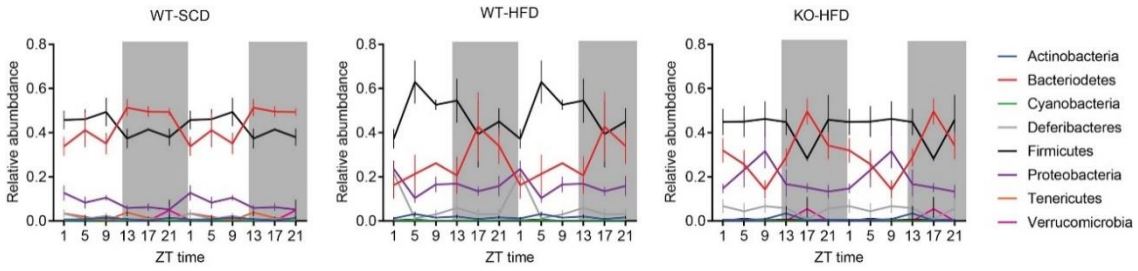

Figure S3. (related to Figure 3) JTK analysis of phylum. (A) Double-plotted JTK analysis of cycling of OTUs from fecal samples collected every four hours from WT-SCD, WT-HFD, and KO-HFD mice. Time is represented in ZT and dark-phase is shaded grey (**Yingnan Gao, Martin Wu**).

	Liver	*Per2*	*Reverba*	*Bmal1*
	Two-way ANOVA Genotype	P = 0.02	p = 0.30	p = 0.38
Bonferroni	WT-SCD vs WT-HFD	ns	ZT 9 ***	ns
	WT-HFD vs KO-HFD	ZT 17 *	ns	ns
	WT-SCD vs KO-HFD	ns	ZT 9 *	ZT 1 **
	GWAT	Per2	Reverb	Bmal
	Two-way ANOVA Genotype	p = 0.07	p = 0.02	p = 0.03
Bonferroni	WT-SCD vs WT-HFD	ZT 9,13 **	ZT1,5* ZT9 ***	ZT 1 *
	WT-HFD vs KO-HFD	ns	ns	ZT 1 ***
	WT-SCD vs KO-HFD	ZT 13 *	ZT9 ***	ns

Table S1: (related to Figure 3) Statistics Summary of Liver and GWAT qPCR. Two-way ANOVA with Bonferroni post hoc comparison. N = 3/time point/group. *p < 0.05, **p < 0.01, ***p < 0.001, ns = no significance.

Re-expression of Drd1 Within the NAc Increases Daytime HFD Consumption without Inducing Obesity.

Energy homeostasis is controlled by a variety of neuronal circuits that influence food intake and energy expenditure, making it likely that protection from obesity in KO mice comes from a reduced central drive overconsume palatable foods (Ferrario et al., 2016; Rossi and Stuber, 2018; Stamatakis et al., 2016). To identify the cell types responsible for HFD-induced obesity, we limited Drd1 ablation to distinct populations of neurons by crossing floxed Drd1 ($Drd1^{fl/fl}$) mice with two different Cre driver lines. We distinguished between forebrain Drd1 neurons and GABAergic populations using either $CaMKII^{Cre/+}$ or $VGAT^{Cre/+}$ driver lines, respectively (Sarinana and Tonegawa, 2016; Vong et al., 2011; Wang et al., 2013). On HFD, $CaMKII^{Cre/+}$;$Drd1^{fl/fl}$ mice gained an equivalent amount of weight

compared to CaMKII$^{Cre/+}$;Drd1$^{+/+}$ controls (Figure 4SA). However, similar to germline Drd1-null animals (Figure S1E), select ablation of Drd1 expression in GABergic neurons (VGAT$^{Cre/+}$;Drd1$^{fl/fl}$ mice) completely protected animals from diet-induced obesity (Figure 4A and 4B).

To identify which GABAergic Drd1 expressing brain region is sufficient for out-of-phase overconsumption of HFD, we restored Drd1 expression to select neuronal populations in Drd1-KO mice by bilaterally delivering an adeno-associated virus 1 (AAV1) containing a Cre recombinase dependent Drd1 transgene (Drd1-HA). Because the Cre recombinase gene is knocked-in to replace the endogenous *Drd1a* gene in these mice, Drd1-HA expression remains confined to the cells with active *Drd1a* promoter at the targeted site (Gore and Zweifel, 2013; Grippo et al., 2017). The nucleus accumbens (NAc) is a primary DA recipient region within the mesolimbic reward pathway and exhibits increased DA turnover in response to HFD (Baik, 2013). Therefore, we initially rescued Drd1 expression specifically in the NAc Drd1-positive medium spiny neurons of Drd1-KO mice (NAc-Rescue, Figure 4C). Successful targeting of Drd1-HA was determined by anti-HA immunohistochemistry (Figure 4C) and functional expression was evaluated by increased locomotor activity in response to intraperitoneal injections of the Drd1 agonist SKF-81297 (i.p.; 7.5 mg/kg) (Figure S4D) (Gore 2013). Drd1-KO mice bilaterally injected with an AAV1 encoding the light-activated, membrane-localized cation channel Channelrhodopsin-2 (ChR2-eYFP) to theNAc were used as controls (NAc-Control). Surprisingly, re-expression of Drd1 within the NAc resulted in no appreciable increase in body weight (NAc-Control: 4.3 ± 2.4%

increase; NAc-Rescue: 6.4 ± 2.3% increase) on HFD (Figure 4D). Additionally, we observed no difference in twenty-four hour consumption compared to controls on either diet, however NAc-Rescue mice significantly increased the portion of daytime HFD consumption (NAc-Control: 19.8 ± 1.2%; NAc-Rescue: 31.1 ± 1.5%) (Figures 4E and Figure 4F). This elevated rest phase consumption resulted in a marginal but statistically significant increase in percentage fat mass and GWAT adipocyte area (Figures 4G and Figure H). However, similar to germline KO mice, NAc-Rescue mice maintained glucose tolerance and insulin sensitivity (Figures 4I and Figure J). Despite increasing the portion of rest-phase feeding, re-expression of Drd1 within the NAc is not sufficient to induce HFD overconsumption and obesity, indicating that another Drd1-expressing brain region governs this response.

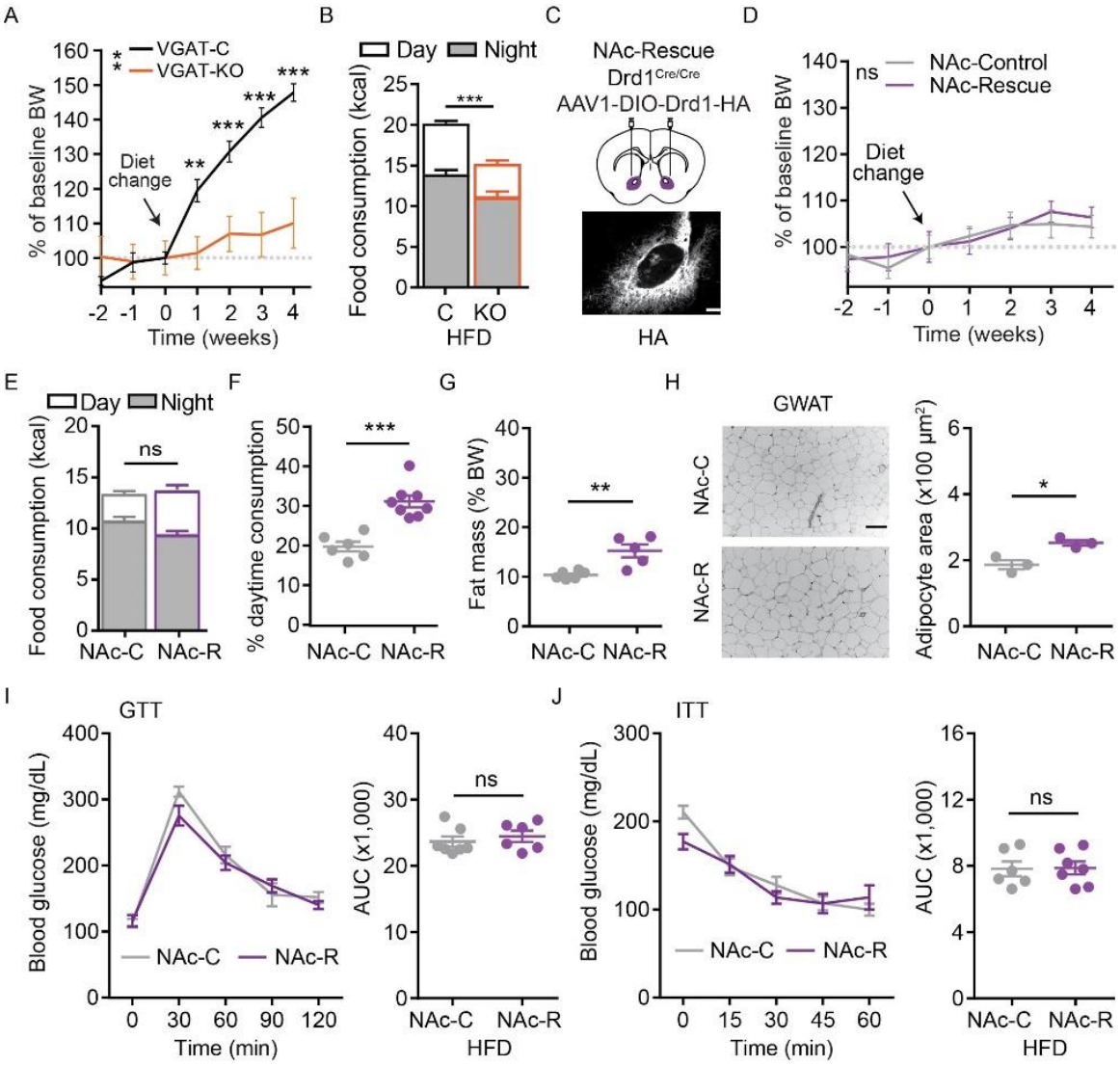

Figure 4. Selective Re-expression of Drd1 Within the NAc of Drd1-KO Mice Partially Rescues HFD Induced Phenotypes Excluding Obesity. (A) Percent body weight (BW) change relative to week 0 for $VGAT^{+/+}$;floxed-Drd1 (VGAT-C), and $VGAT^{Cre/+}$;floxed-Drd1 (VGAT-KO) mice following access to high fat/low sugar diet. Repeated-measures two-way ANOVA with Bonferroni post hoc comparison, n = 7-16/group; $F_{genotype}(1,21) = 10.44$, $p = 0.004$ (**Michael Sidikpramana, Andrew Steele**). (B) Daily total calorie consumption of VGAT-C and VGAT-KO mice on HFD. Light- (white) and dark-phase (grey) consumption are segregated for clarity. Student's two tailed t-test, n = 7-16/group (**Michael Sidikpramana, Andrew Steele**). (C) Top: Schematic diagram illustrating NAc bilateral injection of AAV1-

DIO-D1R-HA or AAV1-ChR2-YFP injection in KO (Drd1$^{cre/cre}$) mice. Bottom: Anti-HA immunohistochemical labeling within the NAc of D1R-HA expressing rescue mice. Scale bar = 100 um (**Qijun Tang**). (D) Percent BW change relative to week 0 for NAc-control (NAc-C) and NAc-rescue (NAc-R) mice on HFD. Repeated-measures two-way ANOVA with Bonferroni post hoc comparison, n = 6-8/group (**Qijun Tang**). (E) Daily total calorie consumption of NAc-control (NAc-C) and NAc-rescue (NAc-R) mice on HFD. Light- (white) and dark-phase (grey) consumption are segregated for clarity. Student's two tailed t-test, n = 6-8/group (**Qijun Tang**). (F) Percent of total daily food intake consumed during the light-phase for groups in (E). Student's two tailed t-test, n = 6-8/group (**Qijun Tang**). (G) Fat mass as percent of BW for groups in (E). Student's two tailed t-test, n = 5-6/group. (H) Representative GWAT histology with H&E stain (left) and quantification of GWAT adipocyte area (right) for groups in (E) (**Aarti Purohit**). Scale bar = 100 μm. Student's two tailed t-test, n = 3/group. (I) Blood glucose levels over time (left; repeated-measures two-way ANOVA with Bonferroni post hoc comparison, n = 6-7/group) and area under the curve (AUC) quantification (right; Student's two tailed t-test, n = 6-7/group) during glucose tolerance test (GTT) for groups in (E) (**Qijun Tang**). (J) Blood glucose levels over time (left; repeated-measures two-way ANOVA with Bonferroni post hoc comparison, n = 6-7/group) and AUC quantification (Student's two tailed t-test, n = 6-7/group) during insulin tolerance test (ITT) for groups in (E) (**Qijun Tang**). Data in all panels are represented as mean ± SEM. *p < 0.05, **p < 0.01, ***p < 0.001, ns = no significance.

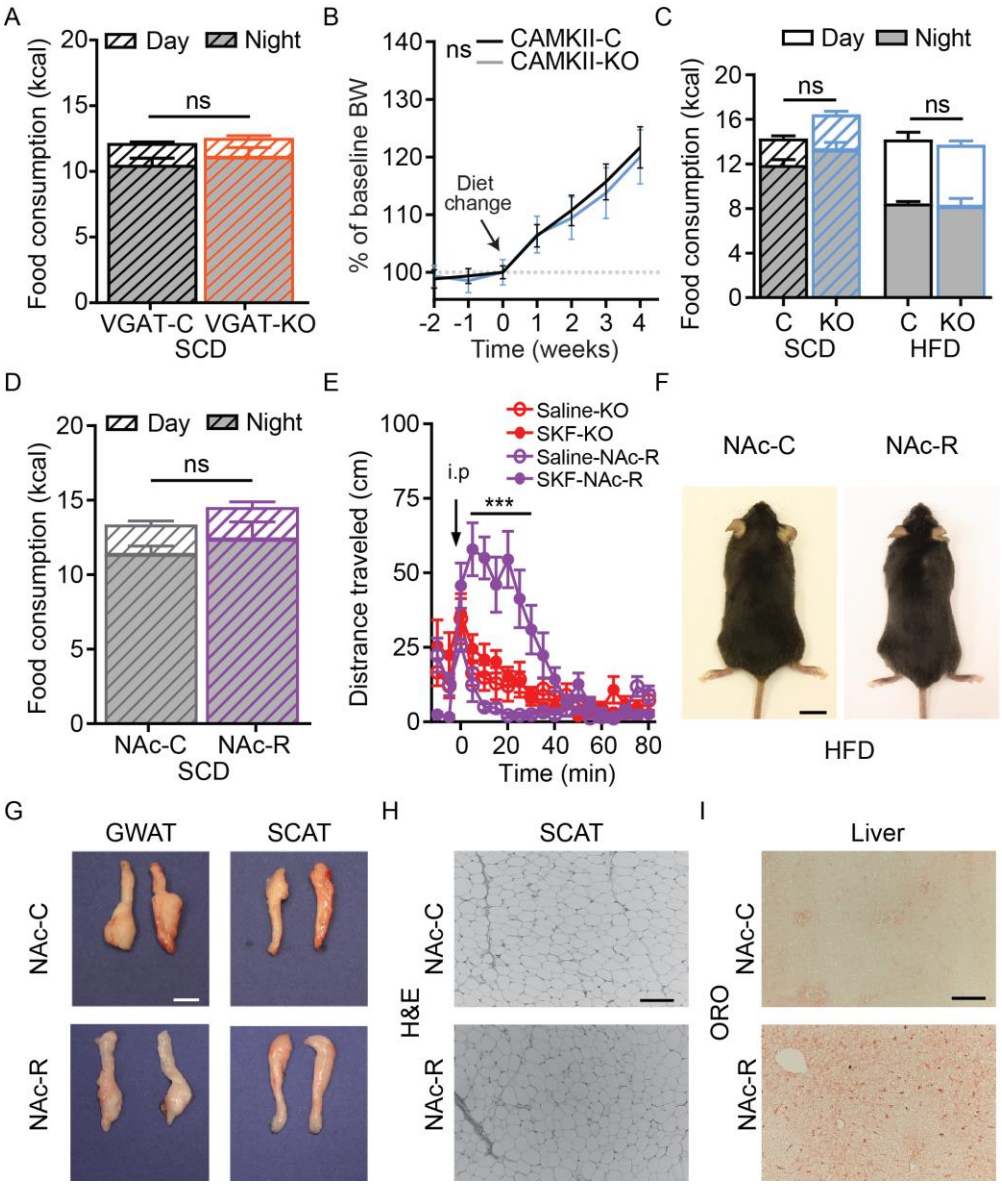

Figure S4. (related to Figure 4) Additional Results Illustrating the Resistance of NAc-rescue Mice to HFD Induced Obesity. (A) Daily total calorie consumption of VGAT-C and VGAT-KO mice on SCD. Light- (white) and dark-phase (grey) consumption are segregated for clarity. Student's two tailed t-test, n = 7-16/group (**Qijun Tang**). (B) Percent body weight (BW) change relative to week 0 for CAMKII$^{+/+}$;floxed-Drd1 (CAMKII-C) and CAMKII$^{Cre/+}$;floxed-Drd1 (CAMKII-KO) mice on HFD. Repeated-measures two-way ANOVA with Bonferroni post hoc comparison, n = 10-11/group (**Michael Sidikpramana, Andrew Steele**). (C) Daily total calorie consumption of CAMKII-C and CAMKII-KO mice on SCD or HFD.

Light- (white) and dark-phase (grey) consumption are segregated for clarity. One-way ANOVA with Bonferroni post hoc comparison, n = 9-11/group (**Michael Sidikpramana, Andrew Steele**). (D) Daily total calorie consumption of NAc-control (NAc-C) and NAc-rescue (NAc-R) mice on SCD. Student's two tailed unpaired t-test, n = 6-8/group (**Qijun Tang**). (E) Distance travelled by NAc-rescue (NAc-R) or KO control mice following vehicle (saline) or D1R agonist SKF-81297 administration (i.p.). Repeated-measures three-way ANOVA with Bonferroni post hoc comparison, n = 7-8/group; $F_{treatment}(1,13) = 16.84$, $p = 0.001$. Statistical significance between SKF-NAc-R and Saline-NAc-R is depicted in the figure (**Qijun Tang**). (F) Representative mouse images of NAc-control (NAc-C) or NAc-rescue (NAc-R) following the HFD feeding paradigm in Figure 1A. Scale bar = 1 cm (**Qijun Tang**). (G) Representative images of dissected GWAT (left) and SCAT (right) for groups in (F). Scale bar = 1 cm (**Qijun Tang, Qi Zhang**). (H) Representative SCAT histology (H&E) for groups in (F), scale bar = 100 μm (**Qijun Tang**). (I) Representative liver histology using Oil-red-O for groups in (F) where hepatic lipid content stains as red. Scale bar = 100 μm. Data in all panels are represented as mean ± SEM. *p < 0.05, **p < 0.01, ***p < 0.001, ns = no significance (**Qijun Tang**).

HFD-induced Increase in the Behavioral Circadian Rhythm Period is Drd1 Dependent

The observed temporal change of feeding pattern in WT-HFD also suggests a disruption in circadian rhythmicity. In addition to alterations in peripheral circadian clock gene expression, access to HFD lengthens centrally regulated circadian activity rhythms in constant darkness (DD) (Kohsaka et al., 2007). While no difference in free running period of wheel running activity rhythms between WT and KO mice was observed on SCD (Grippo et al., 2017), we sought to identify whether HFD-induced disruption of behavioral rhythms is dependent on Drd1

signaling. Following prolonged access to HFD, KO mice maintained a similar free-running period as WT-SCD animals, that was significantly shorter than WT-HFD mice (WT-SCD: 23.66 ± 0.05 h; WT-HFD: 23.87 ± 0.3 h; KO-HFD: 23.65 ± 0.03 h. One-way ANOVA, $p < 0.001$) (Figures 5A-C). Additionally, we observed a rapid, diet-dependent change in the free-running period in WT-HFD mice, which decreases following a switch to SCD (Figure 5SA). The previously lengthened circadian period could be restored upon reintroduction of HFD (HFD 1: 23.88 ± 0.04 h; SCD 1: 23.69 ± 0.05 h; HFD 2: 23.85 ± 0.06 h; Figures 5SA and 5SB). Resistance to HFD induced period lengthening in KO mice suggests a role for Drd1 signaling in disruption of central circadian rhythms during dietary challenge.

HFD Increases DA Turnover within the SCN

Since the HFD-induced circadian period lengthening is Drd1-dependent, we sought to determine whether acute exposure to HFD increases DA tone in the SCN, which would facilitate disrupted circadian rhythmicity. To address this we determined the DOPAC and DA content from hypothalamic tissue punches containing the SCN in WT animals following one-hour access to either SCD or HFD (Figure S5C). The DOPAC/DA ratio is an estimate of DA turnover reflecting active DA release and catabolism, which rapidly increases within the NAc in response to HFD (Carlin et al., 2013; Davis et al., 2008). WT mice given one hour access to HFD at ZT 6 consumed significantly more food than SCD controls (SCD: 0.27 ± 0.08 kcal; HFD: 5.41 ± 0.50 kcal, Student's two-tailed t-test, $p<0.001$). Accordingly, the hypothalamic DOPAC/DA ratio of animals fed HFD were also

elevated (SCD: 0.24 ± 0.02 ; HFD: 0.35 ± 0.02, n = 7/group, Student's t-test p = 0.0093; Figure 5D). Thus, consumption of HFD increases DA turnover within or near the SCN, providing evidence for the direct influence of DA tone on the central circadian clock in response to rewarding food.

Rewarding foods have been shown to reduce the duration of behavioral phase shift in response to photic stimulation and modulate circadian entrainment, as daily presentation of palatable food entrains circadian rhythms to the time of food availability, (Mendoza et al., 2005; Mendoza et al., 2010; Mendoza et al., 2008). Since KO mice fail to show HFD-induced circadian period lengthening, we evaluated the consequence of long-term HFD access on the central circadian clock by quantification of two rhythmic molecular markers within the SCN, c-Fos and Per2, at antiphasic time points (ZT 1 and 13). The immediate early gene c-FOS has a peak expression during the day and a trough at night, while PER2 displays the reverse expression pattern (Fonken et al., 2013; Sumova et al., 2000). We detected a significant time of day effect in both c-FOS and PER2 expression, however, we observed no diet or genotype effect (Figures S5D and Figure S5F). These data further emphasize that while acute access to HFD elevates DA turnover within the SCN, prolonged access to HFD does not significantly disrupt the peak-to-trough expression pattern of circadian regulated proteins.

Increased Drd1 Signaling Reduces Neuronal Firing Rate in the SCN

To resolve the dichotomy between the increased DA turnover in the SCN with the absence of change in circadian gene expression patterns, we evaluated the impact

of increased Drd1 signaling on neuronal activity within the SCN. Thus we determined whether dopaminergic input modulates the firing rate of SCN neurons by incubating acute brain slices from WT mice with the selective Drd1 agonist (SKF-81279; 5μM) and performed loose cell attached recordings at ZT 8-11 (day) and ZT 14-17 (night). In these experiments, we observed that incubation with SKF-81297 significantly decreased the firing rate of neurons within the SCN during both phases (Day: DMSO 4.3 ± 0.4 Hz; Day: SKF 3.2 ± 0.4 Hz; Night: DMSO 2.6 ± 0.4 Hz; Night: SKF 1.5 ± 0.4 Hz, two-way ANOVA, $p = 0.01$) (Figure 5E). Since Drd1 is a G_s-coupled GPCR, and the majority of SCN neurons are GABAergic (Moore and Speh, 1993; Okamura et al., 1989) (Figure S5F), we hypothesized that stimulation of Drd1-expressing SCN neurons attenuates the overall firing rate of the local microcircuitry. Therefore, we performed whole cell current clamp recordings from the SCN of Drd1-Cre mice injected with an AAV2 that expresses ChR2 Cre-dependently (AAV-DIO-ChR2-YFP; Figure 5F). While 26% of recorded cells (n=8 cells) had no response to light stimulation of the SCN, 35% of the cells depolarized within 1-2 ms of the stimulation (n = 11 cells). Additionally, 35% of the SCN-neurons hyperpolarized following a minimum of 4 ms delay (n = 11 cells; Figures 5G-H), while one neuron displayed both light-induced action potentials and post-stimulation hyperpolarization (Figure S5H). Perfusion of a $GABA_A$ channel inhibitor, picrotoxin (PTX; 100 μM), diminished the amplitude of the inhibitory responses, confirming that they are ChR2-driven postsynaptic currents (Figure 5J and 5K). These data identify a local inhibitory response to Drd1-SCN neuron

activation, revealing the possibility for elevated DA tone to directly modulate SCN neuron firing rate.

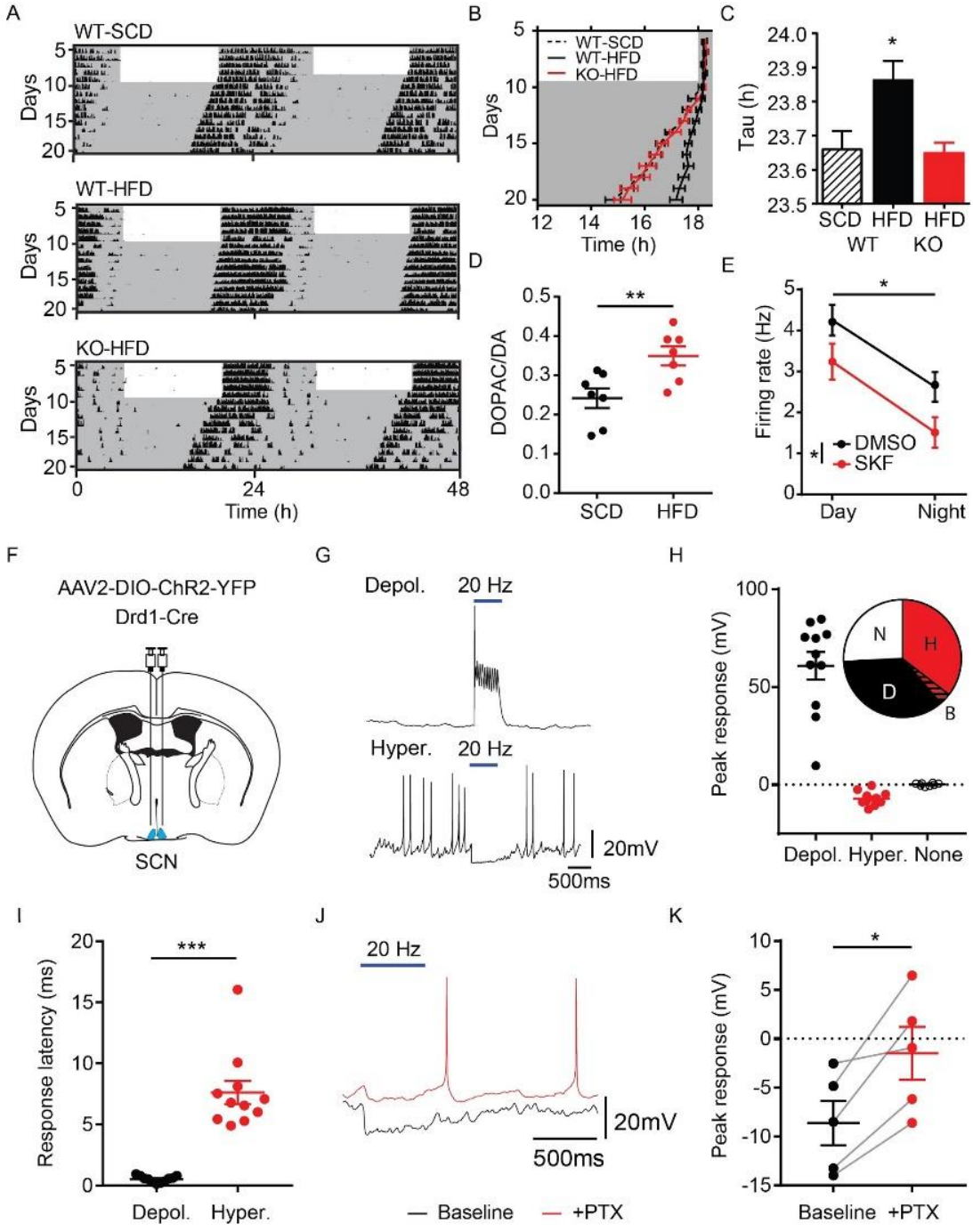

Figure 5 Elevated Drd1 Signaling Reduces Neuronal Firing Rate in the SCN .

(A) Representative double-plotted actogram of wheel running activity in constant

darkness (DD) for WT-SCD (top), WT-HFD (middle) and KO-HFD (bottom) mice. White and grey background indicates the light and dark phase of the LD cycle, respectively. (B) Average daily activity onset time for groups in (A). Repeated-measures two-way ANOVA with Bonferroni post hoc comparison, n = 7-10/group; $F_{genotype}(2,21) = 15.81$, $p < 0.001$. (C) Average DD free running period (Tau) for groups in (A). One-way ANOVA with Bonferroni post hoc comparison, n = 6-9/group; $F(2,20) = 10.92$, $p < 0.001$. (D) Quantification of dopamine turnover (DOPAC/DA ratio) following one-hour SCD or HFD exposure in hypothalamic tissue punches containing the SCN. Student's two tailed t-test, n = 7/group (**Ryan Grippo, Nidhi Purohit, Jay Hirsh**). (E) Mean firing rate of cell attached SCN neuron recordings following 5μM SKF-81297 incubation at ZT 8-11 (Day) or ZT 14-17 (Night) . Two-way ANOVA, n = 13-26/group; $F_{time}(1,70) = 16.9$, $p < 0.001$, $F_{treatment}(1,70) = 6.75$, $p = 0.01$ (**Sean Chadwick**). (F) Schematic diagram illustrating the bilateral AAV2-DIO-ChR2-YFP injection in the SCN of $Drd1^{cre/+}$ mice. (G) Representative traces from whole-cell current-clamp recordings. SCN neurons exhibit both depolarizing (top) and hyperpolarizing (bottom; Hyper.) responses to 20 Hz blue light stimulation (**Sean Chadwick**). (H) ChR2 stimulation induced average peak responses for depolarizing (Depol.), hyperpolarizing (Hyper.) and non-responsive (None) neurons. Distribution of recorded responses are depicted in the inset. B indicates one cell exhibiting both responses (see Figure S5H) (**Sean Chadwick**). (I) Response latency of each group in (H). Student's two tailed t-test, n = 11/group. (J) Representative traces from whole-cell current-clamp recordings for ChR2 stimulation induced postsynaptic responses before and after 5 min 100 μM PTX incubation (**Sean Chadwick**). (K) ChR2 stimulation induced average peak responses before and after PTX incubation. Student's two tailed

paired t-test, n = 5/group. Data in all panels are represented as mean ± SEM. *p < 0.05, **p < 0.01, ***p < 0.001, ns = no significance (**Sean Chadwick**).

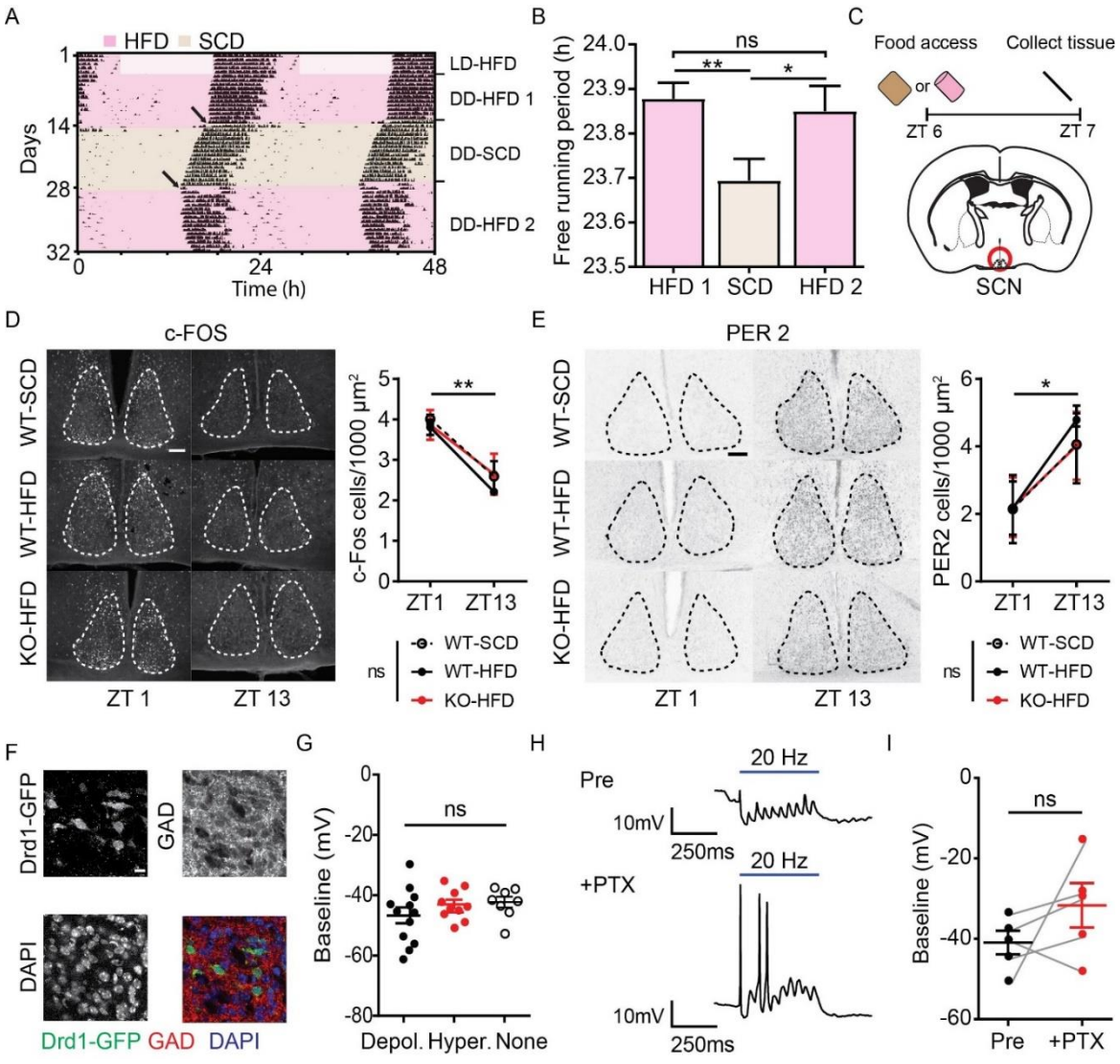

Figure S5. (related to Figure 5) HFD Lengthens the Free Running Period but Does not Dampen the Molecular Oscillation Amplitude. (A) Representative double plotted actogram of wheel running activity for WT-HFD mice exposed to dietary change in DD. The first two weeks following LD entrainment are labeled as DD-HFD 1. Diet change to SCD (DD-SCD) for two weeks preceded the reintroduction of HFD (DD-HFD-2) for an additional two weeks. Tan shading represents SCD and pink shading represents HFD access in DD. Arrows indicate time of the day of diet and cage change. (B) Average free running period in DD

during periods described in (A). Repeated-measures one-way ANOVA with Bonferroni post hoc comparison, n = 5; F(2,8) = 12.92, p = 0.003. (C) Schematic of food access paradigm (top) and location of tissue punch collection (bottom) for HPLC analysis of DA turnover for experiments conducted in Figure 5D. (D) Left: representative images for SCN c-Fos staining at indicated time points. Region of quantification is depicted by dotted lines. Scale bar = 100 μm. Right: Quantification of c-FOS-positive cell density in SCN at day (ZT1) or night (ZT13). Two-way ANOVA, n = 3/group; $F_{time}(1,6) = 20.71$, p = 0.004 (**Qijun Tang, Krystyna Cios**). (E) Left: representative images for SCN Per2 staining at indicated time points. Region of quantification is depicted by dotted lines. Scale bar = 100 um. Right: Quantification of PER2-positive cell density in SCN at day (ZT1) or night (ZT13). Two-way ANOVA, n = 3/group; $F_{time}(1,6) = 10.06$, p = 0.019 (**Qijun Tang, Krystyna Cios**). (F) Representative confocal image of the colocalization for DAPI, GAD65/67 and Drd1 promoter driven cre-GFP in SCN. Scale bar = 10 μm (**Qijun Tang**). (G) Baseline membrane potential of three types of neurons described in Figure 5H) before light stimulation. One-way ANOVA, n = 8-12/group (**Sean Chadwick**). (H) Example trace for one SCN neuron that has both hyperpolarizing and depolarizing response to light stimulation from Figure 5H. Top: Before picrotoxin incubation (Pre), the light stimulation induces hyperpolarization with reoccurring depolarization events time-locked to each light pulse without exhibiting action potentials. Bottom: Following incubation of picrotoxin (+PTX), action potential light stimulation evokes action potentials (**Sean Chadwick**). (I) Baseline membrane potential of neurons that hyperpolarize in response to ChR2 stimulation, before (Pre) or after picrotoxin incubation (+PTX). Student's two tailed paired t-test, n = 5/group. Data in all panels are represented as mean ± SEM, or individual values with mean ± SEM. *p < 0.05, **p < 0.01, ***p < 0.001, ns = no significance (**Sean Chadwick**).

Re-expression of Drd1 Within the SCN Restores Diet-induced Obesity

Although HFD does not significantly dampen circadian gene expression within the SCN (Figure S4), we observed an increase in DA turnover within the SCN in

response to HFD and dampened electrical firing rate in response to Drd1 agonist treatment (Figure 5). These data suggest that SCN-Drd1 signaling may play a prominent role in the increased daytime food intake and obesity observed in WT-HFD mice (Figure 1). To confirm whether this GABAergic population of neurons is sufficient to establish HFD-induced obesity, we virally re-introduced Drd1 within the central circadian pacemaker by delivering Drd1-HA to the SCN of KO mice (SCN-Rescue) (Grippo et al., 2017; McNulty et al., 1998). Mice injected with AAV1 expressing ChR2-eYFP were used as controls (SCN-Control). HFD-induced obesity and the subsequent metabolic consequences were completely restored in SCN-Rescue animals as we observed a significant increase in body weight, food consumption, adipose mass, adipocyte hypertrophy, hepatic steatosis, glucose insensitivity, and insulin intolerance relative to SCN-Controls (Figure 6). SCN-Rescue mice maintained a predominantly nocturnal pattern of food consumption on SCD, while HFD significantly increased daytime consumption (SCD: 20.3 ± 3.1%; HFD: 37.4 ± 2.3%; Student's two tailed t-test, $p<0.001$) (Figures 6D, Figure 6E, and Figure S6A). Most notably, nighttime consumption was not reduced on HFD, leading to an overall increase in food consumption and substantial weight gain (Figure 6D). Unlike restoration in the NAc, genetic reconstruction of Drd1

expression within the SCN of KO mice enabled out-of-phase overconsumption of HFD leading to all of the metabolic consequences observed in WT-HFD mice.

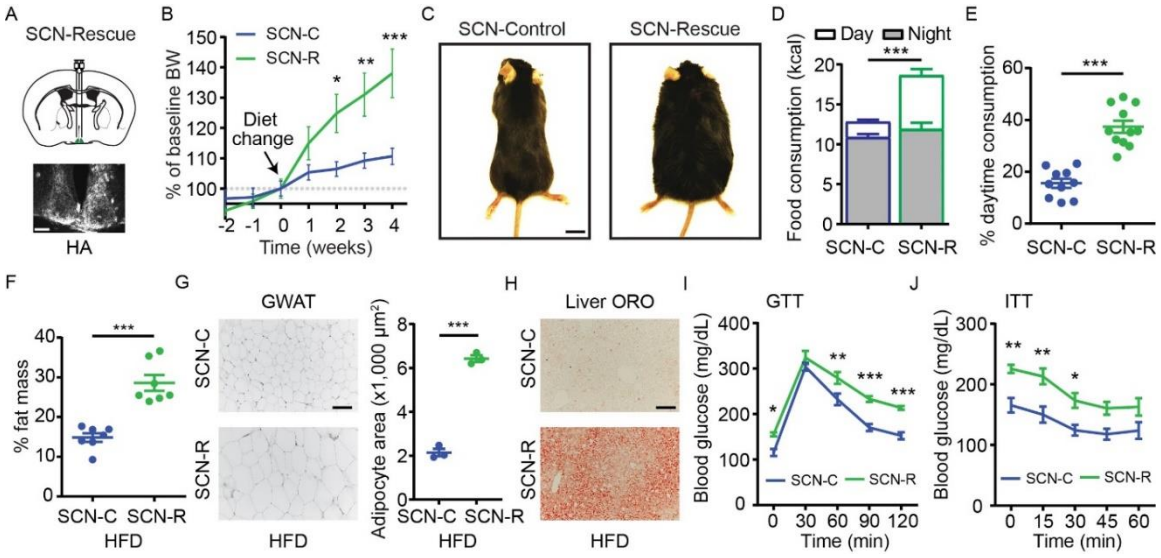

Figure 6 Re-expression of Drd1 Within the SCN of KO Mice Restores HFD Induced Obesity. (A) Top: Schematic diagram illustrating AAV1-DIO-D1R-HA SCN bilateral injection in the Drd1-KO ($Drd1^{cre/cre}$) mice. Bottom: Anti-HA fluorescent immunohistochemistry staining within the SCN of D1R-HA expressing rescue mice. Scale bar = 100 μm. (B) Percent body weight (BW) change relative to week 0 for SCN-control (SCN-C) and SCN-rescue (SCN-R) mice on HFD. Repeated-measures two-way ANOVA with Bonferroni post hoc comparison, n = 10-12/group; $F_{genotype}(1,20) = 4.478$, $p = 0.047$. (C) Representative mouse images of SCN-control (SCN-C) and SCN-rescue (SCN-R) mice following the feeding paradigm in Figure 1A. Scale bar = 1 cm. (D) Daily total calorie consumption of SCN-control (SCN-C) and SCN-rescue (SCN-R) mice on HFD. Light- (white) and dark-phase (grey) consumption are segregated for clarity. Student's two tailed t-test, n = 10-11/group. (E) Percent of total daily food intake consumed during the light-phase for groups in (D). Student's two tailed t-test, n = 10-11/group. (F) Fat mass as percent of BW for groups in (D). Student's two tailed t-test, n = 7/group. (G) Left: representative GWAT histology (H&E) for groups in (D). Scale bar = 100

μm. Right: quantification of GWAT adipocyte area. Student's two tailed t-test, n = 3/group (**Aarti Purohit**). (H) Representative liver histology using Oil-red-O (ORO) for groups in (D) where hepatic lipid content stains as red. Scale bar = 100 μm (**Qijun Tang**). (I) Blood glucose levels over time during glucose tolerance test (GTT) for groups in (D). Repeated-measures two-way ANOVA with Bonferroni post hoc comparison, n = 8-9/group; $F_{genotype}(1,15) = 27.05$, $p < 0.001$ (**Qi Zhang**). (J) Blood glucose levels over time during insulin tolerance test (ITT) for groups in (D). Repeated-measures two-way ANOVA with Bonferroni post hoc comparison, n = 6-8/group; $F_{genotype}(1,12) = 11.2$, $p = 0.006$. Data are represented as mean ± SEM, or individual values with mean ± SEM. *p < 0.05, **p < 0.01, ***p < 0.001, ns = no significance (**Qi Zhang**)

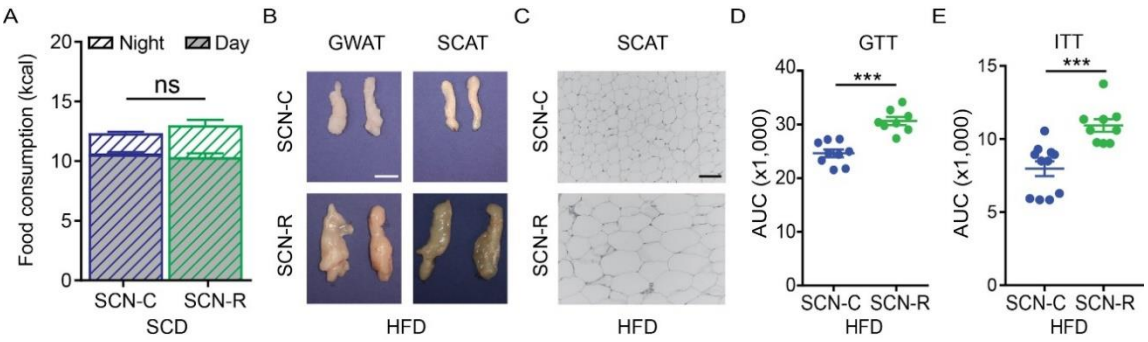

Figure S6. (related to Figure 6) Additional Results Illustrating HFD Induced Obesity in SCN-Rescue Mice. (A) Daily total calorie consumption of SCN-control (SCN-C) and SCN-rescue (SCN-R) mice on SCD. Light- (white) and dark-phase (grey) consumption are segregated for clarity. Student's two tailed t-test, n = 8-10/group. (B) Representative images of dissected GWAT (left) and SCAT (right) following the HFD feeding paradigm in Figure 1A. Scale bar = 1 cm (**Qijun Tang, Qi Zhang**). (C) Representative SCAT H&E histology for groups in (B). Scale bar = 100 μm (**Qijun Tang**). (D) Area under the curve (AUC) for GTT in figure 6I. Student's two tailed t-test, n = 8-9/group (**Qi Zhang**). (E) Area under the curve (AUC) for ITT in figure 6J. Student's two tailed t-test, n = 6-8/group. Data are represented as mean ± SEM. *p < 0.05, **p < 0.01, ***p < 0.001, ns = no significance (**Qi Zhang**).

Figure	Condition (N number)	Body Weight (g)	Liver		GWAT		SCAT	
			Mass (g)	Percent of BW (%)	Mass (g)	Percent of BW (%)	Mass (g)	Percent of BW (%)
Figure 2	WT-SCD (12)	28.97±0.47	1.41±0.05	4.86±0.15	0.50±0.04	1.69±0.10	0.36±0.02	1.23±0.05
	KO-SCD (12)	23.56±0.26	1.22±0.04	5.18±0.17	0.30±0.02	1.28±0.08	0.27±0.01	1.15±0.05
	WT-HFD (12)	34.57±0.91	1.40±0.05	4.06±0.11	1.62±0.12	4.64±0.25	0.99±0.08	2.83±0.18
	KO-HFD (12)	24.64±0.39	1.01±0.02	4.11±0.11	0.47±0.03	1.89±0.12	0.37±0.02	1.51±0.08
Post-hoc comparisons		sig.	sig.	sig.	sig.	sig.	sig.	sig.
WT-SCD vs KO-SCD		***	*	ns	ns	ns	ns	ns
WT-SCD vs WT-HFD		***	ns	**	***	***	***	***
WT-SCD vs KO-HFD		***	***	**	ns	ns	ns	ns
KO-SCD vs WT-HFD		***	*	***	***	***	***	***
KO-SCD vs KO-HFD		ns	**	***	ns	*	ns	ns
WT-HFD vs d KO-HFD		***	***	ns	***	***	***	***
Figure 5	NAc-Control (6)	24.85±0.46	1.00±0.05	4.04±0.19	0.42±0.03	1.69±0.08	0.38±0.02	1.51±0.08
	NAc-Rescue (8)	25.62±0.58	0.99±0.06	3.88±0.22	0.6±0.04	2.35±0.13	0.44±0.03	1.69±0.08
	SCN-Control (10)	25.07±0.64	0.98±0.05	3.92±0.15	0.58±0.05	2.27±0.16	0.49±0.04	1.93±0.12
	SCN-Rescue (8)	38.34±2.32	1.65±0.22	4.22±0.37	1.96±0.22	5.04±0.36	1.72±0.26	4.33±0.46
Post-hoc comparisons		sig.	sig.	sig.	sig.	sig.	sig.	sig.
NAc-C vs SCN-C		ns	ns	ns	ns	ns	ns	ns
NAc-C vs NAc-R		ns	ns	ns	ns	ns	ns	ns
NAc-C vs SCN-R		***	***	ns	***	***	***	***
SCN-C vs NAc-R		ns	ns	ns	ns	ns	ns	ns
SCN-C vs SCN-R		***	***	ns	***	***	***	***
NAc-R vs SCN-R		***	***	ns	***	***	***	***

Table 1: (related to Figure 1, Figure 4 and Figure 6) Summary and Statistics of Body, Liver, GWAT and SCAT Weight. Data are represented as mean ± SEM. Two-way ANOVA with Bonferroni post hoc comparison. (n) number of mice are indicated in the table. *p < 0.05, **p < 0.01, ***p < 0.001, ns = no significance (**Qijun Tang, Qi Zhang, Ryan Grippo**).

Discussion

Robust circadian rhythms are an important determinant of metabolic fitness. Aberrant light conditions and food consumption outside of mealtimes disproportionately contribute to energy storage, obesity and metabolic disease in rodents and humans (Fonken et al., 2013; Gill and Panda, 2015; Turek et al., 2005). Diets rich in fat and sugar increase out-of-phase food consumption,

however, the neuronal correlates of meal timing have remained elusive. Here, we identify a novel mechanism by which energy-rich foods dysregulate properly timed consumption by interfering with neural activity of central circadian pacemaker within the SCN. This modulation results in increased foraging between meals and overconsumption leading to obesity. We observe that Drd1 expression is necessary for HFD-induced rest-phase hyperphagia, amplitude reduction in circadian oscillations of metabolic rhythms, lengthening of behavioral circadian period, and obesity. We also demonstrate that SCN DA turnover increases in response to HFD, while stimulation of the Drd1 signaling in the SCN dampens the overall activity of this nucleus. Lastly, Drd1 expression only within the SCN is sufficient to promote HFD overconsumption and metabolic disease. Therefore, we hypothesize that elevated DA during access to HFD increases out-of-phase foraging and overconsumption by Drd1 mediated reduction in SCN activity (Figure 7).

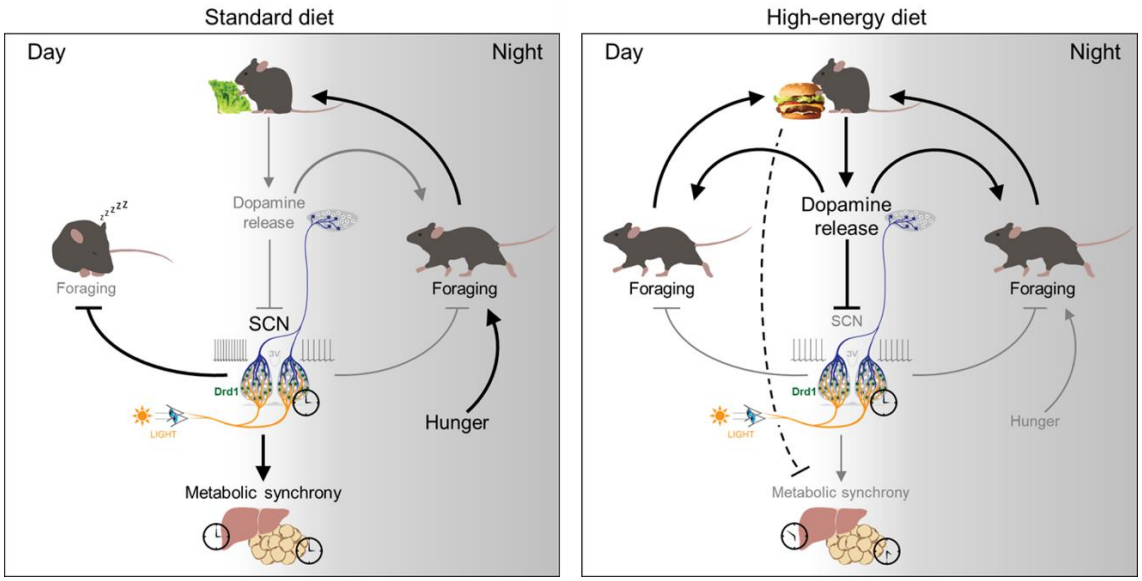

Figure 7. High-energy diet drives ectopic dopaminergic tone in the SCN, resulting in out-of-phase feeding. As nocturnal animals, mice eat 80% of their food during the night when chronically exposed to a healthy diet (left). In contrast, mice on high calorie diet eat roughly 40% of their food during the day. Rewarding high-energy foods induce dopamine release. The increase in SCN dopaminergic tone attenuates overall SCN excitability via Drd1 signaling resulting in: **1.** Increased out-of-phase daytime foraging, **2.** Overconsumption of calories, **3.** Desynchrony of the peripheral clock, **4.** Obesity and metabolic disorder (right). Remarkably, loss of Drd1 signaling in the SCN is sufficient to protect against all of the feeding and metabolic defects associated with chronic exposure to high calorie food (**Ali Güler**).

Diet regimens that involve time restricted feeding are growing in popularity since they attenuate body weight gain and significantly improve metabolic profiles in rodents and humans (Gabel et al., 2018; Hatori et al., 2012; Sutton et al., 2018). Our findings that animals lacking Drd1-signaling in the SCN self-restrict energy-rich food consumption to their active-phase and are protected from obesity, provide much needed insight to how rewarding foods interfere with meal timing and diet adherence. Accordingly, DA, beyond providing hedonistic signal via the

mesolimbic circuit, also hinders anorexic output from the central circadian pacemaker between mealtimes contributing to excessive calorie intake.

Consumption of food beyond regular activity periods generates peripheral circadian desynchrony (Hatori et al., 2012; Kohsaka et al., 2007). We confirmed this previously reported dampening in the amplitude of circadian clock gene expression in adipose tissue of WT-HFD mice compared to WT-SCD controls (Figure 3). However, the effect was blunted in the liver samples in our study, likely due to the shorter duration of HFD access, and differences in the diet composition (Figure 3; (Hatori et al., 2012; Kohsaka et al., 2007). Surprisingly, despite maintaining a lean phenotype, KO-HFD mice show similar circadian gene expression across most time points when compared to WT-HFD mice (Figure 3, Table S1). This indicates that dampened peripheral clock amplitude does not confer an obese phenotype and the observed weight-gain likely precedes the development of peripheral circadian desynchrony, which subsequently compounds the detrimental effects of overnutrition.

In addition to alterations of liver and adipose function, consumption of HFD induces significant changes to the gut microbiome in rodents and humans (David et al., 2014). Gut dysbiosis increasingly has been implicated as a contributing factor to diet-induced obesity, insulin resistance and type 2 diabetes (Baothman et al., 2016; Hartstra et al., 2015; Turnbaugh et al., 2006). Timing of food consumption in TRF has been found to alter circadian cycling of species abundance within the gut microbiome when evaluated at subphylum levels (Zarrinpar et al., 2014). Similar to other reports (Hildebrandt et al., 2009), we

observed that changes in fecal microbial composition are primarily dependent on the diet and not the body composition, as dictated by genotype, of our experimental animals (Figure 3). Additionally, the time of sample collection (day vs night) has a similar effect on microbiome diversity in both WT and KO mice following access to HFD, despite the differences in food intake patterns (Figures 2 and Figure 3). Our data suggest that, rather than the microbiome composition itself, overconsumption and the increased permeability of the intestinal barrier contribute to the negative consequences of a dysbiotic microbiome on insulin resistance and hepatic steatosis (Caricilli and Saad, 2013). Given that WT and KO animals on HFD maintain a similar microbiome and rhythmicity of peripheral clock gene expression, the obesity resistant phenotype of Drd1-ablated animals is primarily driven by the central processes that control the circadian phase and amount of food consumed.

To demonstrate the central cause of HFD overconsumption, we initially identified that genetic ablation of Drd1 from GABAergic cells completely recapitulated the obesity-resistant phenotype of germline KO mice (Figure 4). Surprisingly, re-expression of Drd1 signaling within the NAc fails to induce obesity in KO mice despite increasing daytime HFD consumption (Figure 4). However, these animals, unlike WT and SCN-Rescue mice, compensate for increased daytime food intake by reducing their nighttime consumption and, therefore, maintain twenty-four hour HFD intake at a level similar to the KO mice (Figure 1 and Figure 6). This pattern of consumption in NAc-Rescue mice leads to a moderate increase in adiposity without significant weight gain or alteration in glucose and insulin responsiveness (Figure 4). By contrast, re-expression of Drd1

within the SCN increases daytime foraging, without significantly disrupting feeding at night, resulting in daily overconsumption (Figure 6). We postulate that the restoration of Drd1-dependent DA signaling within the NAc may increase the incentive to consume palatable foods (Berridge and Robinson, 1998), but does not significantly impact energy homeostasis regulation. While our observations reveal the critical role of the Drd1-SCN signaling in energy balance during HFD consumption, it also suggests that increased daytime consumption without an increase in overall energy intake is insufficient for significant weight gain.

There has been a recent resurgence of investigation into the role of DA and rewarding foods on peripheral and central circadian rhythms (Korshunov et al., 2017; Mendoza, 2019; Mendoza and Challet, 2014). Although pharmacological enhancement of Drd1 signaling and diet-induced changes in the feeding pattern perturb the cellular metabolic outputs of the SCN (Figure S4; (Dyar et al., 2018; Rivkees and Lachowicz, 1997), its molecular clock components remain largely unaltered (Pendergast et al., 2013). However, consumption of HFD increases the period length of endogenous activity rhythms, which is driven by the period of Drd1-positive SCN cells (Figure 4; (Kohsaka et al., 2007; Smyllie et al., 2016). Accordingly, Drd1 agonist treatment lengthens the period of *Per2* expression in SCN slices (Landgraf et al., 2016), implicating Drd1-SCN signaling in HFD-induced period lengthening. In line with these reports, free-running period of wheel running activity remains unchanged in Drd1-KO mice following free access to HFD diet (Figure 5).

A vast majority of the SCN neurons are GABAergic and exhibit synchronous neural activity that fluctuates across the day:night cycle (Moore and Speh, 1993). Their activity is high during the day, generating an inhibitory tone within the SCN and its projection sites throughout the hypothalamus, thalamus, and basal forebrain (Kalsbeek et al., 2006). In mice, this diurnal activity suppresses behavioral responses usually observed during the nighttime such as feeding and foraging (Schaap et al., 2003). We discovered that the elevated dopaminergic signaling in response to acute HFD consumption increases DA turnover within in the SCN (Figure 6). Since restoration of Drd1 expression within the SCN is sufficient for development of obesity on HFD, it is evident that diet impacts the SCN function, despite an absence of a change in its molecular clockwork machinery. However, we observed that increased SCN-Drd1 signaling or optogenetic stimulation of Drd1-SCN neurons reduces neuronal activity within the SCN or inhibits postsynaptic SCN neurons, respectively. Therefore, we postulate that in response to rewarding foods, increased DA tone decreases the overall excitability within the SCN . This decrease in activity mimics the nighttime SCN neuronal activity, which is permissive for foraging, leading to overconsumption of available energy-rich foods. The precise downstream targets of the SCN-Drd1 circuit will be the focus of future investigations seeking to uncover how circadian rhythms integrate with the orexigenic signals at the neurocircuit level.

Materials and Methods

Animals

All animal care experiments were conducted in concordance with University of Virginia Institutional Animal Care and Use Committee (IACUC). Animals were housed in a temperature and humidity controlled vivarium (22-24°C, ~40% humidity) until experimental use on a 12-hour:12-hour light:dark (LD) cycle and were provided with food and water ad libitum and cotton nesting material (Ancare, Bellmore, NY) All experiments were conducted with age matched, male controls ranging from 12-14 weeks of age at the onset of food intake experiments. In addition to wild-type C57BL6/J mice, the following mouse lines were used: *Drd1a*$^{Cre/+}$ (Drd1-Cre) (Heusner et al., 2008), CamKIIa-cre$^{T29\text{-}1Stl/}$J (Tsien et al., 1996), Drd1$^{tm2.1Stl}$/J (Floxed-Drd1) (Sarinana and Tonegawa, 2016), Drd1^{tm1Jcd}/J (Drd1 -/-) mice (Drago et al., 1994), and Slc32a1$^{tm2(cre)Lowl}$/MwarJ (Vong et al., 2011). *Drd1a*$^{Cre/Cre}$ (KO) mice and littermates were raised on diet of Teklad 8664 (Envigo, United Kingdom) placed on the cage floor as Drd1-KO mice were more likely to consume food when it was readily accessible.

Mouse Diets

Standard chow diet (SCD):Teklad 8664 (Envigo, United Kingdom: 3.1 kcal/gram; 19% fat, 31% protein, 50% carbohydrates; 3.1% sucrose). High-fat, high-sugar diet (HFD): Open Source D12451 (4.73 kcal/gram; 45% fat, 20% protein, 35% carbohydrates; 17% sucrose). For Cal Poly figure 4, Normal chow diet (NCD) Teklad 2018 (3.1 kcal/gram; 18% fat, 24% protein, 58% carbohydrates). High-fat,

low-sugar diet: BioServ F3282 (Flemington, New Jersey: 5.49 kcal/gram; 60% fat, 15% protein, 26% carbohydrates). Ensure original vanilla (24.3% fat, 16.2% protein, 59.5% carbohydrates).

Food Intake Measurements

Adult male mice were housed individually with *ad libitum* access to SCD food and water throughout all experiments. For longitudinal feeding experiments, 12-14 week old mice were then randomly assigned into two different feeding regimens, SCD or HFD. All mice were maintained on SCD for an additional two weeks to measure baseline food intake and weight change. SCD animals remained on SCD for an additional four weeks at the time of the "diet switch" while the HFD group was given *ad libitum* access to HFD. Pre-weighed food pellets were placed on the cage floor and refreshed weekly. Body mass was measured weekly. For the daily feeding studies, animals were maintained on SCD or habituated to HFD for at least three days prior to the start of intake measurements. Pre-weighed food pellets were given on the cage floor at the start of the experiment, and body mass and food intake was measured at intervals of 12 h (ZT 0 and ZT 12) over a 72 h period starting at ZT 12. Food intake measurements were obtained by subtracting the mass of the residual food pellets from the total food given. Total caloric intake was calculated by multiplying the calories per gram of food and the mass of food consumed (**Ryan Grippo, Qijun Tang, Aarti Purohit, Nidhi Purohit, Meghana Sunkara, Michael Sidikpramana**).

Fecal Bomb Calorimetry Fecal output data was collected over a period of 72 hours. The feces within the bedding was collected, freeze dried (Labconco) and weighed. For analysis of fecal calorie content, samples were collected, 2 mice/ n sample (~1 gram/sample) for fecal bomb calorimetry (Par 6200 isoperibol calorimeter, UT southwestern).

Viral Expression and Stereotaxic Surgery

During surgery, animals were anesthetized with isoflurane (induction 5%, maintenance 2%–2.5%; Isothesia) and placed in a stereotaxic apparatus (Kopf). A heating pad was used for the duration of the surgery to maintain body temperature and ocular lubricant was applied to the eyes to prevent desiccation. A double-floxed inverted open reading frame (DIO) cassette containing recombinant AAV was used to express specific transgenes in Cre-expressing neurons. AAV was delivered using a 10 μl syringe (Hamilton) and 26-gauge needle (Hamilton) at a flow rate of 100 nl/min driven by a microsyringe pump controller (World Precision Instruments, model Micro 4). The syringe needle was left in place for 10 min and was completely withdrawn 20 min after viral delivery. Following surgery, mice were administered ketoprofen (3 mg/kg) subcutaneously as an analgesic. Animals were tested at least two weeks following virus injection to ensure optimal transgene expression. All surgical procedures were performed in sterile conditions and in accordance with University of Virginia IACUC guidelines (**Ryan Grippo, Qijun Tang, Sean Chadwick**).

Viral constructs

AAV2-hSyn-DIO-ChR2-YFP, AAV1-hSyn-ChR2(H134R)-eYFP, AAV1-CAG-DIO-Drd1-HA (500 nl; 1.1 x 10^13 viral genomes/ul) were injected into the NAc (ML: + 1.15 mm, AP: + 0.98 mm, DV: - 5.75 mm), SCN (ML: ± 0.29 mm, AP: - 0.30 mm, DV: -5.75 mm). All coordinates are relative to bregma (George Paxinos and Keith B. J. Franklin).

Circadian Behavioral Analysis

To record the rhythm of locomotor activity, adult male mice were individually housed in activity wheel-equipped cages (Nalgene) in light-tight boxes under a 12h :12h LD cycle for at least 7 days. Fluorescent lights (100 mW/cm^2) were used for behavioral experiments. Food and water were provided ad libitum. Wheel running rhythms were monitored and analyzed with ClockLab collection and analysis system (Actimetrics, Wilmette, IL). The free-running period was calculated according to the onset of activity across seven days in constant darkness. Activity onset was identified through ClockLab software as the first bin above a threshold of 5 counts preceded by at least 6 hr of inactivity and followed by at least 6 hr of activity. When necessary, onset and offset points were edited by eye. All data was analyzed by a trained scorer blind to genotype.

SKF-81297 to NAc-Rescue Locomotor Assay

Mice were habituated to experimental housing conditions for 30 minutes. Following 20 minutes of baseline activity recordings, 7.5 mg/kg SKF-81297 (in saline) was

administered by i.p. Injection. An additional 90 minutes of animal activity was recorded for analysis. Movement was tracked by EthoVision XT 11 (Noldus) and analyzed by EthoVision XT 11 (Noldus) and a custom Matlab script (**Qijun Tang**).

Histological analysis and imaging

Animals were deeply anesthetized (ketamine:xylazine, 280:80 mg/kg, i.p.) and perfused intracardially with ice cold 0.01 M phosphate buffer solution (PBS) followed by fixative solution (4% paraformaldehyde (PFA) in PBS at a pH of 7.4). After perfusion, brains were dissected and post-fixed overnight at 4°C in PFA. Freshly collected brains, after cervical dislocation were incubated in cold 4% PFA for 48 hours. Fixed brains were then rinsed in PBS, transferred into 30% sucrose in PBS for 24 hours, and then frozen on dry ice. Coronal sections (30 µm) were collected with a cryostat (Microm HM 505 E). Sections were permeabilized with 0.3% Triton X-100 in PBS (PBS-T) and blocked with 3% normal donkey serum (Jackson ImmunoResearch) in PBS-T (PBS-T DS) for 30 min at room temperature. Sections were then incubated overnight in primary antibodies diluted in PBS-T DS. For visualization, sections were washed with PBS-T and incubated with appropriate secondary antibodies diluted in the blocking solution for 2 hours at room temperature. Sections were washed three times with PBS and mounted using DAPI Fluoromount-G (Southern Biotech). Images were captured on a Zeiss Axioplan 2 Imaging microscope equipped with an AxioCam MRm camera using AxioVision 4.6 software (Zeiss). Confocal microscope imaging was performed in W.M. Keck Center for Cellular Imaging, University of Virginia, with Leica SP5 X

imaging system. The following primary antibodies were used for fluorescent labelling: anti-Drd1 (rat, 1:500, Sigma D2944), anti-HA (rabbit, 1:500, Cell Signaling Technology C29F4), anti-c-Fos (rabbit, 1:1000, synaptic systems), anti-GAD65/67 (rabbit, 1:2,000, Abcam ab49832). The secondary antibodies (Jackson ImmunoResearch) used were Cy2- or Cy3-conjugated donkey anti-rat IgG (1:250), donkey anti-rabbit (1:250) (**Qijun Tang, Ryan Grippo**).

PER2-DAB

Brains sections were permeabilized and blocked via the process described above. anti-PER2 (rabbit; 1:1000 AlphaDiagnostic International, PER21-A) primary antibody was incubated at 4 ^{o}C for 20 hours. Secondary antibody and DAB staining was processed with a VECTASTAIN Elite ABC-HRP Kit following the company-recommended protocol.

Oil Red O

PFA fixed tissue was rinsed in 1% PBS, transferred to 30% sucrose overnight, then frozen in 2-Methylbutane chilled by dry ice. 8 μm thick sections were collected with a cryostat (Microm HM 505 E) and mounted onto gelatin coated slides. Slides were treated with Oil Red O (ORO) solution (3mg/ml in 60% isopropanol) for 18 hours. Sections were then imaged by Nikon ECLIPSE Ti microscope equipped with a Nikon DS-Ri2 color camera.

Hematoxylin & Eosin (H & E) staining

Bouin's solution fixed tissues were washed 2 x 5 min in PBS and 3 x 5 min in 70% EtOH. Tissues were then sent to UVa Research Histology Core for paraffin embedding, sectioning (6μm) and H&E staining. Sections were imaged in the same way as ORO sections above (**Qijun Tang, Qi Zhang Ryan Grippo**).

Adipose area quantification

Samples of GWAT were collected and fixed for H & E staining as described above. Three digital images (20x) from non-overlapping fields were captured for each sample (Nikon ECLIPSE Ti microscope equipped with Nikon DS-Ri2 color camera). Quantitative analyses of adipocyte area were made using ImageJ (National Institutes of Health, Bethesda, MD). Results are expressed as mean ± SE μm^2 per cell. Exclusions: any cut off adipocytes on the image edge, cells that were artificially divided into multiple cells due to artifact, cells that were combined due to faintness of borders in the original image, and cells <350μm^2 (Parlee et al., 2014) (**Aarti Purohit**).

Western Blot p-HSL

Samples of GWAT were collected from *ad libitum* fed mice at ZT 6 and flash frozen in liquid nitrogen. Adipose samples were homogenized in lysis buffer and centrifuged at 18,000g at 4°C for 20 minutes. The resultant supernatant was collected into a fresh eppendorf tube and protein levels in extracts were determined using the BCA method (Peirce). Protein was loaded equally (30

µg/lane) into lanes of a 4-15% gradient gel (BioRad) and separated by SDS-PAGE, and blotted onto 0.2 micron PVDF membranes. Blots were blocked for 1 hour at room temperature in a half-strength mixture of LiCOR Blocker (LiCOR Blocker (TBS): 1X TBS buffer). Primary antibody against HSL (Cell Signalling Technology 4107), and pHSL 660 (Cell Signalling Technology 4126) rabbit polyclonal used at 1:2000. The blots were washed in 1X TBS containing 0.01% Tween-20, and secondary antibody goat-anti-rabbit LiCOR 800CW was applied in LiCOR Blocker (TBS): 1X TBS buffer, used at 1:10,000 dilution for one hour at room temperature. Signal was normalized against tubulin using hFAB rhodamine-labelled anti-tubulin antibody fragment (BioRad 12004166), used at 1:2,000, and incubated along with LiCor 800 CW secondary. Finally, the blot was washed 6 times for 5-10 minutes each in 1X TBS + 0.01% Tween-20 followed by 2 final rinses for 5-10 minutes in 1X TBS alone. The blot was dried and imaged by fluorescence on a LiCor BioRad ChemiDoc MP station and bands quantified using BioRad ImageLab software. Protein concentrations of pHSL were determined by quantitative blot immunolabeling by a trained experimenter, blind to genotype and dietary conditions (**Anthony Spano, Laura Sipe, Ryan Grippo**)

Metabolic Measurements

Glucose tolerance

Five weeks after the time of diet change, mice were fasted for 16 hours (ZT 10 - ZT 2), and fasted glucose was recorded using a Glucometer (One Touch Ultra) by tail bleeds. Subsequently, mice received an i.p injection of glucose (1g/kg body

weight in saline), and blood glucose was measured in intervals of 30 minutes for 2 hours (**Qi Zhang, Qijun Tang, Ryan Grippo**).

Insulin tolerance

Five weeks after the time of diet change, mice were fasted for 4 hours (ZT 1 - ZT 5), and fasted glucose was recorded using a Glucometer (One Touch Ultra) by tail bleeds. Subsequently, mice received an i.p injection of insulin (0.75units/kg of body weight in saline), and blood glucose was measured in intervals of 15 minutes for 1 hour (**Qi Zhang, Qijun Tang, Ryan Grippo)**.

Body composition

Six weeks after time of diet change SCAT, GWAT, and liver were harvested, weighed, placed into a chilled 4% PFA solution or Bouin's solution (fisher scientific) for fixation. Whole tissue was imaged (Canon EOS Rebel Xsi) before fixation. A ruler was used to scale each tissue (**Qijun Tang, Qi Zhang, Ryan Grippo**).

Echo MRI

Body fat and lean mass four weeks after diet change were assessed using an Echo MRI (The EchoMRI™-100H) following manufacturer's protocol (**Ryan Grippo, Michael Scott**).

Comprehensive Lab Animal Monitoring System (**CLAMS)**

Indirect calorimetry in a CLAMS system (Columbus Instruments) was used to evaluate whole-body states during ad libitum access to SCD or HFD. Four weeks after diet change, mice were acclimated to metabolic cages for 48 hours and then monitored for 72 hours following the manufacturer's instructions. Energy expenditure (EE) in watts per kilogram of lean mass [W/kg] was calculated with the following formula formula described in (Fischer et al., 2018).

EE [W/kg] = 1/60*((0.2716 [W*min/ml]*VO2 [ml/kg/hour])+(0.07616 [W*min/ml]*VCO2 [ml/kg/hour])

The unit Watts was converted to kcal/hour by multiplying factor of 0.86 to report EE as kcal/hour/kg of lean mass. The resting metabolic rate (RMR) was quantified and defined as the average of the lowest 5 consecutive energy expenditure values (18 minute intervals) across a twenty-four hour day (**Ryan Grippo, Qijun Tang, Michael Scott**).

QPCR

6 weeks after diet change, WT-SCD, WT-HFD, and D1R-KO mice were sacrificed by cervical dislocation every four hours along the LD cycle (3 mice/timepoint: ZT 1,5,9,13,17,21). Tissue collected from mice during the night phase were sacrificed in the dark under IR light with night-vision goggles. Dissected liver and GWAT tissue was flash frozen in liquid nitrogen. RNA was extracted with the RNeasy Lipid Tissue Mini Kit (QIAGEN). For liver and GWAT, 1100 ng of RNA was reverse-transcribed using a SuperScript™ IV First-Strand Synthesis System kit (Thermo Fisher). Quantitative PCR was performed using the iQ™ SYBR® Green Supermix system (BIO-RAD). *Beta-actin* was used as a housekeeping gene for the analysis

of *Bmal-1*, *Per2*, and *Rev-erbα*. The relative mRNA levels were calculated using the 2−ΔCt method. The ΔCt values were obtained by calculating the differences: Ct(gene of interest) – Ct(housekeeping gene) in each sample (**Qi Zhang**).

Gene	Forward Primer (5' to 3')	Reverse Primer (5' to 3')	Cited Paper
Bmal-1	TGACCCTCATGG AAGGTTAGAA	GGACATTGCATTG CATGTTGG	(Solt et al., 2012)
Per2	GAAAGCTGTCAC CACCATAGAA	AACTCGCACTTCCT TTTCAGG	(Vollmers et al., 2009)
Actin	GGCTGTATTCCC CTCCATCG	CAGTTGGTAACAAT GCCATGT	(Vollmers et al., 2009)
Rev-erbα	TGGCATGGTGCT ACTGTGTAAGG	ATATTCTGTTGGAT GCTCCGGCG	(Solt et al., 2012)

FITC-Dextran

For the intestinal permeability assay, tracer FITC-labeled dextran (4kDa; Sigma-Aldrich) was used to assess in vivo intestinal permeability. Mice were deprived of food 4 hours prior to and 4 hours following an oral gavage using 150 µl of 80 mg/ml FITC-dextran. Blood (50µl) was collected from tail bleeds, and fluorescence

intensity was measured on fluorescence plates using an excitation wavelength of 485 nm and an emission wavelength of 530 nm.

Foraging assay

Animals were habituated to experimental conditions for 4 days prior to testing. On the 1st and 2nd day 1 pellet of HFD was placed on the homecage floor for diet habituation. On the 3rd day mice were moved to a larger testing cage (144 in^2; 18 (L) x 8 (W) x 8 (H)) with ad libitum access to SCD and 1 pellet of HFD on cage floor. 4th day: ad libitum access to SCD in home cage. After this habituation, the foraging assay was performed at either ZT 8 (day) or ZT 15 (night). Mice were habituated to the testing cage with 1~1.5cm deep bedding for 30 minutes. A pellet of HFD diet was buried beneath the bedding at one end of the testing cage. Mice were then placed onto the opposite end of the testing cage, video recorded, and tracked by EthoVision XT 11 (Noldus) (day) or a night-vision sports camera (night) for 10 minutes. The latency of the animals' first intentional foraging of the food area scored by an investigator blind to genotype. For the mice that failed to perform a foraging behavior within 10 minutes, the latency was recorded as 600s when analyzing the data (**Qijun Tang**).

HPLC

WT mice were habituated to HFD or SCD on cage floor on the day prior to tissue collection. Mice were given 1 hour access to either HFD or SCD and sacrificed by cervical dislocation. Fresh brains were dissected from adult wild-type male animals

and 1 mm coronal slices were collected using a mouse brain matrix (Zivic Instruments). Hypothalamic samples containing the SCN were collected with a 1.5 mm in diameter tissue biopsy punch (Miltex), frozen in liquid nitrogen, and stored at 80°C until further processing. Tissue punches were homogenized by sonication in 50 µL of 0.04N perchloric acid solution. The homogenate was centrifuged at 13,200 rmp for 12 min at 4°C, followed by spin filtration (Sigma Aldrich) at 11,000 rpm for 4 min at 4°C. 15 µL of the resulting supernatant was loaded into an autosampler connected to a high-performance liquid chromatography instrument with an electrochemical detector (Decade, Antec Leyden B.V., Zoeterwoude,the Netherlands) to measure the levels DA and 3,4-Dihydroxyphenylacetic acid (DOPAC) and serotonin. Retention time for was determined through comparison with standards diluted in 0.04N perchloric acid. DOPAC tR range 4.56 ± 0.015 min, DA: tR range 10.01 ± 0.24 min, Serotonin: tR range: 22.165 ± 0.035 min. Mobile phase: pH 3, 10% acetonitrile, 0.50mmol DSA. 0.8V 0.125 ml/min, 26 °C 24 minutes 0.5µM of DSA. Identification of serotonin within the chromatogram was used to confirm the SCN in collected tissue punch (Morin, 1999) (**Ryan Grippo, Nidhi Purohit, Jay Hirsh**).

Microbiome

Six weeks after diet change, fresh fecal samples from WT-SCD, WT-HFD and KO-HFD mice were collected, flash frozen in liquid nitrogen and stored at -80 until further processing. One or two fecal pellets weighing 10 to 100 mg from each sample were used for DNA extraction with the ZR-96 Fecal DNA Kit (Zymo

Research). Bacterial 16S rRNA gene (V4 region) was amplified with barcodes from the extracted DNA, quantified and pooled for Illumina Miseq sequencing at the Genomic Core Facility of UVa. Demultiplexed sequence reads were trimmed based on quality score and checked for chimeric reads, and *de novo* operational taxonomic units (OTUs) were then picked at 97% similarity threshold using QIIME (Caporaso et al., 2010). Mitochondrial and chloroplast OTUs and OTUs with no more than 100 sequences across all samples were filtered out. For each sample, sequences were rarefied to 64,455 sequences per sample to normalize the sequencing effort for diversity analysis. The weighted Unifrac metric was applied to calculate the dissimilarity between samples, and alpha diversity was measured as the observed number of OTUs. PERMANOVA test was applied to examine the effect of diet and genotype on the microbiome composition. The non-parametric JTK analysis that detects cycling elements was performed to determine whether a particular taxonomic group was cyclically fluctuating (Hughes et al., 2010). A taxonomic group was considered cyclical if both its adjusted permutation-based p-value (ADJ.P) and Benjamini-Hochberg q-values (BH.Q) were smaller than 0.05 (**Yingnan Gao, Martin Wu**).

Temperature recordings

Body temperature were measured using a rectal probe attached to a digital thermometer (Physitemp Instruments, Clifton, NJ). Temperatures were collected at ZT 6 and ZT 18.

Slice electrophysiology

Slice visualization and data collection

SCN cells were visualized with infrared DIC in an upright Slicescope 6000 microscope. The SCN was identified by shape of the both 3rd ventricle and most inferior middle region of the slice, as well as the presence of the optic chiasm. Images of patched brain regions were taken using Scientifica SciPro camera and Ocular imaging software. A Multiclamp 700B amplifier and Digidata 1550B digitizer (Molecular Devices; San Jose, California) were used to perform all patch clamp experiments. All experiments were conducted using 2.5-6MΩ microelectrodes pulled with a Sutter P97 puller. All brain slice solutions were saturated with 95% O2 and 5% CO2 gas. SKF-81297 was used at 5μM concentration in all incubation experiments.

Cell attached recordings

Male and female WT mice were individually housed in light-tight boxes under a 12 hr:12 hr LD cycle for at least 7 days. Mice between P31 and P55 were deeply anesthetized with isoflurane and brains were rapidly dissected and mounted for slicing in the compresstome slicer. Slices were taken with in ice cold HEPES based holding ACSF solution containing (in mM): 92 NaCl, 2.5 KCl, 1.25 NaH2PO4, 30 NaHCO3, 20 HEPES, 25 glucose, 2 thiourea, 5 Na-ascorbate, 3 Na-pyruvate, 2 CaCl2·4H2O and 2 MgSO4·7H2O with pH ranging from 7.3 to 7.4 and osmolarity ranging from 300 to 310 mOsm (J Ting 2014). Slices were allowed to recover for ≤12 min at 34°C in the same HEPES based holding ACSF solution, and then allowed to come to room temperature. ‘Day’ collections condition (sacrificed at ZT

5-6) were incubated for a minimum of 90 minutes, and data was collected between ZT 8 and 11 and for ‘night’ collections condition (sacrificed at ZT 11-12) were incubated and data was collected at ZT 14 to 17. After a minimum of 90 minutes of incubation slices were transferred to the microscope recording bath and superfused with a continuous flow (1.5 - 2 ml/min) recording ACSF which consisted of (in mM): 124 NaCl, 2.5 KCl, 1.2 NaH_2PO_4, 24 $NaHCO_3$, 5 HEPES, 10 glucose, 2 $CaCl_2 \cdot 4H_2O$ and 2 $MgSO_4 \cdot 7H_2O$ with pH ranging from 7.3 to 7.4 and osmolarity ranging from 300 to 310 mOsm, and included the vehicle or agonist. The resulting DMSO concentration in these buffers ranged from 0.01% to 0.12%. Vehicle control solutions contained the same amount of DMSO as the treatment conditions. Drug solutions were added directly to the bath after the recovery incubation. Cell attached recordings were made at 32 °C. For cell attached recordings the pipette was filled with ACSF, slight positive pressure applied when approaching the cell was released and the seal was allowed. Seal magnitude ranged from 5 to 50MΩ. In all experiments the pipette offset was <15mV, typically ranging from 1 to 11mV. Pipette offset was set just before initiating a recording, and the seal resistance was monitored closely. Recordings measuring spontaneous spiking lasted approximately one minute. Recordings were filtered offline at 1kHz and baseline was manually adjusted using ClampFit (Molecular devices) software. Action potential events were then extracted using ClampFit and analyzed using custom scripts in Matlab (Mathworks). Statistical tests were performed in Prism 7 (Graphpad).

Optogenetic stimulation

Heterozygous Drd1-HET mice minimum of 8 weeks of age received bilateral injections of AAV2-DIO-ChR2-YFP to the SCN as previously described. After minimum of 5 weeks recovery animals were deeply anesthetized (ketamine:xylazine, 280:80 mg/kg, i.p.) and transcardially perfused with an NMDG recovery ACSF solution containing (in mM): 92 NMDG, 2.5 KCl, 1.25 NaH_2PO_4, 30 $NaHCO_3$, 20 HEPES, 25 glucose, 2 thiourea, 5 Na-ascorbate, 3 Na-pyruvate, 0.5 $CaCl_2 \cdot 4H_2O$ and 10 $MgSO_4 \cdot 7H_2O$, pH adjusted to 7.3 to 7.4, osmolarity 300 to 310 mOsm (Ting et al., 2014). Slices were held in the NMDG recovery ACSF for ≤12 min at 34°C, and then transferred to recording ACSF (described above)/and allowed to rest at room temperature for 45 minutes before being transferred to microscope bath for data collection. All recordings were made at room temperature and the same K-Glu intracellular solution was used as described above. SCN cells were randomly patched without regard for YFP expression. After formation of gigaohm seal (>2GΩ), cell membrane was ruptured, and current clamp recordings acquired. A minimal current injection hold of 0 to -15pA was used to compensate for minor current leakage. Whole cell voltage measurements made as described for whole cell incubation recordings. Optogenetic stimulation consisted a 500ms 20 Hz square pulses of 488 nm light (10 pulses total, each pulse 10ms). Light was delivered at the beginning of each 10 second trace. For a subset of cells (n=5) which showed a hyperpolarized response to blue light stimulation, recording ACSF with 100μM Picrotoxin (PTX) was perfused for 6 minutes and cell responses to the optogenetic stimulation protocol were recorded.

No further recordings were made on slices which were exposed to PTX. Response magnitudes and latencies were manually extracted in ClampFit and consisted of an average of 5 to 6 traces. Statistical tests were performed in Prism 7 (Graphpad) (**Sean Chadwick**).

Statistical Analysis

When comparing two groups of normally distributed data, Student's two tailed t-test was used. To compare the effects of genotype and diet with 4 groups, a two way ANOVA test was used. When the data were measured multiple times at different time points, a three way ANOVA test would be performed to analyze time effect along with genotype and diet effect. With three groups, a one way ANOVA was performed. A Bonferroni's post hoc comparison would be used to further analyze the difference in the event with significance in ANOVA test. Permutational multivariate analysis of variance PERMANOVA was used to evaluate microbiome OTUs. Analyses were conducted using the GraphPad Prism 6 and 7 statistical software for Windows, or Prism 8 for Mac OS. All data are presented as means ± standard error of the mean with $p < 0.05$ considered statistically significant (**Qijun Tang, Ryan Grippo**).

Chapter IV: Conclusions and Future Directions

Outlook

Circadian rhythms perform a vital role in orchestrating all aspects of physiology to ensure that rest and active states are properly aligned with the solar day. However, obligatory schedules of modern society disrupt natural oscillations of biological clocks. Disturbing these rhythms increases the likelihood of metabolic, mental and physical disorders, thereby increasing the burden on healthcare around the globe. A challenge for researchers and clinicians is to elucidate the precise mechanisms of circadian rhythm disruptions and how to reduce their negative impact on well-being.

In our investigation to define a neural circuit between DA producing neurons and the central pacemaker, we uncovered a role for Drd1 signaling within the SCN that influences the time required to resynchronize to a shift in the LD cycle (Chapters II and IV). Adjustment to a shifted photoperiod is initiated by discrete phase shifts of retino-recipient SCN neurons, which in turn synchronize the surrounding non-retinorecipient neurons within the central pacemaker (Nagano et al., 2003; Rohling et al., 2011). The time it takes for these two components to generate a cohesive rhythm synchronized to the new light cycle determines the rate of photoentrainment. Although increased Drd1 signaling within the developed SCN does not elicit an immediate circadian behavioral effect in constant conditions (Duffield et al., 1998; Weaver et al., 1992), we believe that when challenged by a light cycle shift, central oscillator enters a more “entrainment susceptible” state by acting as a coincidence detector to set the gain for other entrainment cues such as light.

This has been observed previously by evidence that entrainment to a shift in photoperiod is regulated by vasoactive intestinal peptide (VIP), a small neuropeptide expressed within the SCN (Aton et al., 2005). Application of VIP permits rapid entrainment of behavioral and physiological rhythms through phase-tumbling, a process by which coupled oscillators enhance their entrainment rate through transient phase desynchronization (Abraham et al., 2010; An et al., 2013; Buhr et al., 2010; Mazuski and Herzog, 2015; Roberts et al., 2015). It is compelling to propose that dopaminergic tone feeds into this mechanism as VIP and DA signaling share several similarities: 1) Both Drd1 and the VIP receptor VPAC2 are G_s-coupled receptors, (Beaulieu and Gainetdinov, 2011; Grinninger et al., 2004) 2) Sustained VPAC2 agonist administration directly to the SCN increases period length (Pantazopoulos et al., 2010) akin to hyperdopaminergic DAT knockdown mice (Landgraf et al., 2016). 3) SCN slices treated with the VPAC2 agonist BAY 55-9837 or selective Drd1 agonist SKF81297 lengthen the period of Per2 driven luciferase expression (Landgraf et al., 2016; Pantazopoulos et al., 2010). Therefore, like Drd1-dependent dopaminergic signaling, G_s-coupled receptors within the SCN might offer a convergence point for inputs that modulate the circadian entrainment susceptibility and will be the basis of future studies. In sum, DA neurotransmission via Drd1-expressing neurons within the SCN is an integral component of rate setting during entrainment following changes in the LD cycle. Delineation of how DA-neurons modulate the central circadian clock provides novel therapeutic targets for alleviating the harmful effects of circadian rhythm misalignment. Furthermore, it could help uncover novel principles employed by

other oscillatory neuronal networks modulated by DA during information processing. Notably, our work has additionally implicated this system in permitting palatable food induced overconsumption and obesity (Chapters IV and V). From these studies, we postulate that Drd1 signaling within the SCN enables flexibility of the circadian pacemaker to challenges brought on by changes in lighting or food availability conditions.

Modern society places a significant burden on the primitive circadian machinery whereby the central pacemaker is under constant dysregulation by artificial lighting. Moreover, easy access to palatable foods likely contributes to maladaptive feeding behavioral responses causing overconsumption and obesity. In this dissertation, I have demonstrated that Drd1-mediated dopamine neurotransmission within the SCN is a critical component of metabolic regulation in the presence of rewarding, energy dense foods. Elevated DA signaling within the SCN, enables out-of-phase foraging and overconsumption of these palatable foods leading to a dysregulation of homeostatic control of feeding. This feeding behavior changes the metabolic state from one of fat utilization to that of excessive fat storage. Here we have unearthed one possible mechanism by which rewarding foods induce perturbation of feeding and metabolic rhythms.

I believe that the SCN normally functions to reduce foraging when it is less advantageous for the organism (at risk of predation). However, in the context of self-preservation, when energy dense food becomes available, the system restructures to enable excessive food intake and foraging to ensure maximal energy storage as fat. While the SCN is sufficient to establish the timing of food

consumption, we believe other hypothalamic nuclei are responsible for the initiation and perpetuation of intake.

As such, this work opens many more questions and lines of research for discovery. We fully intend to investigate the influence of light on Drd1-KO mice as well as their sleep physiology. It will be fascinating to investigate whether HFD consumption throughout the rest phase results in sleep deprivation in WT mice and results in disrupted metabolism. Additionally we will evaluate the motivational state of Drd1-KO mice and their willingness to “work” for food during operant conditioning experiments. Full characterization of the behavioral responses in these mice to palatable foods will be critical toward developing a better understanding of the mechanism driving these behaviors. The next step toward a greater understanding of this circuit will be to determine the anatomical projection sites of SCN-Drd1 neurons to other feeding centers within the hypothalamus. Identifying these will further establish the DA-Drd1-SCN axis as a therapeutic target to combat obesity and type 2 diabetes.

While significant advances have been made in the field of circadian biology, pressing issues remain. For instance, the processing of light information from the retina to the SCN has been well characterized, however, the mechanism of how the SCN communicates with the rest of the brain and body is less understood (Kalsbeek et al., 2011). A mechanistic understanding of how the SCN integrates and relays photic and non-photic information to generate high amplitude biological rhythms is necessary to understand how daily physiological and metabolic rhythms

deteriorate under certain conditions. Furthermore, it is still unclear whether restoring the SCN oscillation amplitude would be enough to alleviate pathologies associated with circadian misalignment. In addition, maladaptive changes in the dopaminergic system underlie many neurological diseases such as depression, bipolar disease and Parkinson's disease, which share symptoms of circadian and sleep disruption. Thus, a mechanistic understanding of how dopamine signaling coordinates with the circadian system to govern daily physiological and behavioral functions will provide novel therapeutic avenues for these disorders.

References

Abarca, C., Albrecht, U., and Spanagel, R. (2002). Cocaine sensitization and reward are under the influence of circadian genes and rhythm. Proc Natl Acad Sci U S A *99*, 9026-9030.

Abraham, U., Granada, A.E., Westermark, P.O., Heine, M., Kramer, A., and Herzel, H. (2010). Coupling governs entrainment range of circadian clocks. Mol Syst Biol *6*, 438.

Adamovich, Y., Ladeuix, B., Golik, M., Koeners, M.P., and Asher, G. (2017). Rhythmic Oxygen Levels Reset Circadian Clocks through HIF1alpha. Cell Metab *25*, 93-101.

Akasheh, R.T., Pini, M., Pang, J., and Fantuzzi, G. (2013). Increased adiposity in annexin A1-deficient mice. PLoS One *8*, e82608.

Albrecht, U. (2012). Timing to perfection: the biology of central and peripheral circadian clocks. Neuron *74*, 246-260.

Alsio, J., Olszewski, P.K., Norback, A.H., Gunnarsson, Z.E., Levine, A.S., Pickering, C., and Schioth, H.B. (2010). Dopamine D1 receptor gene expression decreases in the nucleus accumbens upon long-term exposure to palatable food and differs depending on diet-induced obesity phenotype in rats. Neuroscience *171*, 779-787.

Altimus, C.M., Guler, A.D., Alam, N.M., Arman, A.C., Prusky, G.T., Sampath, A.P., and Hattar, S. (2010). Rod photoreceptors drive circadian photoentrainment across a wide range of light intensities. Nat Neurosci *13*, 1107-1112.

An, S., Harang, R., Meeker, K., Granados-Fuentes, D., Tsai, C.A., Mazuski, C., Kim, J., Doyle, F.J., 3rd, Petzold, L.R., and Herzog, E.D. (2013). A neuropeptide speeds circadian entrainment by reducing intercellular synchrony. Proc Natl Acad Sci U S A *110*, E4355-4361.

Antle, M.C., and Silver, R. (2005). Orchestrating time: arrangements of the brain circadian clock. Trends Neurosci *28*, 145-151.

Arble, D.M., Bass, J., Laposky, A.D., Vitaterna, M.H., and Turek, F.W. (2009). Circadian timing of food intake contributes to weight gain. Obesity (Silver Spring) *17*, 2100-2102.

Arble, D.M., Ramsey, K.M., Bass, J., and Turek, F.W. (2010). Circadian disruption and metabolic disease: findings from animal models. Best Pract Res Clin Endocrinol Metab *24*, 785-800.

Armbruster, B.N., Li, X., Pausch, M.H., Herlitze, S., and Roth, B.L. (2007). Evolving the lock to fit the key to create a family of G protein-coupled receptors potently activated by an inert ligand. Proc Natl Acad Sci U S A *104*, 5163-5168.

Aschoff, J. (1960). Exogenous and endogenous components in circadian rhythms. Cold Spring Harb Symp Quant Biol *25*, 11-28.

Asher, G., and Sassone-Corsi, P. (2015). Time for food: the intimate interplay between nutrition, metabolism, and the circadian clock. Cell *161*, 84-92.

Astrup, A., Greenway, F.L., Ling, W., Pedicone, L., Lachowicz, J., Strader, C.D., Kwan, R., and Ecopipam Obesity Study, G. (2007). Randomized controlled trials of the D1/D5 antagonist ecopipam for weight loss in obese subjects. Obesity (Silver Spring) *15*, 1717-1731.

Aton, S.J., Colwell, C.S., Harmar, A.J., Waschek, J., and Herzog, E.D. (2005). Vasoactive intestinal polypeptide mediates circadian rhythmicity and synchrony in mammalian clock neurons. Nat Neurosci *8*, 476-483.

Baik, J.H. (2013). Dopamine signaling in reward-related behaviors. Front Neural Circuits *7*, 152.

Balleine, B.W., Delgado, M.R., and Hikosaka, O. (2007). The role of the dorsal striatum in reward and decision-making. J Neurosci *27*, 8161-8165.

Baothman, O.A., Zamzami, M.A., Taher, I., Abubaker, J., and Abu-Farha, M. (2016). The role of Gut Microbiota in the development of obesity and Diabetes. Lipids Health Dis *15*, 108.

Barion, A., and Zee, P.C. (2007). A clinical approach to circadian rhythm sleep disorders. Sleep Med *8*, 566-577.

Beaulieu, J.M., and Gainetdinov, R.R. (2011). The physiology, signaling, and pharmacology of dopamine receptors. Pharmacol Rev *63*, 182-217.

Bender, M., Drago, J., and Rivkees, S.A. (1997). D1 receptors mediate dopamine action in the fetal suprachiasmatic nuclei: studies of mice with targeted deletion of the D1 dopamine receptor gene. Brain Res Mol Brain Res *49*, 271-277.

Berridge, K.C., and Robinson, T.E. (1998). What is the role of dopamine in reward: hedonic impact, reward learning, or incentive salience? Brain Res Brain Res Rev *28*, 309-369.

Berson, D.M., Dunn, F.A., and Takao, M. (2002). Phototransduction by retinal ganglion cells that set the circadian clock. Science *295*, 1070-1073.

Blancas-Velazquez, A., Mendoza, J., Garcia, A.N., and la Fleur, S.E. (2017). Diet-Induced Obesity and Circadian Disruption of Feeding Behavior. Front Neurosci *11*, 23.

Blum, I.D., Zhu, L., Moquin, L., Kokoeva, M.V., Gratton, A., Giros, B., and Storch, K.F. (2014). A highly tunable dopaminergic oscillator generates ultradian rhythms of behavioral arousal. Elife *3*.

Bobrzynska, K.J., and Mrosovsky, N. (1998). Phase shifting by novelty-induced running: activity dose-response curves at different circadian times. J Comp Physiol A *182*, 251-258.

Boulos, Z., and Terman, M. (1980). Food availability and daily biological rhythms. Neurosci Biobehav Rev *4*, 119-131.

Breen, D.P., Vuono, R., Nawarathna, U., Fisher, K., Shneerson, J.M., Reddy, A.B., and Barker, R.A. (2014). Sleep and circadian rhythm regulation in early Parkinson disease. JAMA Neurol *71*, 589-595.

Brun, P., Castagliuolo, I., Di Leo, V., Buda, A., Pinzani, M., Palu, G., and Martines, D. (2007). Increased intestinal permeability in obese mice: new evidence in the pathogenesis of nonalcoholic steatohepatitis. Am J Physiol Gastrointest Liver Physiol *292*, G518-525.

Bucan, M., and Abel, T. (2002). The mouse: genetics meets behaviour. Nat Rev Genet *3*, 114-123.

Buhr, E.D., Yoo, S.H., and Takahashi, J.S. (2010). Temperature as a universal resetting cue for mammalian circadian oscillators. Science *330*, 379-385.

Cahill, G.M., and Besharse, J.C. (1991). Resetting the circadian clock in cultured Xenopus eyecups: regulation of retinal melatonin rhythms by light and D2 dopamine receptors. J Neurosci *11*, 2959-2971.

Cao, R., Robinson, B., Xu, H., Gkogkas, C., Khoutorsky, A., Alain, T., Yanagiya, A., Nevarko, T., Liu, A.C., Amir, S.*, et al.* (2013). Translational control of entrainment and synchrony of the suprachiasmatic circadian clock by mTOR/4E-BP1 signaling. Neuron *79*, 712-724.

Caporaso, J.G., Kuczynski, J., Stombaugh, J., Bittinger, K., Bushman, F.D., Costello, E.K., Fierer, N., Pena, A.G., Goodrich, J.K., Gordon, J.I.*, et al.* (2010). QIIME allows analysis of high-throughput community sequencing data. Nat Methods *7*, 335-336.

Caricilli, A.M., and Saad, M.J. (2013). The role of gut microbiota on insulin resistance. Nutrients *5*, 829-851.

Carlin, J., Hill-Smith, T.E., Lucki, I., and Reyes, T.M. (2013). Reversal of dopamine system dysfunction in response to high-fat diet. Obesity (Silver Spring) *21*, 2513-2521.

Challet, E., Caldelas, I., Graff, C., and Pevet, P. (2003). Synchronization of the molecular clockwork by light- and food-related cues in mammals. Biol Chem *384*, 711-719.

Chang, C.J., Lu, C.C., Lin, C.S., Martel, J., Ko, Y.F., Ojcius, D.M., Wu, T.R., Tsai, Y.H., Yeh, T.S., Lu, J.J.*, et al.* (2018). Antrodia cinnamomea reduces obesity and modulates the gut microbiota in high-fat diet-fed mice. Int J Obes (Lond) *42*, 231-243.

Chung, S., Lee, E.J., Yun, S., Choe, H.K., Park, S.B., Son, H.J., Kim, K.S., Dluzen, D.E., Lee, I., Hwang, O.*, et al.* (2014). Impact of circadian nuclear receptor REV-ERBalpha on midbrain dopamine production and mood regulation. Cell *157*, 858-868.

Coccurello, R., and Maccarrone, M. (2018). Hedonic Eating and the "Delicious Circle": From Lipid-Derived Mediators to Brain Dopamine and Back. Front Neurosci *12*, 271.

Corthell, J.T., Stathopoulos, A.M., Watson, C.C., Bertram, R., and Trombley, P.Q. (2013). Olfactory bulb monoamine concentrations vary with time of day. Neuroscience *247*, 234-241.

Czeisler, C.A., and Brown, E.N. (1999). Commentary: models of the effect of light on the human circadian system: current state of the art. J Biol Rhythms *14*, 538-543.

Czeisler, C.A., and Gooley, J.J. (2007). Sleep and circadian rhythms in humans. Cold Spring Harb Symp Quant Biol *72*, 579-597.

Daan, S. (1977). Tonic and phasic effects of light in the entrainment of circadian rhythms. Ann N Y Acad Sci *290*, 51-59.

Dandona, P., Aljada, A., and Bandyopadhyay, A. (2004). Inflammation: the link between insulin resistance, obesity and diabetes. Trends Immunol *25*, 4-7.

David, L.A., Maurice, C.F., Carmody, R.N., Gootenberg, D.B., Button, J.E., Wolfe, B.E., Ling, A.V., Devlin, A.S., Varma, Y., Fischbach, M.A.*, et al.* (2014). Diet rapidly and reproducibly alters the human gut microbiome. Nature *505*, 559-563.

Davidson, A.J., Sellix, M.T., Daniel, J., Yamazaki, S., Menaker, M., and Block, G.D. (2006). Chronic jet-lag increases mortality in aged mice. Curr Biol *16*, R914-916.

Davis, J.F., Tracy, A.L., Schurdak, J.D., Tschop, M.H., Lipton, J.W., Clegg, D.J., and Benoit, S.C. (2008). Exposure to elevated levels of dietary fat attenuates psychostimulant reward and mesolimbic dopamine turnover in the rat. Behav Neurosci *122*, 1257-1263.

de Mutsert, R., Sun, Q., Willett, W.C., Hu, F.B., and van Dam, R.M. (2014). Overweight in early adulthood, adult weight change, and risk of type 2 diabetes, cardiovascular diseases, and certain cancers in men: a cohort study. Am J Epidemiol *179*, 1353-1365.

Del Corral, P., Bryan, D.R., Garvey, W.T., Gower, B.A., and Hunter, G.R. (2011). Dietary adherence during weight loss predicts weight regain. Obesity (Silver Spring) *19*, 1177-1181.

Denis, R.G., Joly-Amado, A., Webber, E., Langlet, F., Schaeffer, M., Padilla, S.L., Cansell, C., Dehouck, B., Castel, J., Delbes, A.S.*, et al.* (2015). Palatability Can Drive Feeding Independent of AgRP Neurons. Cell Metab *22*, 646-657.

Doi, M., Yujnovsky, I., Hirayama, J., Malerba, M., Tirotta, E., Sassone-Corsi, P., and Borrelli, E. (2006). Impaired light masking in dopamine D2 receptor-null mice. Nat Neurosci *9*, 732-734.

Doyle, S.E., McIvor, W.E., and Menaker, M. (2002). Circadian rhythmicity in dopamine content of mammalian retina: role of the photoreceptors. J Neurochem *83*, 211-219.

Drago, J., Gerfen, C.R., Lachowicz, J.E., Steiner, H., Hollon, T.R., Love, P.E., Ooi, G.T., Grinberg, A., Lee, E.J., Huang, S.P.*, et al.* (1994). Altered striatal function in

a mutant mouse lacking D1A dopamine receptors. Proc Natl Acad Sci U S A *91*, 12564-12568.

Duffield, G.E., Hastings, M.H., and Ebling, F.J. (1998). Investigation into the regulation of the circadian system by dopamine and melatonin in the adult Siberian hamster (Phodopus sungorus). J Neuroendocrinol *10*, 871-884.

Duffield, G.E., McNulty, S., and Ebling, F.J. (1999). Anatomical and functional characterisation of a dopaminergic system in the suprachiasmatic nucleus of the neonatal Siberian hamster. J Comp Neurol *408*, 73-96.

Dyar, K.A., Lutter, D., Artati, A., Ceglia, N.J., Liu, Y., Armenta, D., Jastroch, M., Schneider, S., de Mateo, S., Cervantes, M.*, et al.* (2018). Atlas of Circadian Metabolism Reveals System-wide Coordination and Communication between Clocks. Cell *174*, 1571-1585 e1511.

Eban-Rothschild, A., Rothschild, G., Giardino, W.J., Jones, J.R., and de Lecea, L. (2016). VTA dopaminergic neurons regulate ethologically relevant sleep-wake behaviors. Nat Neurosci *19*, 1356-1366.

Eckel, R.H., Kahn, S.E., Ferrannini, E., Goldfine, A.B., Nathan, D.M., Schwartz, M.W., Smith, R.J., and Smith, S.R. (2011). Obesity and type 2 diabetes: what can be unified and what needs to be individualized? J Clin Endocrinol Metab *96*, 1654-1663.

Espinosa-Carrasco, J., Burokas, A., Fructuoso, M., Erb, I., Martin-Garcia, E., Gutierrez-Martos, M., Notredame, C., Maldonado, R., and Dierssen, M. (2018). Time-course and dynamics of obesity-related behavioral changes induced by energy-dense foods in mice. Addict Biol *23*, 531-543.

Ferguson, S.A., Rowe, S.A., Krupa, M., and Kennaway, D.J. (2000). Prenatal exposure to the dopamine agonist SKF-38393 disrupts the timing of the initial response of the suprachiasmatic nucleus to light. Brain Res *858*, 284-289.

Ferrario, C.R., Labouebe, G., Liu, S., Nieh, E.H., Routh, V.H., Xu, S., and O'Connor, E.C. (2016). Homeostasis Meets Motivation in the Battle to Control Food Intake. J Neurosci *36*, 11469-11481.

Ferris, M.J., Espana, R.A., Locke, J.L., Konstantopoulos, J.K., Rose, J.H., Chen, R., and Jones, S.R. (2014). Dopamine transporters govern diurnal variation in extracellular dopamine tone. Proc Natl Acad Sci U S A *111*, E2751-2759.

Fifel, K., and Cooper, H.M. (2014). Loss of dopamine disrupts circadian rhythms in a mouse model of Parkinson's disease. Neurobiol Dis *71*, 359-369.

Fifel, K., and DeBoer, T. (2014). The central clock in patients with Parkinson disease. JAMA Neurol *71*, 1455-1456.

Fischer, A.W., Cannon, B., and Nedergaard, J. (2018). Optimal housing temperatures for mice to mimic the thermal environment of humans: An experimental study. Mol Metab *7*, 161-170.

Fonken, L.K., Aubrecht, T.G., Melendez-Fernandez, O.H., Weil, Z.M., and Nelson, R.J. (2013). Dim light at night disrupts molecular circadian rhythms and increases body weight. J Biol Rhythms *28*, 262-271.

Fonken, L.K., Workman, J.L., Walton, J.C., Weil, Z.M., Morris, J.S., Haim, A., and Nelson, R.J. (2010). Light at night increases body mass by shifting the time of food intake. Proc Natl Acad Sci U S A *107*, 18664-18669.

Franken, P., Cao, V., Heller, H.C., and Miller, J.D. (1999). The glutamate induced phase shift in the SCN slice: a two pulse study. Brain Res *818*, 34-40.

Frazier, T.H., DiBaise, J.K., and McClain, C.J. (2011). Gut microbiota, intestinal permeability, obesity-induced inflammation, and liver injury. JPEN J Parenter Enteral Nutr *35*, 14S-20S.

Friend, D.M., Devarakonda, K., O'Neal, T.J., Skirzewski, M., Papazoglou, I., Kaplan, A.R., Liow, J.S., Guo, J., Rane, S.G., Rubinstein, M.*, et al.* (2017). Basal

Ganglia Dysfunction Contributes to Physical Inactivity in Obesity. Cell Metab *25*, 312-321.

Gabel, K., Hoddy, K.K., Haggerty, N., Song, J., Kroeger, C.M., Trepanowski, J.F., Panda, S., and Varady, K.A. (2018). Effects of 8-hour time restricted feeding on body weight and metabolic disease risk factors in obese adults: A pilot study. Nutr Healthy Aging *4*, 345-353.

Gallardo, C.M., Darvas, M., Oviatt, M., Chang, C.H., Michalik, M., Huddy, T.F., Meyer, E.E., Shuster, S.A., Aguayo, A., Hill, E.M.*, et al.* (2014). Dopamine receptor 1 neurons in the dorsal striatum regulate food anticipatory circadian activity rhythms in mice. Elife *3*, e03781.

Garaulet, M., Gomez-Abellan, P., Alburquerque-Bejar, J.J., Lee, Y.C., Ordovas, J.M., and Scheer, F.A. (2013). Timing of food intake predicts weight loss effectiveness. Int J Obes (Lond) *37*, 604-611.

Gill, S., and Panda, S. (2015). A Smartphone App Reveals Erratic Diurnal Eating Patterns in Humans that Can Be Modulated for Health Benefits. Cell Metab *22*, 789-798.

Glass, J.D., DiNardo, L.A., and Ehlen, J.C. (2000). Dorsal raphe nuclear stimulation of SCN serotonin release and circadian phase-resetting. Brain Res *859*, 224-232.

Golombek, D.A., and Rosenstein, R.E. (2010). Physiology of circadian entrainment. Physiol Rev *90*, 1063-1102.

Gooley, J.J., Lu, J., Chou, T.C., Scammell, T.E., and Saper, C.B. (2001). Melanopsin in cells of origin of the retinohypothalamic tract. Nat Neurosci *4*, 1165.

Gore, B.B., and Zweifel, L.S. (2013). Genetic reconstruction of dopamine D1 receptor signaling in the nucleus accumbens facilitates natural and drug reward responses. J Neurosci *33*, 8640-8649.

Grinninger, C., Wang, W., Oskoui, K.B., Voice, J.K., and Goetzl, E.J. (2004). A natural variant type II G protein-coupled receptor for vasoactive intestinal peptide with altered function. J Biol Chem *279*, 40259-40262.

Grippo, R.M., Purohit, A.M., Zhang, Q., Zweifel, L.S., and Guler, A.D. (2017). Direct Midbrain Dopamine Input to the Suprachiasmatic Nucleus Accelerates Circadian Entrainment. Curr Biol *27*, 2465-2475 e2463.

Grosse, J., and Davis, F.C. (1999). Transient entrainment of a circadian pacemaker during development by dopaminergic activation in Syrian hamsters. Brain Res Bull *48*, 185-194.

Guh, D.P., Zhang, W., Bansback, N., Amarsi, Z., Birmingham, C.L., and Anis, A.H. (2009). The incidence of co-morbidities related to obesity and overweight: a systematic review and meta-analysis. BMC Public Health *9*, 88.

Guler, A.D., Ecker, J.L., Lall, G.S., Haq, S., Altimus, C.M., Liao, H.W., Barnard, A.R., Cahill, H., Badea, T.C., Zhao, H.*, et al.* (2008). Melanopsin cells are the principal conduits for rod-cone input to non-image-forming vision. Nature *453*, 102-105.

Hampp, G., and Albrecht, U. (2008). The circadian clock and mood-related behavior. Commun Integr Biol *1*, 1-3.

Hampp, G., Ripperger, J.A., Houben, T., Schmutz, I., Blex, C., Perreau-Lenz, S., Brunk, I., Spanagel, R., Ahnert-Hilger, G., Meijer, J.H.*, et al.* (2008). Regulation of monoamine oxidase A by circadian-clock components implies clock influence on mood. Curr Biol *18*, 678-683.

Hannibal, J. (2002). Neurotransmitters of the retino-hypothalamic tract. Cell Tissue Res *309*, 73-88.

Hariri, N., and Thibault, L. (2010). High-fat diet-induced obesity in animal models. Nutr Res Rev *23*, 270-299.

Harrington, M.E., and Rusak, B. (1989). Photic responses of geniculo-hypothalamic tract neurons in the Syrian hamster. Vis Neurosci *2*, 367-375.

Hartstra, A.V., Bouter, K.E., Backhed, F., and Nieuwdorp, M. (2015). Insights into the role of the microbiome in obesity and type 2 diabetes. Diabetes Care *38*, 159-165.

Hasler, B.P., Smith, L.J., Cousins, J.C., and Bootzin, R.R. (2012). Circadian rhythms, sleep, and substance abuse. Sleep Med Rev *16*, 67-81.

Hastings, M., and Maywood, E.S. (2000). Circadian clocks in the mammalian brain. Bioessays *22*, 23-31.

Hastings, M.H., Duffield, G.E., Ebling, F.J., Kidd, A., Maywood, E.S., and Schurov, I. (1997). Non-photic signalling in the suprachiasmatic nucleus. Biol Cell *89*, 495-503.

Hastings, M.H., Duffield, G.E., Smith, E.J., Maywood, E.S., and Ebling, F.J. (1998). Entrainment of the circadian system of mammals by nonphotic cues. Chronobiol Int *15*, 425-445.

Hatori, M., and Panda, S. (2010). The emerging roles of melanopsin in behavioral adaptation to light. Trends Mol Med *16*, 435-446.

Hatori, M., Vollmers, C., Zarrinpar, A., DiTacchio, L., Bushong, E.A., Gill, S., Leblanc, M., Chaix, A., Joens, M., Fitzpatrick, J.A.*, et al.* (2012). Time-restricted feeding without reducing caloric intake prevents metabolic diseases in mice fed a high-fat diet. Cell Metab *15*, 848-860.

Hattar, S., Liao, H.W., Takao, M., Berson, D.M., and Yau, K.W. (2002). Melanopsin-containing retinal ganglion cells: architecture, projections, and intrinsic photosensitivity. Science *295*, 1065-1070.

Hernandez, L., and Hoebel, B.G. (1988). Feeding and hypothalamic stimulation increase dopamine turnover in the accumbens. Physiol Behav *44*, 599-606.

Herzog, E.D., Takahashi, J.S., and Block, G.D. (1998). Clock controls circadian period in isolated suprachiasmatic nucleus neurons. Nat Neurosci *1*, 708-713.

Heusner, C.L., Beutler, L.R., Houser, C.R., and Palmiter, R.D. (2008). Deletion of GAD67 in dopamine receptor-1 expressing cells causes specific motor deficits. Genesis *46*, 357-367.

Hildebrandt, M.A., Hoffmann, C., Sherrill-Mix, S.A., Keilbaugh, S.A., Hamady, M., Chen, Y.Y., Knight, R., Ahima, R.S., Bushman, F., and Wu, G.D. (2009). High-fat diet determines the composition of the murine gut microbiome independently of obesity. Gastroenterology *137*, 1716-1724 e1711-1712.

Honma, K., and Honma, S. (1986). Effects of methamphetamine on development of circadian rhythms in rats. Brain Dev *8*, 397-401.

Hood, S., Cassidy, P., Cossette, M.P., Weigl, Y., Verwey, M., Robinson, B., Stewart, J., and Amir, S. (2010). Endogenous dopamine regulates the rhythm of expression of the clock protein PER2 in the rat dorsal striatum via daily activation of D2 dopamine receptors. J Neurosci *30*, 14046-14058.

Horvitz, J.C. (2000). Mesolimbocortical and nigrostriatal dopamine responses to salient non-reward events. Neuroscience *96*, 651-656.

Hughes, M.E., Hogenesch, J.B., and Kornacker, K. (2010). JTK_CYCLE: an efficient nonparametric algorithm for detecting rhythmic components in genome-scale data sets. J Biol Rhythms *25*, 372-380.

Hurt, R.T., Kulisek, C., Buchanan, L.A., and McClave, S.A. (2010). The obesity epidemic: challenges, health initiatives, and implications for gastroenterologists. Gastroenterol Hepatol (N Y) *6*, 780-792.

Imbesi, M., Yildiz, S., Dirim Arslan, A., Sharma, R., Manev, H., and Uz, T. (2009). Dopamine receptor-mediated regulation of neuronal "clock" gene expression. Neuroscience *158*, 537-544.

Ingram, C.D., Ciobanu, R., Coculescu, I.L., Tanasescu, R., Coculescu, M., and Mihai, R. (1998). Vasopressin neurotransmission and the control of circadian rhythms in the suprachiasmatic nucleus. Prog Brain Res *119*, 351-364.

Isobe, Y., and Nishino, H. (2001). Circadian rhythm of drinking and running-wheel activity in rats with 6-hydroxydopamine lesions of the ventral tegmental area. Brain Res *899*, 187-192.

Jackson, C.R., Ruan, G.X., Aseem, F., Abey, J., Gamble, K., Stanwood, G., Palmiter, R.D., Iuvone, P.M., and McMahon, D.G. (2012). Retinal dopamine mediates multiple dimensions of light-adapted vision. J Neurosci *32*, 9359-9368.

James, S.M., Honn, K.A., Gaddameedhi, S., and Van Dongen, H.P.A. (2017). Shift Work: Disrupted Circadian Rhythms and Sleep-Implications for Health and Well-Being. Curr Sleep Med Rep *3*, 104-112.

Johnson, P.M., and Kenny, P.J. (2010). Dopamine D2 receptors in addiction-like reward dysfunction and compulsive eating in obese rats. Nat Neurosci *13*, 635-641.

Johnson, R.F., Smale, L., Moore, R.Y., and Morin, L.P. (1988). Lateral geniculate lesions block circadian phase-shift responses to a benzodiazepine. Proc Natl Acad Sci U S A *85*, 5301-5304.

Jones, J.R., Tackenberg, M.C., and McMahon, D.G. (2015). Manipulating circadian clock neuron firing rate resets molecular circadian rhythms and behavior. Nat Neurosci *18*, 373-375.

Jud, C., Schmutz, I., Hampp, G., Oster, H., and Albrecht, U. (2005). A guideline for analyzing circadian wheel-running behavior in rodents under different lighting conditions. Biol Proced Online *7*, 101-116.

Kahn, S.E., Hull, R.L., and Utzschneider, K.M. (2006). Mechanisms linking obesity to insulin resistance and type 2 diabetes. Nature *444*, 840-846.

Kalsbeek, A., Palm, I.F., La Fleur, S.E., Scheer, F.A., Perreau-Lenz, S., Ruiter, M., Kreier, F., Cailotto, C., and Buijs, R.M. (2006). SCN outputs and the hypothalamic balance of life. J Biol Rhythms *21*, 458-469.

Kalsbeek, A., Yi, C.X., Cailotto, C., la Fleur, S.E., Fliers, E., and Buijs, R.M. (2011). Mammalian clock output mechanisms. Essays Biochem *49*, 137-151.

Kelley, A.E., and Berridge, K.C. (2002). The neuroscience of natural rewards: relevance to addictive drugs. J Neurosci *22*, 3306-3311.

Kizer, J.S., Palkovits, M., and Brownstein, M.J. (1976). The projections of the A8, A9 and A10 dopaminergic cell bodies: evidence for a nigral-hypothalamic-median eminence dopaminergic pathway. Brain Res *108*, 363-370.

Kohsaka, A., Laposky, A.D., Ramsey, K.M., Estrada, C., Joshu, C., Kobayashi, Y., Turek, F.W., and Bass, J. (2007). High-fat diet disrupts behavioral and molecular circadian rhythms in mice. Cell Metab *6*, 414-421.

Kopelman, P.G. (2000). Obesity as a medical problem. Nature *404*, 635-643.

Korshunov, K.S., Blakemore, L.J., and Trombley, P.Q. (2017). Dopamine: A Modulator of Circadian Rhythms in the Central Nervous System. Front Cell Neurosci *11*, 91.

Kosobud, A.E., Gillman, A.G., Leffel, J.K., 2nd, Pecoraro, N.C., Rebec, G.V., and Timberlake, W. (2007). Drugs of abuse can entrain circadian rhythms. ScientificWorldJournal *7*, 203-212.

Kraemer, F.B., and Shen, W.J. (2002). Hormone-sensitive lipase: control of intracellular tri-(di-)acylglycerol and cholesteryl ester hydrolysis. J Lipid Res *43*, 1585-1594.

Krieger, D.T., Hauser, H., and Krey, L.C. (1977). Suprachiasmatic nuclear lesions do not abolish food-shifted circadian adrenal and temperature rhythmicity. Science *197*, 398-399.

Lammel, S., Steinberg, E.E., Foldy, C., Wall, N.R., Beier, K., Luo, L., and Malenka, R.C. (2015). Diversity of transgenic mouse models for selective targeting of midbrain dopamine neurons. Neuron *85*, 429-438.

Land, B.B., Narayanan, N.S., Liu, R.J., Gianessi, C.A., Brayton, C.E., Grimaldi, D.M., Sarhan, M., Guarnieri, D.J., Deisseroth, K., Aghajanian, G.K.*, et al.* (2014). Medial prefrontal D1 dopamine neurons control food intake. Nat Neurosci *17*, 248-253.

Landgraf, D., Joiner, W.J., McCarthy, M.J., Kiessling, S., Barandas, R., Young, J.W., Cermakian, N., and Welsh, D.K. (2016). The mood stabilizer valproic acid opposes the effects of dopamine on circadian rhythms. Neuropharmacology *107*, 262-270.

Lee, I.T., Chang, A.S., Manandhar, M., Shan, Y., Fan, J., Izumo, M., Ikeda, Y., Motoike, T., Dixon, S., Seinfeld, J.E.*, et al.* (2015). Neuromedin s-producing neurons act as essential pacemakers in the suprachiasmatic nucleus to couple clock neurons and dictate circadian rhythms. Neuron *85*, 1086-1102.

Lin, L.H., and Pivorun, E.B. (1989). Analysis of serotonin, dopamine and their metabolites in the caudate putamen, the suprachiasmatic nucleus and the median raphe nucleus of euthermic and torpid deermice, Peromyscus maniculatus. Pharmacol Biochem Behav *33*, 309-314.

Liu, C.M., and Kanoski, S.E. (2018). Homeostatic and non-homeostatic controls of feeding behavior: Distinct vs. common neural systems. Physiol Behav *193*, 223-231.

Liu, Y.Y., Liu, T.Y., Qu, W.M., Hong, Z.Y., Urade, Y., and Huang, Z.L. (2012). Dopamine is involved in food-anticipatory activity in mice. J Biol Rhythms *27*, 398-409.

Logan, R.W., and McClung, C.A. (2018). Rhythms of life: circadian disruption and brain disorders across the lifespan. Nat Rev Neurosci.

Logan, R.W., Williams, W.P., 3rd, and McClung, C.A. (2014). Circadian rhythms and addiction: mechanistic insights and future directions. Behav Neurosci *128*, 387-412.

Longo, V.D., and Panda, S. (2016). Fasting, Circadian Rhythms, and Time-Restricted Feeding in Healthy Lifespan. Cell Metab *23*, 1048-1059.

Luo, S., Zhang, Y., Ezrokhi, M., Li, Y., Tsai, T.H., and Cincotta, A.H. (2018). Circadian peak dopaminergic activity response at the biological clock pacemaker (suprachiasmatic nucleus) area mediates the metabolic responsiveness to a high-fat diet. J Neuroendocrinol *30*.

Madisen, L., Zwingman, T.A., Sunkin, S.M., Oh, S.W., Zariwala, H.A., Gu, H., Ng, L.L., Palmiter, R.D., Hawrylycz, M.J., Jones, A.R.*, et al.* (2010). A robust and high-throughput Cre reporting and characterization system for the whole mouse brain. Nat Neurosci *13*, 133-140.

Maywood, E.S., O'Neill, J., Wong, G.K., Reddy, A.B., and Hastings, M.H. (2006). Circadian timing in health and disease. Prog Brain Res *153*, 253-269.

Mazuski, C., and Herzog, E.D. (2015). Circadian rhythms: to sync or not to sync. Curr Biol *25*, R337-339.

McClung, C.A. (2007). Circadian rhythms, the mesolimbic dopaminergic circuit, and drug addiction. ScientificWorldJournal *7*, 194-202.

McClung, C.A., Sidiropoulou, K., Vitaterna, M., Takahashi, J.S., White, F.J., Cooper, D.C., and Nestler, E.J. (2005). Regulation of dopaminergic transmission and cocaine reward by the Clock gene. Proc Natl Acad Sci U S A *102*, 9377-9381.

McNulty, S., Schurov, I.L., Sloper, P.J., and Hastings, M.H. (1998). Stimuli which entrain the circadian clock of the neonatal Syrian hamster in vivo regulate the phosphorylation of the transcription factor CREB in the suprachiasmatic nucleus in vitro. Eur J Neurosci *10*, 1063-1072.

Meijer, J.H., and Robbers, Y. (2014). Wheel running in the wild. Proc Biol Sci *281*.

Meijer, J.H., van der Zee, E.A., and Dietz, M. (1988). Glutamate phase shifts circadian activity rhythms in hamsters. Neurosci Lett *86*, 177-183.

Mendoza, J. (2019). Eating Rewards the Gears of the Clock. Trends Endocrinol Metab *30*, 299-311.

Mendoza, J., Angeles-Castellanos, M., and Escobar, C. (2005). A daily palatable meal without food deprivation entrains the suprachiasmatic nucleus of rats. Eur J Neurosci *22*, 2855-2862.

Mendoza, J., and Challet, E. (2014). Circadian insights into dopamine mechanisms. Neuroscience *282C*, 230-242.

Mendoza, J., Clesse, D., Pevet, P., and Challet, E. (2010). Food-reward signalling in the suprachiasmatic clock. J Neurochem *112*, 1489-1499.

Mendoza, J., Pevet, P., and Challet, E. (2008). High-fat feeding alters the clock synchronization to light. J Physiol *586*, 5901-5910.

Mills, E.L., Pierce, K.A., Jedrychowski, M.P., Garrity, R., Winther, S., Vidoni, S., Yoneshiro, T., Spinelli, J.B., Lu, G.Z., Kazak, L.*, et al.* (2018). Accumulation of succinate controls activation of adipose tissue thermogenesis. Nature *560*, 102-106.

Missale, C., Nash, S.R., Robinson, S.W., Jaber, M., and Caron, M.G. (1998). Dopamine receptors: from structure to function. Physiol Rev *78*, 189-225.

Mistlberger, R.E. (1994). Circadian food-anticipatory activity: formal models and physiological mechanisms. Neurosci Biobehav Rev *18*, 171-195.

Mistlberger, R.E. (2011). Neurobiology of food anticipatory circadian rhythms. Physiol Behav *104*, 535-545.

Mistlberger, R.E., and Antle, M.C. (2011). Entrainment of circadian clocks in mammals by arousal and food. Essays Biochem *49*, 119-136.

Moga, M.M., and Moore, R.Y. (1997). Organization of neural inputs to the suprachiasmatic nucleus in the rat. J Comp Neurol *389*, 508-534.

Mohawk, J.A., Green, C.B., and Takahashi, J.S. (2012). Central and peripheral circadian clocks in mammals. Annu Rev Neurosci *35*, 445-462.

Mohawk, J.A., Pezuk, P., and Menaker, M. (2013). Methamphetamine and dopamine receptor D1 regulate entrainment of murine circadian oscillators. PLoS One *8*, e62463.

Montesi, L., El Ghoch, M., Brodosi, L., Calugi, S., Marchesini, G., and Dalle Grave, R. (2016). Long-term weight loss maintenance for obesity: a multidisciplinary approach. Diabetes Metab Syndr Obes *9*, 37-46.

Moore, R.Y., and Eichler, V.B. (1972). Loss of a circadian adrenal corticosterone rhythm following suprachiasmatic lesions in the rat. Brain Res *42*, 201-206.

Moore, R.Y., and Speh, J.C. (1993). GABA is the principal neurotransmitter of the circadian system. Neurosci Lett *150*, 112-116.

Morin, L.P. (1999). Serotonin and the regulation of mammalian circadian rhythmicity. Ann Med *31*, 12-33.

Morin, L.P., Blanchard, J.H., and Provencio, I. (2003). Retinal ganglion cell projections to the hamster suprachiasmatic nucleus, intergeniculate leaflet, and visual midbrain: bifurcation and melanopsin immunoreactivity. J Comp Neurol *465*, 401-416.

Morris, G., Nevet, A., Arkadir, D., Vaadia, E., and Bergman, H. (2006). Midbrain dopamine neurons encode decisions for future action. Nat Neurosci *9*, 1057-1063.

Mrosovsky, N. (1995). A non-photic gateway to the circadian clock of hamsters. Ciba Found Symp *183*, 154-167; discussion 167-174.

Mrosovsky, N., Reebs, S.G., Honrado, G.I., and Salmon, P.A. (1989). Behavioural entrainment of circadian rhythms. Experientia *45*, 696-702.

Nagano, M., Adachi, A., Nakahama, K., Nakamura, T., Tamada, M., Meyer-Bernstein, E., Sehgal, A., and Shigeyoshi, Y. (2003). An abrupt shift in the day/night cycle causes desynchrony in the mammalian circadian center. J Neurosci *23*, 6141-6151.

Nakagawa, H., Sack, R.L., and Lewy, A.J. (1992). Sleep propensity free-runs with the temperature, melatonin and cortisol rhythms in a totally blind person. Sleep *15*, 330-336.

Nakamura, T., Sato, A., Kitsukawa, T., Momiyama, T., Yamamori, T., and Sasaoka, T. (2014). Distinct motor impairments of dopamine D1 and D2 receptor knockout mice revealed by three types of motor behavior. Front Integr Neurosci *8*, 56.

Nakamura, T.J., Nakamura, W., Yamazaki, S., Kudo, T., Cutler, T., Colwell, C.S., and Block, G.D. (2011). Age-related decline in circadian output. J Neurosci *31*, 10201-10205.

Nirenberg, M.J., Chan, J., Liu, Y., Edwards, R.H., and Pickel, V.M. (1996). Ultrastructural localization of the vesicular monoamine transporter-2 in midbrain dopaminergic neurons: potential sites for somatodendritic storage and release of dopamine. J Neurosci *16*, 4135-4145.

Okamura, H., Berod, A., Julien, J.F., Geffard, M., Kitahama, K., Mallet, J., and Bobillier, P. (1989). Demonstration of GABAergic cell bodies in the suprachiasmatic nucleus: in situ hybridization of glutamic acid decarboxylase (GAD) mRNA and immunocytochemistry of GAD and GABA. Neurosci Lett *102*, 131-136.

Panda, S., Hogenesch, J.B., and Kay, S.A. (2002). Circadian rhythms from flies to human. Nature *417*, 329-335.

Pantazopoulos, H., Dolatshad, H., and Davis, F.C. (2010). Chronic stimulation of the hypothalamic vasoactive intestinal peptide receptor lengthens circadian period in mice and hamsters. Am J Physiol Regul Integr Comp Physiol *299*, R379-385.

Parlee, S.D., Lentz, S.I., Mori, H., and MacDougald, O.A. (2014). Quantifying size and number of adipocytes in adipose tissue. Methods Enzymol *537*, 93-122.

Pendergast, J.S., Branecky, K.L., Yang, W., Ellacott, K.L., Niswender, K.D., and Yamazaki, S. (2013). High-fat diet acutely affects circadian organisation and eating behavior. Eur J Neurosci *37*, 1350-1356.

Pilorz, V., Cunningham, P.S., Jackson, A., West, A.C., Wager, T.T., Loudon, A.S., and Bechtold, D.A. (2014). A novel mechanism controlling resetting speed of the circadian clock to environmental stimuli. Curr Biol *24*, 766-773.

Provencio, I., Rollag, M.D., and Castrucci, A.M. (2002). Photoreceptive net in the mammalian retina. This mesh of cells may explain how some blind mice can still tell day from night. Nature *415*, 493.

Ralph, M.R., Foster, R.G., Davis, F.C., and Menaker, M. (1990). Transplanted suprachiasmatic nucleus determines circadian period. Science *247*, 975-978.

Riera, C.E., Tsaousidou, E., Halloran, J., Follett, P., Hahn, O., Pereira, M.M.A., Ruud, L.E., Alber, J., Tharp, K., Anderson, C.M.*, et al.* (2017). The Sense of Smell Impacts Metabolic Health and Obesity. Cell Metab *26*, 198-211 e195.

Rivkees, S.A., and Lachowicz, J.E. (1997). Functional D1 and D5 dopamine receptors are expressed in the suprachiasmatic, supraoptic, and paraventricular nuclei of primates. Synapse *26*, 1-10.

Roberts, L., Leise, T.L., Noguchi, T., Galschiodt, A.M., Houl, J.H., Welsh, D.K., and Holmes, T.C. (2015). Light evokes rapid circadian network oscillator desynchrony followed by gradual phase retuning of synchrony. Curr Biol *25*, 858-867.

Roeper, J. (2013). Dissecting the diversity of midbrain dopamine neurons. Trends Neurosci *36*, 336-342.

Rogan, S.C., and Roth, B.L. (2011). Remote control of neuronal signaling. Pharmacol Rev *63*, 291-315.

Rohling, J.H., vanderLeest, H.T., Michel, S., Vansteensel, M.J., and Meijer, J.H. (2011). Phase resetting of the mammalian circadian clock relies on a rapid shift of a small population of pacemaker neurons. PLoS One *6*, e25437.

Rollag, M.D., Berson, D.M., and Provencio, I. (2003). Melanopsin, ganglion-cell photoreceptors, and mammalian photoentrainment. J Biol Rhythms *18*, 227-234.

Rosenwasser, A.M., and Dwyer, S.M. (2001). Circadian phase shifting: Relationships between photic and nonphotic phase-response curves. Physiol Behav *73*, 175-183.

Rossi, M.A., and Stuber, G.D. (2018). Overlapping Brain Circuits for Homeostatic and Hedonic Feeding. Cell Metab *27*, 42-56.

Ruan, G.X., Allen, G.C., Yamazaki, S., and McMahon, D.G. (2008). An autonomous circadian clock in the inner mouse retina regulated by dopamine and GABA. PLoS Biol *6*, e249.

Sack, R.L., Lewy, A.J., Blood, M.L., Keith, L.D., and Nakagawa, H. (1992). Circadian rhythm abnormalities in totally blind people: incidence and clinical significance. J Clin Endocrinol Metab *75*, 127-134.

Saper, C.B., Chou, T.C., and Elmquist, J.K. (2002). The need to feed: homeostatic and hedonic control of eating. Neuron *36*, 199-211.

Sarinana, J., and Tonegawa, S. (2016). Differentiation of forebrain and hippocampal dopamine 1-class receptors, D1R and D5R, in spatial learning and memory. Hippocampus *26*, 76-86.

Schaap, J., Pennartz, C.M., and Meijer, J.H. (2003). Electrophysiology of the circadian pacemaker in mammals. Chronobiol Int *20*, 171-188.

Schultz, W. (1997). Dopamine neurons and their role in reward mechanisms. Curr Opin Neurobiol *7*, 191-197.

Schultz, W. (1998). Predictive reward signal of dopamine neurons. J Neurophysiol *80*, 1-27.

Seeman, P. (1980). Brain dopamine receptors. Pharmacol Rev *32*, 229-313.

Sleipness, E.P., Sorg, B.A., and Jansen, H.T. (2007a). Contribution of the suprachiasmatic nucleus to day:night variation in cocaine-seeking behavior. Physiol Behav *91*, 523-530.

Sleipness, E.P., Sorg, B.A., and Jansen, H.T. (2007b). Diurnal differences in dopamine transporter and tyrosine hydroxylase levels in rat brain: dependence on the suprachiasmatic nucleus. Brain Res *1129*, 34-42.

Smolensky, M.H., Hermida, R.C., Reinberg, A., Sackett-Lundeen, L., and Portaluppi, F. (2016). Circadian disruption: New clinical perspective of disease pathology and basis for chronotherapeutic intervention. Chronobiol Int *33*, 1101-1119.

Smyllie, N.J., Chesham, J.E., Hamnett, R., Maywood, E.S., and Hastings, M.H. (2016). Temporally chimeric mice reveal flexibility of circadian period-setting in the suprachiasmatic nucleus. Proc Natl Acad Sci U S A *113*, 3657-3662.

Solt, L.A., Wang, Y., Banerjee, S., Hughes, T., Kojetin, D.J., Lundasen, T., Shin, Y., Liu, J., Cameron, M.D., Noel, R.*, et al.* (2012). Regulation of circadian behaviour and metabolism by synthetic REV-ERB agonists. Nature *485*, 62-68.

Song, A.J., and Palmiter, R.D. (2018). Detecting and Avoiding Problems When Using the Cre-lox System. Trends Genet *34*, 333-340.

Stamatakis, A.M., Van Swieten, M., Basiri, M.L., Blair, G.A., Kantak, P., and Stuber, G.D. (2016). Lateral Hypothalamic Area Glutamatergic Neurons and Their Projections to the Lateral Habenula Regulate Feeding and Reward. J Neurosci *36*, 302-311.

Stenvers, D.J., Scheer, F., Schrauwen, P., la Fleur, S.E., and Kalsbeek, A. (2019). Circadian clocks and insulin resistance. Nat Rev Endocrinol *15*, 75-89.

Stephan, F.K., Swann, J.M., and Sisk, C.L. (1979). Anticipation of 24-hr feeding schedules in rats with lesions of the suprachiasmatic nucleus. Behav Neural Biol *25*, 346-363.

Stephan, F.K., and Zucker, I. (1972). Circadian rhythms in drinking behavior and locomotor activity of rats are eliminated by hypothalamic lesions. Proc Natl Acad Sci U S A *69*, 1583-1586.

Steppan, C.M., Bailey, S.T., Bhat, S., Brown, E.J., Banerjee, R.R., Wright, C.M., Patel, H.R., Ahima, R.S., and Lazar, M.A. (2001). The hormone resistin links obesity to diabetes. Nature *409*, 307-312.

Stevens, R.G., Blask, D.E., Brainard, G.C., Hansen, J., Lockley, S.W., Provencio, I., Rea, M.S., and Reinlib, L. (2007). Meeting report: the role of environmental lighting and circadian disruption in cancer and other diseases. Environ Health Perspect *115*, 1357-1362.

Stokkan, K.A., Yamazaki, S., Tei, H., Sakaki, Y., and Menaker, M. (2001). Entrainment of the circadian clock in the liver by feeding. Science *291*, 490-493.

Strother, W.N., Norman, A.B., and Lehman, M.N. (1998). D1-dopamine receptor binding and tyrosine hydroxylase-immunoreactivity in the fetal and neonatal hamster suprachiasmatic nucleus. Brain Res Dev Brain Res *106*, 137-144.

Sumova, A., Travnickova, Z., and Illnerova, H. (2000). Spontaneous c-Fos rhythm in the rat suprachiasmatic nucleus: location and effect of photoperiod. Am J Physiol Regul Integr Comp Physiol *279*, R2262-2269.

Sutton, E.F., Beyl, R., Early, K.S., Cefalu, W.T., Ravussin, E., and Peterson, C.M. (2018). Early Time-Restricted Feeding Improves Insulin Sensitivity, Blood Pressure, and Oxidative Stress Even without Weight Loss in Men with Prediabetes. Cell Metab *27*, 1212-1221 e1213.

Takahashi, J.S. (2017). Transcriptional architecture of the mammalian circadian clock. Nat Rev Genet *18*, 164-179.

Takahashi, J.S., DeCoursey, P.J., Bauman, L., and Menaker, M. (1984). Spectral sensitivity of a novel photoreceptive system mediating entrainment of mammalian circadian rhythms. Nature *308*, 186-188.

Tataroglu, O., Davidson, A.J., Benvenuto, L.J., and Menaker, M. (2006). The methamphetamine-sensitive circadian oscillator (MASCO) in mice. J Biol Rhythms *21*, 185-194.

Terry, P., and Katz, J.L. (1994). A comparison of the effects of the D1 receptor antagonists SCH 23390 and SCH 39166 on suppression of feeding behavior by the D1 agonist SKF38393. Psychopharmacology (Berl) *113*, 328-333.

Thevaranjan, N., Puchta, A., Schulz, C., Naidoo, A., Szamosi, J.C., Verschoor, C.P., Loukov, D., Schenck, L.P., Jury, J., Foley, K.P.*, et al.* (2017). Age-Associated Microbial Dysbiosis Promotes Intestinal Permeability, Systemic Inflammation, and Macrophage Dysfunction. Cell Host Microbe *21*, 455-466 e454.

Tilg, H., and Kaser, A. (2011). Gut microbiome, obesity, and metabolic dysfunction. J Clin Invest *121*, 2126-2132.

Ting, J.T., Daigle, T.L., Chen, Q., and Feng, G. (2014). Acute brain slice methods for adult and aging animals: application of targeted patch clamp analysis and optogenetics. Methods Mol Biol *1183*, 221-242.

Tosini, G., Pozdeyev, N., Sakamoto, K., and Iuvone, P.M. (2008). The circadian clock system in the mammalian retina. Bioessays *30*, 624-633.

Tsien, J.Z., Chen, D.F., Gerber, D., Tom, C., Mercer, E.H., Anderson, D.J., Mayford, M., Kandel, E.R., and Tonegawa, S. (1996). Subregion- and cell type-restricted gene knockout in mouse brain. Cell *87*, 1317-1326.

Turek, F.W., Joshu, C., Kohsaka, A., Lin, E., Ivanova, G., McDearmon, E., Laposky, A., Losee-Olson, S., Easton, A., Jensen, D.R.*, et al.* (2005). Obesity and metabolic syndrome in circadian Clock mutant mice. Science *308*, 1043-1045.

Turnbaugh, P.J., Ley, R.E., Mahowald, M.A., Magrini, V., Mardis, E.R., and Gordon, J.I. (2006). An obesity-associated gut microbiome with increased capacity for energy harvest. Nature *444*, 1027-1031.

Ugrumov, M.V., Tixier-Vidal, A., Taxi, J., Thibault, J., and Mitskevich, M.S. (1989). Ontogenesis of tyrosine hydroxylase-immunopositive structures in the rat hypothalamus. Fiber pathways and terminal fields. Neuroscience *29*, 157-166.

Vadnie, C.A., and McClung, C.A. (2017). Circadian Rhythm Disturbances in Mood Disorders: Insights into the Role of the Suprachiasmatic Nucleus. Neural Plast *2017*, 1504507.

van der Weyden, L., White, J.K., Adams, D.J., and Logan, D.W. (2011). The mouse genetics toolkit: revealing function and mechanism. Genome Biol *12*, 224.

Van Someren, E.J., Kessler, A., Mirmiran, M., and Swaab, D.F. (1997). Indirect bright light improves circadian rest-activity rhythm disturbances in demented patients. Biol Psychiatry *41*, 955-963.

Van Veen, M.M., Kooij, J.J., Boonstra, A.M., Gordijn, M.C., and Van Someren, E.J. (2010). Delayed circadian rhythm in adults with attention-deficit/hyperactivity disorder and chronic sleep-onset insomnia. Biol Psychiatry *67*, 1091-1096.

Videnovic, A., and Golombek, D. (2013). Circadian and sleep disorders in Parkinson's disease. Exp Neurol *243*, 45-56.

Viswanathan, N., Weaver, D.R., Reppert, S.M., and Davis, F.C. (1994). Entrainment of the fetal hamster circadian pacemaker by prenatal injections of the dopamine agonist SKF 38393. J Neurosci *14*, 5393-5398.

Volkow, N.D., Wang, G.J., Fowler, J.S., Logan, J., Jayne, M., Franceschi, D., Wong, C., Gatley, S.J., Gifford, A.N., Ding, Y.S.*, et al.* (2002). "Nonhedonic" food motivation in humans involves dopamine in the dorsal striatum and methylphenidate amplifies this effect. Synapse *44*, 175-180.

Volkow, N.D., Wang, G.J., Fowler, J.S., Tomasi, D., and Baler, R. (2012). Food and drug reward: overlapping circuits in human obesity and addiction. Curr Top Behav Neurosci *11*, 1-24.

Volkow, N.D., Wang, G.J., Telang, F., Fowler, J.S., Thanos, P.K., Logan, J., Alexoff, D., Ding, Y.S., Wong, C., Ma, Y.*, et al.* (2008). Low dopamine striatal D2 receptors are associated with prefrontal metabolism in obese subjects: possible contributing factors. Neuroimage *42*, 1537-1543.

Vollmers, C., Gill, S., DiTacchio, L., Pulivarthy, S.R., Le, H.D., and Panda, S. (2009). Time of feeding and the intrinsic circadian clock drive rhythms in hepatic gene expression. Proc Natl Acad Sci U S A *106*, 21453-21458.

Vong, L., Ye, C., Yang, Z., Choi, B., Chua, S., Jr., and Lowell, B.B. (2011). Leptin action on GABAergic neurons prevents obesity and reduces inhibitory tone to POMC neurons. Neuron *71*, 142-154.

Wan, M., Easton, R.M., Gleason, C.E., Monks, B.R., Ueki, K., Kahn, C.R., and Birnbaum, M.J. (2012). Loss of Akt1 in mice increases energy expenditure and protects against diet-induced obesity. Mol Cell Biol *32*, 96-106.

Wang, G.J., Volkow, N.D., Logan, J., Pappas, N.R., Wong, C.T., Zhu, W., Netusil, N., and Fowler, J.S. (2001). Brain dopamine and obesity. Lancet *357*, 354-357.

Wang, X., Zhang, C., Szabo, G., and Sun, Q.Q. (2013). Distribution of CaMKIIalpha expression in the brain in vivo, studied by CaMKIIalpha-GFP mice. Brain Res *1518*, 9-25.

Weaver, D.R., and Reppert, S.M. (1995). Definition of the developmental transition from dopaminergic to photic regulation of c-fos gene expression in the rat suprachiasmatic nucleus. Brain Res Mol Brain Res *33*, 136-148.

Weaver, D.R., Rivkees, S.A., and Reppert, S.M. (1992). D1-dopamine receptors activate c-fos expression in the fetal suprachiasmatic nuclei. Proc Natl Acad Sci U S A *89*, 9201-9204.

Webb, I.C., Baltazar, R.M., Wang, X., Pitchers, K.K., Coolen, L.M., and Lehman, M.N. (2009). Diurnal variations in natural and drug reward, mesolimbic tyrosine hydroxylase, and clock gene expression in the male rat. J Biol Rhythms *24*, 465-476.

Webb, V.L., and Wadden, T.A. (2017). Intensive Lifestyle Intervention for Obesity: Principles, Practices, and Results. Gastroenterology *152*, 1752-1764.

Welsh, D.K., Logothetis, D.E., Meister, M., and Reppert, S.M. (1995). Individual neurons dissociated from rat suprachiasmatic nucleus express independently phased circadian firing rhythms. Neuron *14*, 697-706.

Welsh, D.K., Takahashi, J.S., and Kay, S.A. (2010). Suprachiasmatic nucleus: cell autonomy and network properties. Annu Rev Physiol *72*, 551-577.

West, A.C., and Bechtold, D.A. (2015). The cost of circadian desynchrony: Evidence, insights and open questions. Bioessays *37*, 777-788.

Wilson, S., and Argyropoulos, S. (2012). Sleep in schizophrenia: time for closer attention. Br J Psychiatry *200*, 273-274.

Winzell, M.S., and Ahren, B. (2004). The high-fat diet-fed mouse: a model for studying mechanisms and treatment of impaired glucose tolerance and type 2 diabetes. Diabetes *53 Suppl 3*, S215-219.

Wise, R.A. (2004). Dopamine, learning and motivation. Nat Rev Neurosci *5*, 483-494.

Wise, R.A. (2006). Role of brain dopamine in food reward and reinforcement. Philos Trans R Soc Lond B Biol Sci *361*, 1149-1158.

Wise, R.A., and Rompre, P.P. (1989). Brain dopamine and reward. Annu Rev Psychol *40*, 191-225.

Wulff, K., Gatti, S., Wettstein, J.G., and Foster, R.G. (2010). Sleep and circadian rhythm disruption in psychiatric and neurodegenerative disease. Nat Rev Neurosci *11*, 589-599.

Xu, H., Barnes, G.T., Yang, Q., Tan, G., Yang, D., Chou, C.J., Sole, J., Nichols, A., Ross, J.S., Tartaglia, L.A.*, et al.* (2003). Chronic inflammation in fat plays a crucial role in the development of obesity-related insulin resistance. J Clin Invest *112*, 1821-1830.

Xu, M., Moratalla, R., Gold, L.H., Hiroi, N., Koob, G.F., Graybiel, A.M., and Tonegawa, S. (1994). Dopamine D1 receptor mutant mice are deficient in striatal expression of dynorphin and in dopamine-mediated behavioral responses. Cell *79*, 729-742.

Yamanaka, Y., Honma, S., and Honma, K. (2008). Scheduled exposures to a novel environment with a running-wheel differentially accelerate re-entrainment of mice peripheral clocks to new light-dark cycles. Genes Cells *13*, 497-507.

Zaidi, F.H., Hull, J.T., Peirson, S.N., Wulff, K., Aeschbach, D., Gooley, J.J., Brainard, G.C., Gregory-Evans, K., Rizzo, J.F., 3rd, Czeisler, C.A.*, et al.* (2007). Short-wavelength light sensitivity of circadian, pupillary, and visual awareness in humans lacking an outer retina. Curr Biol *17*, 2122-2128.

Zanini, M.A., Castro, J., Cunha, G.R., Asevedo, E., Pan, P.M., Bittencourt, L., Coelho, F.M., Tufik, S., Gadelha, A., Bressan, R.A.*, et al.* (2015). Abnormalities in sleep patterns in individuals at risk for psychosis and bipolar disorder. Schizophr Res.

Zarrinpar, A., Chaix, A., Yooseph, S., and Panda, S. (2014). Diet and feeding pattern affect the diurnal dynamics of the gut microbiome. Cell Metab *20*, 1006-1017.

Zee, P.C., and Goldstein, C.A. (2010). Treatment of shift work disorder and jet lag. Curr Treat Options Neurol *12*, 396-411.

Zhou, Q.Y., and Palmiter, R.D. (1995). Dopamine-deficient mice are severely hypoactive, adipsic, and aphagic. Cell *83*, 1197-1209.

Zhuang, X., Masson, J., Gingrich, J.A., Rayport, S., and Hen, R. (2005). Targeted gene expression in dopamine and serotonin neurons of the mouse brain. J Neurosci Methods *143*, 27-32.